

博士論文

**Molecular design of amphiphilic polyaspartamide derivatives
with hydrophobic moieties for efficient nucleic acids delivery**

(核酸送達効率の向上を目指した疎水性官能基導入

ポリアスパルタミド誘導体の分子設計)

廉 鐘旻

**Molecular design of amphiphilic polyaspartamide derivatives
with hydrophobic moieties for efficient nucleic acids delivery**

Jongmin Yum

**Department of Materials Engineering
School of Engineering
The University of Tokyo**

December 2021

Referee in chief: *Professor* Dr. Kanjiro Miyata

Referee: *Professor* Dr. Ryo Yoshida

Associate Professor Dr. Yuichi Yamasaki

Associate Professor Dr. Horacio Cabral

Professor Dr. Shinsuke Sando

Table of contents

Chapter 1. General introduction

1.1 Nucleic acid-based therapeutics	4
1.2 Development of delivery technologies of nucleic acids.....	6
1.3 Design of polymeric carriers for efficient nucleic acid drug delivery.....	11
1.4 Amphiphilic polyaspartamide derivatives	19
1.5 Purpose of this study and structure of the thesis.....	21
References	23

Chapter 2. Polyaspartamide derivatives with varying hydrophobicity for antisense oligonucleotide delivery

2.1 Chapter introduction.....	29
2.2 Materials and methods.....	31
2.3 Results and discussion	37
2.4 Conclusions	51
References	52

Chapter 3. Molecular design of polyaspartamide derivatives for efficient messenger RNA delivery

3.1 Chapter introduction.....	55
3.2 Materials and methods.....	58
3.3 Results and discussion.....	67
3.4 Conclusions	85
References	86

Chapter 4. Systemic messenger RNA delivery by using polyaspartamide derivatives

4.1 Chapter introduction.....	88
4.2 Materials and methods.....	90

4.3 Results and discussions	95
4.4 Conclusions	105
References	106

Chapter 5. Concluding remarks

5.1. Concluding remarks.....	110
Appendix	113
Acknowledgement.....	115

Chapter 1
General introduction

1.1. Nucleic acid-based therapeutics

Nucleic acid drugs have been attracting considerable attention for the treatment of various intractable diseases by regulating the expression of the target gene [1-3]. Antisense oligonucleotide (ASO), small interfering RNA (siRNA), and *in vitro* transcribed messenger RNA (IVT mRNA) are representative nucleic acid drugs. ASO and siRNA can inhibit target gene expression *via* a complementary interaction to target mRNA (**Fig. 1-1**) [4]. Despite similar activities to target RNA, ASO and siRNA exhibit different gene silencing mechanisms. After transfection, ASO, being single-stranded DNA, forms an ASO-RNA heteroduplex by complementary bonding with the mRNA target and activates RNase H [3,5]. This activated enzyme cleaves the RNA in the heteroduplex, inducing target gene silencing. In addition, ASO can modulate gene expression by targeting transcripts and forming steric blocking, leading to alternative splicing. On the other hand, siRNA, as double-stranded RNA (dsRNA), is incorporated into the RNA-induced silencing complex (RISC). In the RISC, the sense strand of the siRNA is degraded and removed. Consequently, the residual antisense strand binds complementary messenger RNA (mRNA) to suppress the translation of the mRNA or cleave the mRNA [6]. Compared to ASO and siRNA, IVT mRNA can produce coded-protein in the cytoplasm of the target cells, after cellular internalization (**Fig. 1-1**). Compared to gene therapy using plasmid DNAs, the insertional mutagenesis risk is trivial in mRNA-based therapies, due to the mRNA nature of not integrating into the host genome. Even though nucleic acid drugs are promising biopharmaceuticals, as abovementioned, there are several hurdles to achieving effective delivery to target sites. When naked nucleic acids are administered into a body, they are readily degraded by nucleases or interact with serum proteins in the biological fluids, mainly in the bloodstream. Moreover, such negatively charged nucleic acids elicit inefficient cellular uptake due to the electrostatic repulsion against the negatively charged cytoplasmic membrane. These obstacles

hamper the arrival rate of intact nucleic acids to the cytoplasm of the target cell, thereby limiting the clinical applications of nucleic acid drugs.

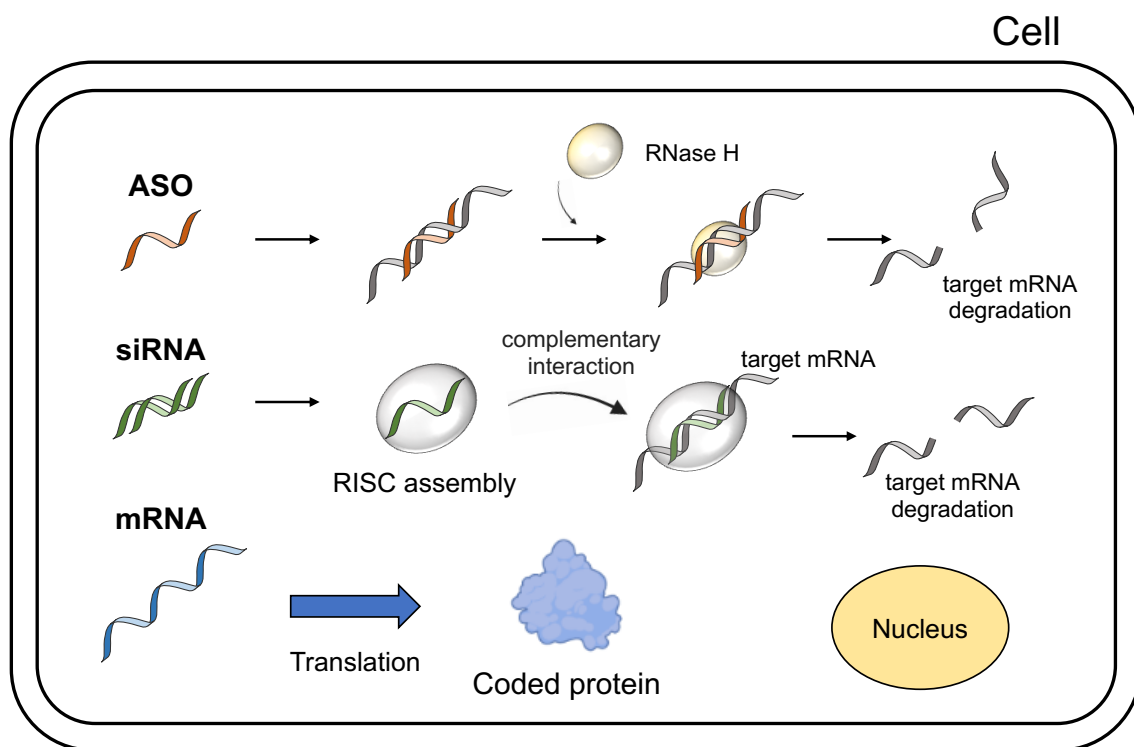


Fig. 1-1. The types of nucleic acids and their mechanisms of action.

1.2. Development of delivery technologies of nucleic acids

To overcome the limitations and improve the bioavailability of naked nucleic acids, various delivery technologies have been studied and developed, such as chemical modifications and delivery vehicles.

- **Chemical modification**

Nucleic acid chemical modification technology has developed significantly since the gene silencing ability of ASO to targeted RNA was reported in the 1970s [7]. To date, all ASO drugs approved by the U.S. Food and Drug Administration (FDA) are chemically modified (**Table 1-1**) [3,8], of which the phosphorothioate (PS) backbone and 2'-ribose modifications are representative (**Fig. 1-2**). The PS backbone has a structure in which one oxygen element in the phosphate group linking nucleotides is substituted with a sulfur element. The PS backbone not only enhances the cellular uptake efficiency of the nucleotides but also increases stability against enzyme degradation [8]. However, the PS backbone alone cannot completely protect the payloads. Furthermore, nucleic acids can achieve greater stability and an improved binding affinity to target RNA through additional 2'-ribose modification, including 2'-*O*-methyl (2'-OMe), 2'-*O*-methoxyethyl (2'-MOE), 2'-deoxy-2'-fluoro (2'-F), 2'-*O*,4'-*C*-methylene bridged nucleic acid (LNA) [8]. Additionally, there are morpholinos, which are nucleotide analogs with alternative chemically modified structures. Compared to other nucleic acids, morpholinos are neutrally charged, leading to the elimination of non-antisense effects by reducing the interactions with cationic serum proteins. In this way, various nucleic acid drugs have found practical application through the use of developed chemical modification techniques.

Table 1-1. ASO- and siRNA-based drugs approved by the FDA.

ASO	Chemistry	Organ (indication)	FDA approval
Fomivirsen	PS (21 mer)	Eye (cytomegalovirus retinitis)	1998
Mipomersen	PS, 2'-MOE (20 mer)	Liver (homozygous familial hypercholesterolaemia)	2013
Eteplirsen	PMO (30 mer)	Skeletal muscle (Duchenne muscular dystrophy)	2016
Nusinersen	PS, 2'-MOE (18 mer)	Spinal cord (spinal muscular atrophy)	2016
Inotersen	PS, 2'-MOE (20 mer)	Liver (hereditary transthyretin amyloidosis, polyneuropathy)	2018
Golodirsen	PMO (25 mer)	Skeletal muscle (Duchenne muscular dystrophy)	2019
Viltolarsen	PMO (21 mer)	Skeletal muscle (Duchenne muscular dystrophy)	2020
Casimersen	PMO (22 mer)	Skeletal muscle (Duchenne muscular dystrophy)	2021
siRNA	Chemistry	Organ (indication)	FDA approval
Patisiran	2'-OMe (19 + 2 mer, LNP formulation)	Liver (hereditary transthyretin amyloidosis, polyneuropathy)	2018
Givosiran	PS, 2'-Ome, 2'-F (21/23 mer, GalNAc conjugate)	Liver (acute hepatic porphyria)	2019
Lumasiran	PS, 2'-Ome, 2'-F (21/23 mer, GalNAc conjugate)	Liver (primary hyperoxaluria type 1)	2020

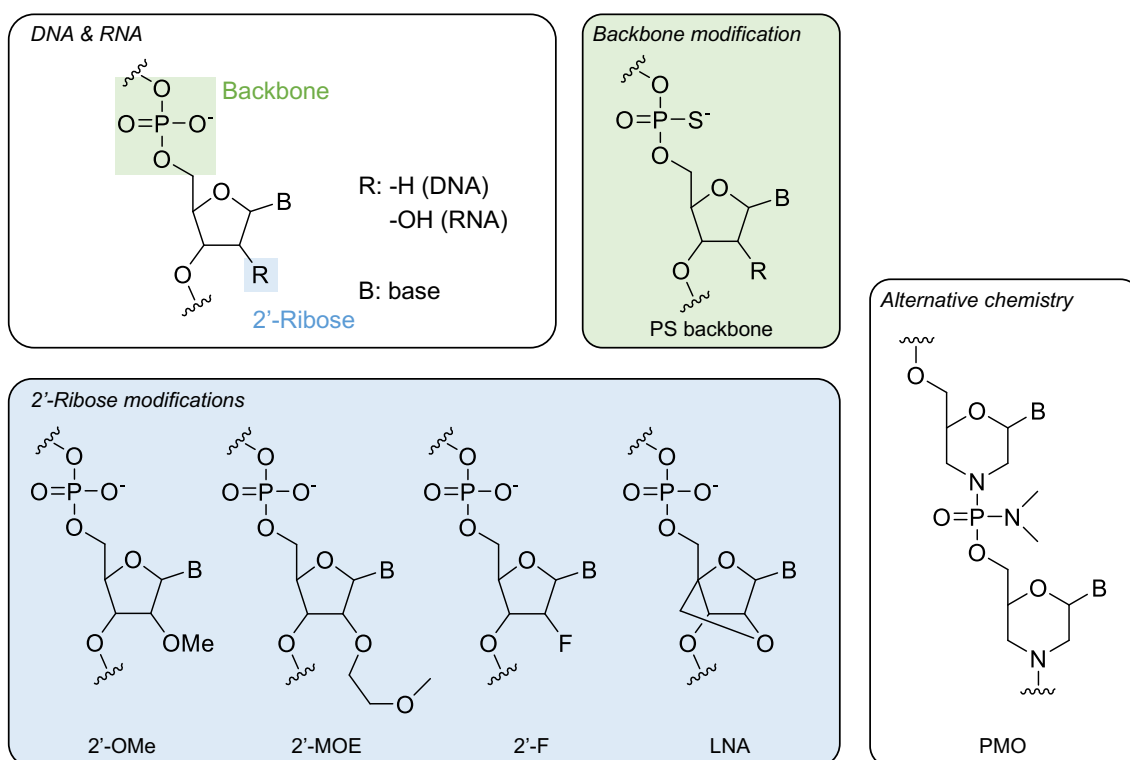


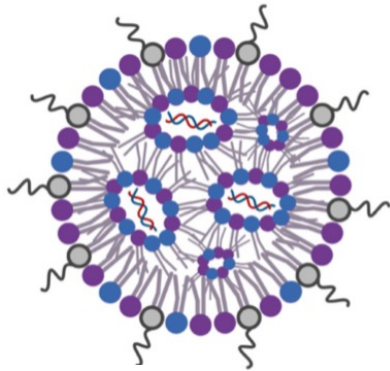
Fig. 1-2. Chemical structures for the modification of nucleic acids





- **Delivery vehicles**

Another alternative method is the utilization of delivery vehicles, *e.g.*, lipid nanoparticles (LNPs) and polymeric nanoparticles (polyplexes) for the protection of payloads from nucleases and improvement of cellular internalization into the target cells [9–11]. These vehicles are also effective for the systemic delivery of nucleic acid drugs. Although chemically modified nucleic acids have a dramatically enhanced resistance to enzymatic degradation and increased the cellular uptake and binding affinity to target nucleic acids, they are rapidly removed when systemically administrated due to their small size [12,13]. However, the loading of nucleic acids into vehicles, which become larger than the size range suitable for renal excretion, leads to an increase in blood circulation time. Patisiran (or Onpattro[®]) is the first approved siRNA-based drug, which is a siRNA-loaded PEGylated lipid nanoparticle (LNP) with a size of 60–100 nm.

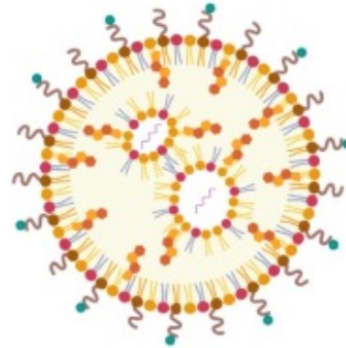
This LNP formulation is composed of a chemically modified siRNA, an ionizable lipid (DLin-MC3-DMA; MC3), a neutral lipid (1,2-distearoyl-*sn*-glycero-3-phosphocholine; DSPC), PEGylated lipid (PEG_{2K}-C-DMG), and cholesterol (**Fig. 1-3**) [14,15]. The administration of LNP is *via* intravenous infusion to deliver siRNA to the liver for the treatment of hereditary transthyretin (hATTR) amyloidosis (previously called familial amyloid polyneuropathy (FAP) or familial amyloid cardiomyopathy (FAC)) [16-18]. Various LNPs, including Patisiran, generally deliver the payloads into the liver, due to the opsonization with apolipoprotein E (apoE) in the bloodstream, leading to efficient cellular uptake by hepatocytes *via* a low-density lipoprotein receptor (LDLR) [16,19]. Furthermore, two lipid nanoparticle delivery systems have been recently approved for mRNA-based vaccines for COVID19, which are BNT162b2 and mRNA-1273, developed by Pfizer-BioNTech and Moderna, respectively. Heptadecane-9-yl-8-((2-hydroxyethyl)(6-oxo-6-(undecyloxy)hexyl)amino)octanoate (Lipid H) was utilized in mRNA-1273 as an ionizable lipid (**Fig. 1-3**) [20,23]. Polyplexes have also great potential as nucleic acid-loaded vesicles in terms of the ease of preparation in aqueous buffers. Although, compared to previous procedures, LNP preparation has become easier using developed technologies such as microfluidics, processes such as pH control and dialysis are required. On the other hand, polyplexes can be more easily prepared by the simple mixing of cationic polymers with nucleic acids. Moreover, polyplexes can be highly functionalized by chemical fine-tuning of the components [11,21,22]. Based on these merits, various polyplexes have been developed and translated to clinical trials.

Patisiran (siRNA)



-  **siRNA**
-  **DSPC**
-  **Dlin-MC3-DMA**
-  **PEG-DMG**

mRNA-vaccine









-  **Helper lipid**
(e.g., DOPE, DSPC)
-  **Ionizable lipid**
(e.g., C12-200, MC3)
-  **Cholesterol**
-  **Lipid-anchored PEG**
-  **Targeting moiety**
(e.g., monoclonal antibody, peptide)
-  **mRNA**

Fig. 1-3. Lipid nanoparticles encapsulating nucleic acids [36,37].

1.3. Design of polymeric carriers for efficient nucleic acid drug delivery

For the nucleic acid drugs to be effective *via* polyplex-based delivery, polyplexes must pass through a series of processes in the intracellular environment (**Fig. 1-4**). After reaching the target tissues, nanoparticles are internalized into the cell, followed by enclosure within the endosome. Next, the nanoparticles escape the endosome and reach the cytoplasm, where they release their payloads (nucleic acid drugs) to undertake their activities. Fine-tuning of the polymer design can facilitate efficient polyplex delivery into the cells. In **Chapter 1.3**, the design of polymeric carriers that efficiently pass through each process is briefly discussed.

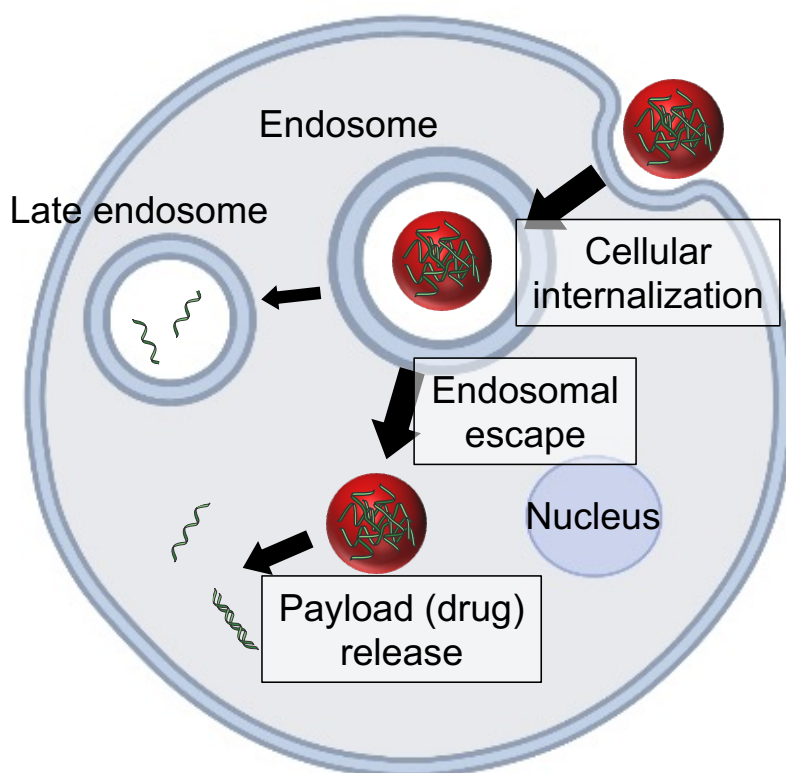


Figure 1-4. Intracellular delivery route of a polyplex.

- **Stability of nanoparticles in the extracellular milieu**

The stability of polyplexes is an important factor for the transfection of nucleic acids in the extracellular milieu until reaching the cells. Generally, polyplexes are formed *via* electrostatic interactions between cationic polymers and nucleic acids, which can be destabilized by competitive interactions with anionic components in the extracellular matrix and cell surface and/or by the diluted conditions in the bloodstream after administration into the body. Therefore, various other interactions have been utilized to enhance polyplex stability. One of the representatives is the use of hydrophobic interactions. The hydrophobic segments introduced into the polymers interact with each other, enhancing the polyplex stability. It has been reported that various types of hydrophobic molecules, *i.e.*, cholesterol and alkyl chains, have been used as components for fine-tuning the hydrophobicity by insertion into the polymer [24-26]. However, since an excessive increase of polyplex stability induces difficulties with payload release in the cytoplasm, optimization of the hydrophobicity is required [25,26]. Cross-linkage between polymers forming polyplexes can also increase colloidal stability. Cationic guanidinium groups have hydrogen bond donors, which facilitate synergetic ionic and hydrogen interactions with the anionic components of nucleic acids, *i.e.*, the phosphate moiety. It has been reported that polyplex stability is enhanced by introducing guanidinium moieties into the polymers [27,28]. Disulfide cross-linking has also been widely used to increase polyplex stability. For example, a cationic block copolymer tailored with 3-mercaptopropyl amidine (MPA) and 2-thiolaneimine (IM) moieties exhibited improved stability due to disulfide cross-linking [29,30]. This link also can be effective for tumor targeting, because of the high glutathione (GSH) concentration in tumor cells, which elicits cleavage of the disulfide bond and the release of the cargo. Furthermore, this was also studied with cationic polymers bearing the 4-carboxy-3-fluorophenylboronic acid (FPBA) moiety [31]. The FPBA moieties form the ester-linkage between the boronate and ribose group at

the 3' ends of siRNA, leading to an increase in the polyplex stability. After cellular internalization, the linkage is rapidly cleaved to promote siRNA release *via* the ATP response in the intercellular environment.

- **Endosomal escape**

Cationic polymers forming polyplexes have increased protonation rates in the endosomes, due to their acidic environments (pH ~5.5) compared to the extracellular milieu (pH ~7.3). This prompts membrane destabilization by the influx of large amounts of protons and counter-ions into endosomes, resulting in elevated osmotic pressure; termed the proton sponge hypothesis (**Fig. 1-5**). It is also reported that the increased protonated amines trigger an interaction with the endosomal membrane, leading to efficient membrane destabilization. For efficient endosomal escape, cationic polymers containing amines with slightly lower pK_a than ~7.3, which can effectively respond to stimuli at much lower pH in endosomes, have been widely used. Indeed, both MC3 and Lipid H (both approved by the FDA), consisting of LNP, have an amine with pK_a at 6.35 and 6.68, respectively, which are lower than the endosomal pH [14,20]. Meanwhile, polymer libraries having aminoethylene units have been studied, due to their special protonation behavior (**Fig. 1-6**) [22,32,33]. Among the polyaspartamide derivatives (PAsp(EDA), PAsp(DET), PAsp(TET), and PAsp(TEP)) bearing aminoethylene units with various numbers of repeats (ethylenediamine (EDA), diethylenetriamine (DET), triethylenetetramine (TET), and tetraethylenepentamine (TEP)), PAsp(DET) and PAsp(TEP) exhibited a relatively large decrease in the degree of protonation ($\Delta\alpha$) from pH 7.4 (extracellular milieu) to 5.5 (endosome) compared to PAsp(EDA) and PAsp(TET), leading to their rapid and efficient endosomal escape. In particular, PAsp(DET) showed the highest $\Delta\alpha$ value (31%), which is also higher than that of linear PEI (10%) with high endosomal escape [33]. Moreover, in the case of PAsp(DET) and

PAsp(TEP), an increase of the protonated amine number occurs in each DET and TEP moiety (protonated amine number, 1 to 2, DET; 2 to 3, TEP) by reducing the pH from 7.3 to 5.5 (**Fig. 1-6, Table 1-2**). This causes a disruption of the membrane, resulting in efficient endosomal escape with low toxicity, compared with polyethyleneimine (PEI).

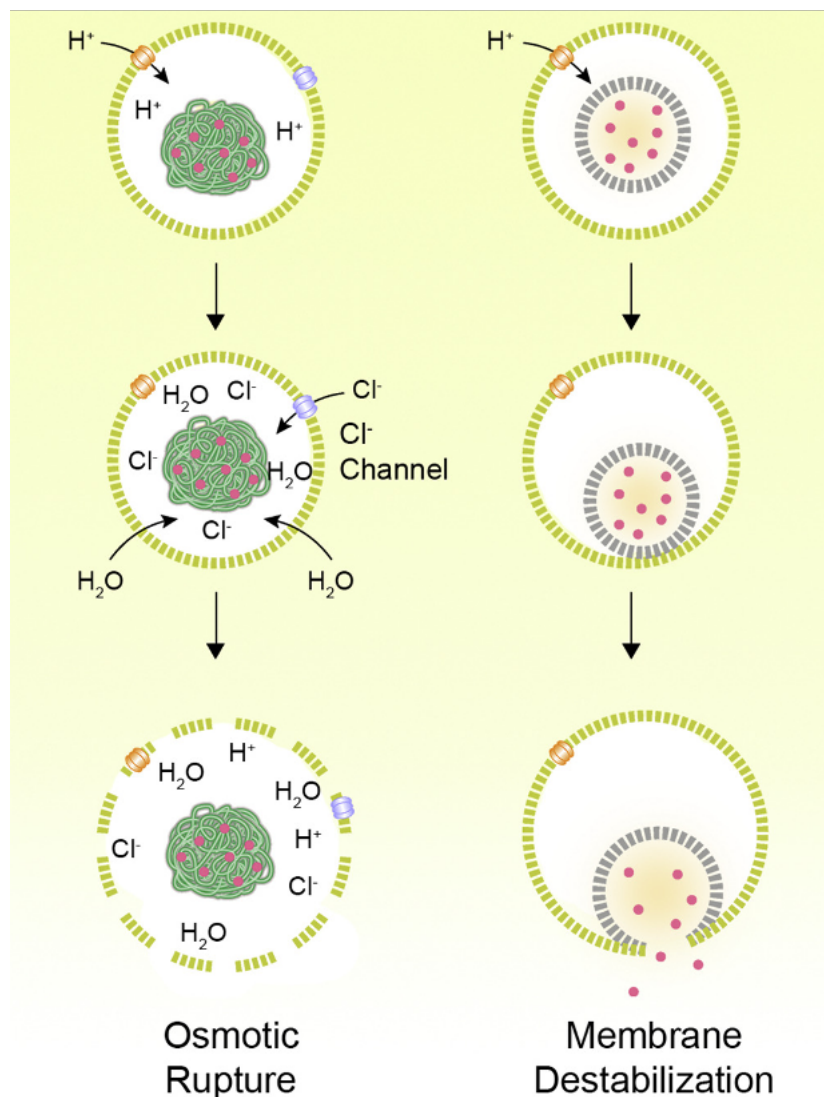


Figure 1-5. Schematic illustration of polyplex endosomal escape [38].

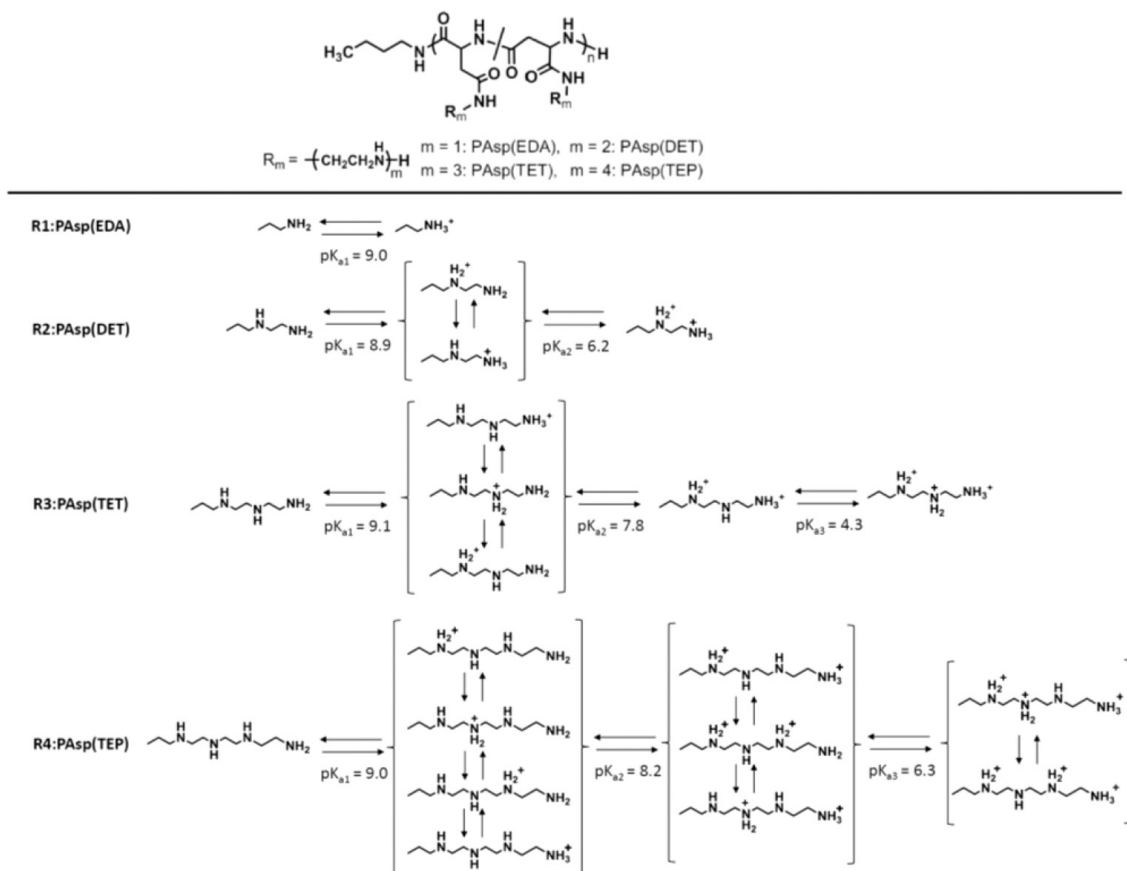


Fig. 1-6. Protonation states of polyaspartimide derivatives bearing repeated aminoethylene moieties [33].

Table 1-2. Degrees of protonation (α) and pK_a values of polyaspartimide derivatives bearing repeated aminoethylene moieties.

Polycation	α		$\Delta\alpha$	pK_{a1}	pK_{a2}	pK_{a3}
	pH 7.4	pH 5.5				
PAsp(EDA)	0.93	0.99	0.06	9.0		
PAsp(DET)	0.51	0.82	0.31	8.9	6.2	
PAsp(TET)	0.56	0.66	0.10	9.1	7.8	4.3
PAsp(TEP)	0.49	0.68	0.19	9.0	8.2	6.3

- **Biodegradability**

The biodegradability of polycations is also an important factor for safe and efficient drug delivery. After the polymer degrades, the segments are easily metabolized or removed from the body. Therefore, biodegradable polymers can achieve lower toxicity than non-degradable alternatives. PEI is one of the representative polycations for nucleic acid delivery due to its facilitation of endosomal escape and enhancement of gene expression. However, its non-degradable nature induces substantial cytotoxicity at a high molecular weight [34]. Moreover, since excessive nanoparticle stability decreases the efficiency of payload release, as aforementioned, polycation biodegradability is a desirable property that elicits efficient drug release with low cytotoxicity. To date, there have been various studies on the development of cationic polymers with biodegradable linkages, such as ester bonds, amide bonds, and disulfide bonds. These bonds can be hydrolyzed by the enzymes in the body. Additionally, it was recently reported that *N*-substituted polyaspartamide derivatives have nonenzymatic degradability with the introduction of the 2-aminoethyl group in the side chain, and the chemical structure of the side chains affects the degradability of the derivatives [35]. *N*-substituted polyaspartamide derivatives exhibit different degradability trends due to the possession of a primary amine with varying alkyl spacer lengths in the side chains (**Fig. 1-7a**). The derivative with the 2-aminoethyl moiety (PAsp(AE)) exhibited efficient degradability, followed by the derivatives with the 3-aminopropyl moiety (PAsp(AP)) and the derivatives with the 4-aminobutyl moiety (PAsp(AB)), under physiological conditions. This is because the primary amine forms a ring-like structure with the amide nitrogen in the side chains and activates the amide nitrogen. The activated nitrogen attacks and cleaves the amide in the main chain. PAsp(AP) and PAsp(AB) have relatively longer spacer lengths, which increases the difficulty of inducing the ring-like formation, resulting in lower degradation than PAsp(AE) (**Fig. 1-7b**). Due to its higher degradability, PAsp(AE) exhibited

lower cytotoxicity and higher transfection efficiency. Similarly, a polyglutamate derivative with DET moieties (PGlu(DET)) in the side chains displayed limited degradability, due to the difficulty in forming the ring-like structure, which is attributed to the presence of an additional carbon between the main chain and amide of the DET moieties. This leads to it having a higher cytotoxicity than a polyaspartamide derivative with DET moieties (PAsp(DET)) possessing nonenzymatic degradability.

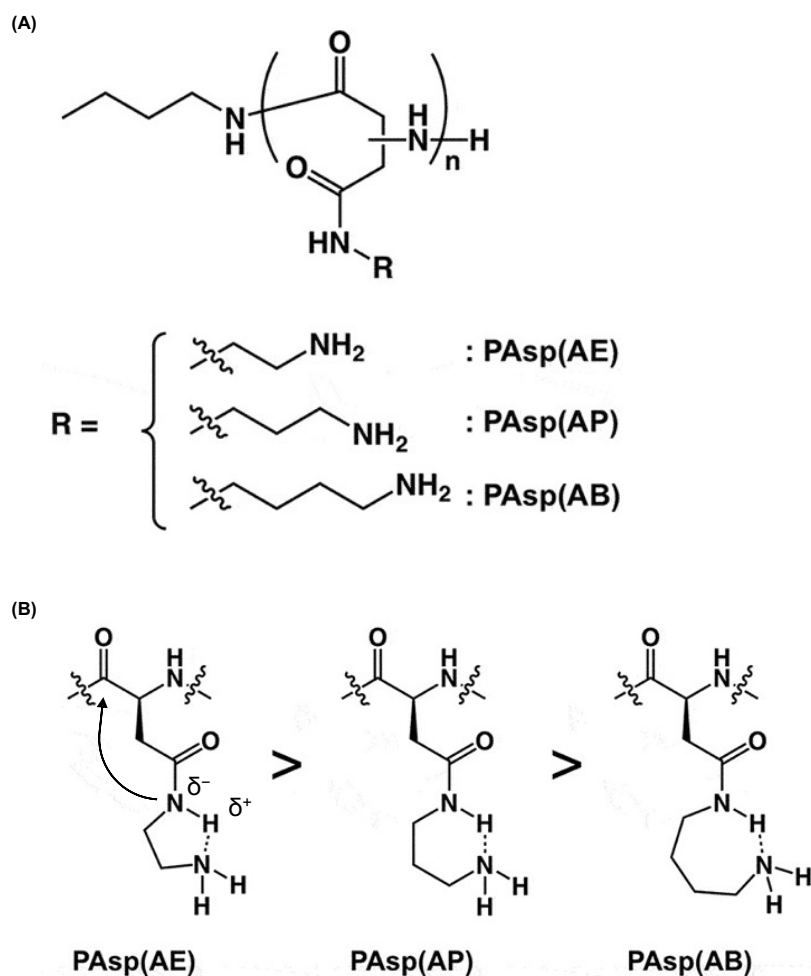


Figure 1-7. The chemical structures of *N*-substituted polyaspartamides (PAsp(R)) bearing a primary amine with various lengths of alkyl spacers (R) in the side chains. AE, 2-aminoethyl; AP, 3-aminopropyl; AB, 4-aminobutyl. (B) The degradation mechanism is the deprotonation of the amide nitrogen in the side chains and the stabilization of the ring conformation causing deprotonated amide nitrogen.

1.4. Amphiphilic polyaspartamide derivatives

In a previous report, a series of amphiphilic polyaspartamide derivatives (PAsp(DET/R)s) were developed by tailoring with DET and various hydrophobic (R) moieties in the side chains for efficient mRNA delivery (**Fig. 1-8a**) [25]. The DET moiety possesses two functional features, which are interactions with mRNA and endosomal escape. The cationic DET moiety can bind mRNA *via* electrostatic interactions, allowing the formation of a polyplex. Moreover, as abovementioned, DET moieties, which adopted a mono-protonated ($-\text{NHCH}_2\text{CH}_2\text{NH}_3^+$) state at physiologically neutral pH, were distinctively converted to a di-protonated ($-\text{NH}_2^+\text{CH}_2\text{CH}_2\text{NH}_3^+$) state at acidic pH in the endosome, leading to destabilization of the endosomal membrane, followed by efficient endosomal escape. R moieties can stabilize the polyplex formation in an aqueous milieu *via* hydrophobic interactions. In fact, although PAsp(DET) with no hydrophobic units exhibited efficient plasmid DNA delivery, it resulted in negligible siRNA delivery ability due to insufficient stability of the polyplex. Interestingly, a previous study revealed that the mRNA expression efficiencies in cultured cells were nicely correlated with the distribution coefficient ($\log D_{7.3}$) obtained in an octanol–aqueous buffer (pH 7.3), which serves as an indicator of the hydrophobicity of nanoparticle-forming PAsp(DET/R)s (**Fig. 1-8b**). In particular, the $\log D_{7.3}$ threshold for efficient mRNA delivery was observed to be approximately -2.4 . PAsp(DET/R)s with $\log D_{7.3}$ values larger than -2.4 exhibited appreciably higher mRNA expression efficiencies compared with the counterparts with $\log D_{7.3}$ values lower than -2.4 . In the comparison among PAsp(DET/R)s with larger hydrophobicity than the threshold, the transfection efficiency slightly decreased, as $\log D_{7.3}$ of the polymer increased, due to retarded detachment of mRNA caused by excess hydrophobicity. Ultimately, a polyaspartamide derivative comprising cyclohexylethyl (CHE) moieties, PAsp(DET/CHE), accomplished the highest transfection efficiency, because of the hydrophobicity resulted in the optimal polyplex stability in

the extracellular milieu and the mRNA release in the cell cytoplasm. In addition, it achieved IVT-mRNA-mediated gene editing in the brain *via* intracerebroventricular (ICV) injection into the reporter mouse model.

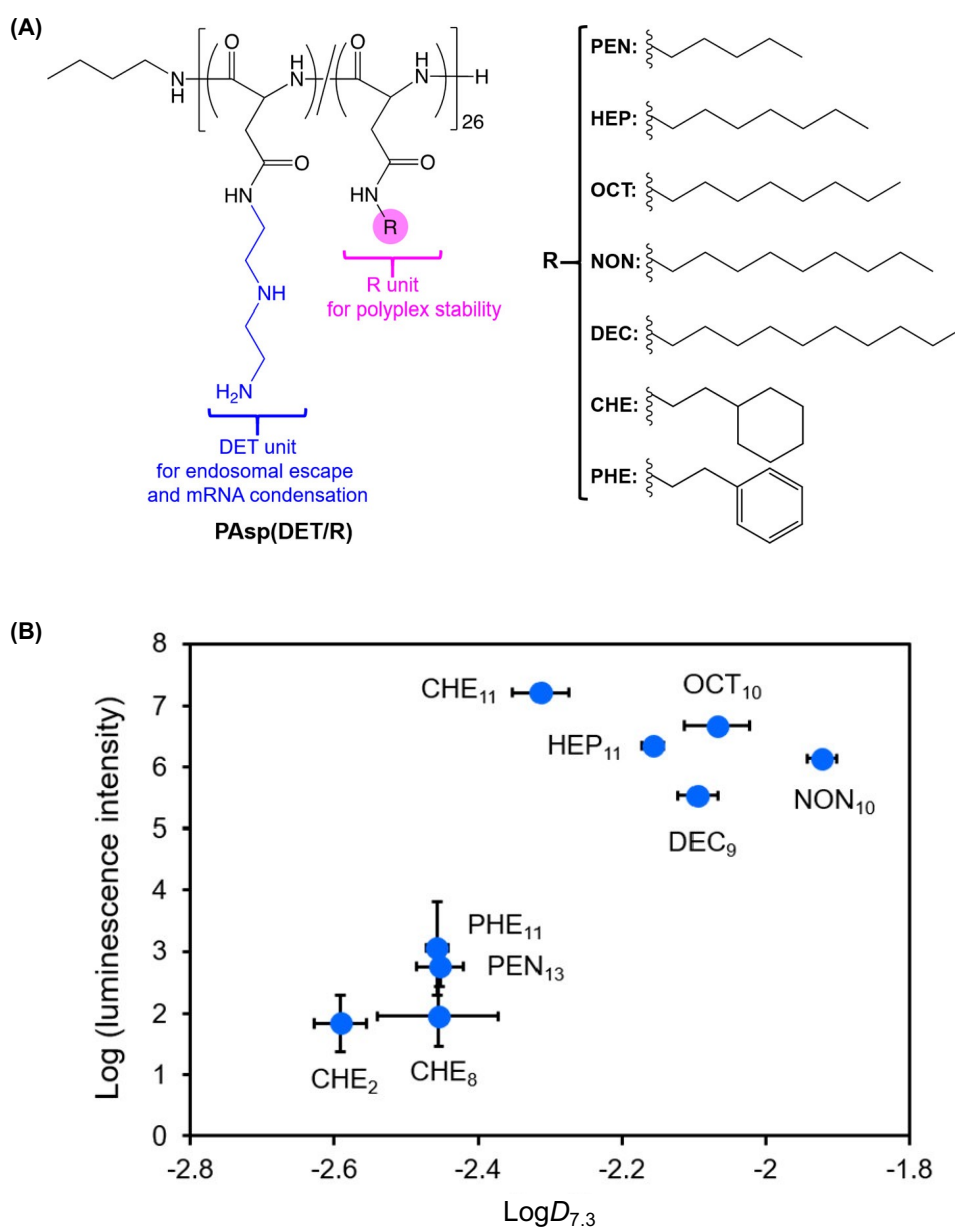


Figure 1-8. (A) Chemical structures of polyaspartamide derivatives with DET and hydrophobic moieties reported in a previous study. (B) Correlation between mRNA transfection efficiency and the hydrophobicity ($\log D_{7.3}$) of PAsp(DET/R)s.

1.5. Purpose of this study and structure of the thesis

As aforementioned, mRNA transfection efficiency can change considerably depending on the $\log D_{7.3}$ value of PAsp(DET/R), and it has been found that hydrophobicity is a crucial parameter for efficient mRNA delivery by polyplexes. Furthermore, PAsp(DET/CHE), exhibiting the highest mRNA transfection among derivatives, achieved mRNA delivery in the brain *via* local injection. However, previous results revealed the effect of the R moieties of PAsp(DET/R) carriers only for mRNA delivery. Further investigations are needed on the impact of hydrophobicity (or R moiety) for the delivery of other nucleic acid drugs. Moreover, it has not been demonstrated that PAsp(DET/R) carriers can systemically deliver mRNA and how R moieties affect the *in vivo* activities of polyplexes and their mRNA payload. In this study, the molecular structure of PAsp(DET/R), particularly the R moiety, was optimized for the delivery of other nucleic acid drugs and systemic mRNA delivery. In **Chapter 2**, application of the PAsp(DET/R) library to ASO delivery is described. The structure of ASO molecules is different from that of mRNAs. ASO molecules are chemically modified and shorter than mRNA. Considering the structures differ from those of mRNAs, the effect of the R moiety (hydrophobicity) in ASO delivery was investigated and the molecular structures of PAsp(DET/R)s were optimized. **Chapters 3 and 4** present investigations into the utilization of PAsp(DET/R) carriers for systemic mRNA delivery. In detail, a series of polyaspartamide derivatives with new R moieties were synthesized in consideration of systemic mRNA delivery, and the results are presented in **Chapter 3**. A new PAsp(DET/R) library was tested for *in vitro* transfection, and the impact of new R moieties was studied with respect to *in vitro* transfection efficiency. In **Chapter 4**, tests of a newly synthesized PAsp(DET/R) library for systemic mRNA delivery are presented. The effect of R moieties on *in vivo* activities was evaluated after

intravenous administration of mRNA-loaded polyplexes. In addition, the optimized structure of PAsp(DET/R)s for systemic mRNA delivery was investigated.

References

1. Opalinska, J. B., Gewirtz, A. M. Nucleic-acid therapeutics: basic principles and recent applications. *Nat. Rev. Drug Discov.* **1**, 503–514 (2002).
2. Kulkarni, J. A., Witzigmann, D., Thomson, S. B., Chen, S., Leavitt, B. R., Cullis, P. R., van der Meel, R. The current landscape of nucleic acid therapeutics. *Nat. Nanotechnol.* **16**, 630–643 (2021).
3. Crooke, S. T., Baker, B. F., Crooke, R. M., Liang, X. H. Antisense technology: an overview and prospectus. *Nat. Rev. Drug Discov.* **20**, 427–453 (2021).
4. Watts, J. K., Corey, D. R. Gene silencing by siRNAs and antisense oligonucleotides in the laboratory and the clinic. *J Pathol.* **226**, 365–379 (2012).
5. Juliano, R. L., Carver, K. Cellular uptake and intracellular trafficking of oligonucleotides. *Adv. Drug Deliv. Rev.* **87**, 35–45 (2015).
6. Alshaer, W., Zureigat, H., Karaki, A. A., Al-Kadash, A., Gharaibeh, L., Hatmal, M. M., Aljabali, A. A. A., Awidi, A. siRNA: Mechanism of action, challenges, and therapeutic approaches. *Eur. J. Pharmacol.* **905**, 174178.
7. Sharma, V. K., Sharma, R. K., Singh, S. K. Antisense oligonucleotides: modifications and clinical trials. *Med. Chem. Comm.* **5**, 1454–1471 (2014).
8. Roberts, T. C., Langer, R., Wood, M. J. A. Advances in oligonucleotide drug delivery. *Nat. Rev. Drug Discov.* **19**, 673–694 (2020).
9. Kowalski, P. S., Rudra, A., Miao, L., Anderson, D. G. Delivering the messenger: advances in technologies for therapeutic mRNA delivery. *Mol. Ther.* **27**, 710–728 (2019).
10. Weng, Y., Li, C., Yang, T., Hu, B., Zhang, M., Guo, S., Xiao, H., Liang, X. J., Huang, Y. The challenge and prospect of mRNA therapeutics landscape. *Biotechnol. Adv.* **40**, 107534 (2020).
11. Cabral, H., Miyata, K., Osada, K., Kataoka, K. Block copolymer micelles in nanomedicine applications. *Chem. Rev.* **118**, 6844–6892 (2018).
12. Seymour, L. W., Duncan, R., Strohal, J., Kopecek, J. Effect of molecular weight of N-(2-hydroxypropyl) methacrylamide copolymers on body distribution and rate of excretion after subcutaneous, intraperitoneal, and intravenous administration to rats. *J Biomed Mater Res.* **21**, 1341–1358 (1987).

13. Choi, H. S., Liu, W., Misra, P., Tanaka, E., Zimmer, J. P., Ipe, B. I., Bawendi, M. G., Frangioni, J. V. Renal clearance of quantum dots. *Nat. Biotechnol.* **25**, 1165–1170 (2007).
14. Jayaraman, M., Ansell, S. M., Mui, B. L., Tam, Y. K., Chen, J., Du, X., Butler, D., Eltepu, L., Matsuda, S., Narayanannair, J. K., Rajeev, K. G., Hafez, I. M., Akinc, A., Maier, M. A., Tracy, M. A., Cullis, P. R., Madden, T. D., Manoharan, M., Hope, M. J. Maximizing the potency of siRNA lipid nanoparticles for hepatic gene silencing in vivo. *Angew. Chem. Int. Ed.* **51**, 8529–8533 (2012).
15. Setten, R. L., Rossi, J. J., Han, S. P. The current state and future directions of RNAi-based therapeutics. *Nat Rev Drug Discov.* **18**, 421–446 (2019).
16. Zhang, X., Goel, V., Robbie, G. J. Pharmacokinetics of Patisiran, the first approved RNA interference therapy in patients with hereditary transthyretin-mediated amyloidosis. *J. Clin. Pharmacol.* **60**, 573–585 (2020).
17. Adams, D., Gonzalez-Duarte, A., O'Riordan, W. D., Yang, C. C., Ueda, M., Kristen, A. V., Tournev, I., Schmidt, H. H., Coelho, T., Berk, J. L., Lin, K. P., Vita G., Attarian, S., Planté-Bordeneuve, V., Mezei, M. M., Campistol, J. M., Buades, J., Brannagan, T. H. 3rd, Kim, B. J., Oh, J., Parman, Y., Sekijima, Y., Hawkins, P. N., Solomon, S. D., Polydefkis, M., Dyck, P. J., Gandhi, P. J., Goyal, S., Chen, J., Strahs, A. L., Nochur, S. V., Sweetser, M. T., Garg, P. P., Vaishnaw, A. K., Gollob, J. A., Suhr, O. B. *N. Engl. J. Med.* **379**, 11–21 (2018).
18. Solomon, S. D., Adams, D., Kristen, A., Grogan, M., González-Duarte, A., Maurer, M. S., Merlini, G., Damy, T., Slama, M. S., Brannagan, T. H. 3rd., Dispenzieri, A., Berk, J. L., Shah, A. M., Garg, P., Vaishnaw, A., Karsten, V., Chen, J., Gollob, J., Vest, J., Suhr, O. *Circulation.* **139**, 431–443 (2019).
19. Akinc, A., Querbes, W., De, S., Qin, J., Frank-Kamenetsky, M., Jayaprakash, K. N., Jayaraman, M., Rajeev, K. G., Cantley, W. L., Dorkin, J. R., Butler, J. S., Qin, L., Racie, T., Sprague, A., Fava, E., Zeigerer, A., Hope, M. J., Zerial, M., Sah, D. W., Fitzgerald, K., Tracy, M. A., Manoharan, M., Kotliansky, V., de Fougerolles, A., Maier, M. A. *Mol. Ther.* **18**, 1357–1364 (2010).
20. Hassett, K. J., Benenato, K. E., Jacquinet, E., Lee, A., Woods, A., Yuzhakov, O., Himansu, S., Deterling, J., Geilich, B. M., Ketova, T., Mihai, C., Lynn, A., McFadyen, I., Moore, M. J., Senn, J. J., Stanton, M. G., Almarsson, Ö., Ciaramella, G., Brito, L. A. Optimization of

- lipid nanoparticles for intramuscular administration of mRNA vaccines. *Mol. Ther. Nucleic Acids* **15**, 1–11 (2019).
21. Kataoka, K., Harada, A., Nagasaki, Y. Block copolymer micelles for drug delivery: design, characterization and biological significance. *Adv. Drug Deliv. Rev.* **47**, 113–131 (2001).
 22. Miyata, K., Nishiyama, N., Kataoka, K. Rational design of smart supramolecular assemblies for gene delivery: chemical challenges in the creation of artificial viruses. *Chem. Soc. Rev.* **41**, 2562–2574 (2012).
 23. Vogel, A. B., Kanevsky, I., Che, Y., Swanson, K. A., Muik, A., Vormehr, M., Kranz, L. M., Walzer, K. C., Hein, S., Güler, A., Loschko, J., Maddur, M. S., Ota-Setlik, A., Tompkins, K., Cole, J., Lui, B. G., Ziegenhals, T., Plaschke, A., Eisel, D., Dany, S. C., Fesser, S., Erbar, S., Bates, F., Schneider, D., Jesionek, B., Sängler, B., Wallisch, A. K., Feuchter, Y., Junginger, H., Krumm, S. A., Heinen, A. P., Adams-Quack, P., Schlereth, J., Schille, S., Kröner, C., Garcia, R. C. G., Hiller, T., Fischer, L., Sellers, R. S., Choudhary, S., Gonzalez, O., Vascotto, F., Gutman, M. R., Fontenot, J. A., Hall-Ursone, S., Brasky, K., Griffor, M. C., Han, S., Su, A. A. H., Lees, J. A., Nedoma, N. L., Mashalidis, E. H., Sahasrabudhe, P. V., Tan, C. Y., Pavliakova, D., Singh, G., Fontes-Garfias, C., Pride, M., Scully, I. L., Ciolino, T., Obregon, J., Gazi, M., Carrion, R. Jr., Alfson, K. J., Kalina, W. V., Kaushal, D., Shi, P. Y., Klamp, T., Rosenbaum, C., Kuhn, A. N., Türeci, Ö., Dormitzer, P. R., Jansen, K. U., Sahin, U. BNT162b vaccines protect rhesus macaques from SARS-CoV-2. *Nature* **592**, 283–289 (2021).
 24. Uchida, S., Kinoh, H., Ishii, T., Matsui, A., Tockary, T. A., Takeda, K. M., Uchida, H., Osada, K., Itaka, K., Kataoka, K. Systemic delivery of messenger RNA for the treatment of pancreatic cancer using polyplex nanomicelles with a cholesterol moiety. *Biomaterials* **82**, 221–228 (2016).
 25. Kim, H. J., Ogura, S., Otabe, T., Kamegawa, R., Sato, M., Kataoka, K., Miyata, K. Fine-tuning of hydrophobicity in amphiphilic polyaspartamide derivatives for rapid and transient expression of messenger RNA directed toward genome engineering in brain. *ACS Cent. Sci.* **5**, 1866–1875 (2019).
 26. Yu, X., Liu, S., Cheng, Q., Lee, S. M., Wei, T., Zhang, D., Farbiak, L., Johnson, L. T., Wang, X., Siegwart, D. J. Hydrophobic optimization of functional Poly(TPAE-co-suberoyl chloride) for extrahepatic mRNA delivery following intravenous administration. *Pharmaceutics* **21**, 1914 (2021).

27. Miyazaki, T., Uchida, S., Hatano, H., Miyahara, Y., Matsumoto, A., Cabral, H. Guanidine-phosphate interactions stabilize polyion complex micelles based on flexible cationomers to improve mRNA delivery. *Euro. Polym. J.* **140**, 1100282 (2020).
28. Hori, M., Cabral, H., Toh, K., Kishimura, A., Kataoka, K. Robust polyion complex vesicles (PICsomes) under physiological conditions reinforced by multiple hydrogen bond formation derived by guanidinium groups. *Biomacromolecules* **19**, 4113–4121 (2018).
29. Dirisala, A., Uchida, S., Tockary, T. A., Yoshinaga, N., Li, J., Osawa, S., Gorantla, L., Fukushima, S., Osada, K., Kataoka, K. Precise tuning of disulphide crosslinking in mRNA polyplex micelles for optimizing extracellular and intracellular nuclease tolerability. *J. Drug Target.* **27**, 670–680 (2019).
30. Min, H. S., Kim, H. J., Naito, M., Ogura, S., Toh, K., Hayashi, K., Kim, B. S., Fukushima, S., Anraku, Y., Miyata, K., Kataoka, K. Systemic brain delivery of antisense oligonucleotides across the blood–brain barrier with a glucose-coated polymeric nanocarrier. *Angew. Chem. Int. Ed.* **59**, 8173–8180 (2020).
31. Naito, M., Yoshinaga, N., Ishii, T., Matsumoto, A., Miyahara, Y., Miyata, K., Kataoka, K. Enhanced intracellular delivery of siRNA by controlling ATP-responsivity of phenylboronic acid-functionalized polyion complex micelles. *Macromol. Biosci.* **18**, 1700357 (2018).
32. Miyata, K., Oba, M., Nakanishi, M., Fukushima, S., Yamasaki, Y., Koyama, H., Nishiyama, N., Kataoka, K. Polyplexes from poly(aspartamide) bearing 1,2-diaminoethene side chains induce pH-selective, endosomal membrane destabilization with amplified transfection and negligible cytotoxicity. *J. Am. Chem. Soc.* **130**, 16287–16294 (2008).
33. Uchida, H., Itaka, K., Nomoto, T., Ishii, T., Suma, T., Ikegami, M., Miyata, K., Oba, M., Nishiyama, N., Kataoka, K. Modulated protonation of side chain aminoethylene repeats in N-substituted poly-aspartamides promotes mRNA transfection. *J. Am. Chem. Soc.* **136**, 2396–2405 (2014).
34. Jiang, H. L., Arote, R., Jere, D., Kim Y. K., Cho, M. H., Cho, C. S. Degradable polyethylenimines as gene carriers. *Mater. Sci. and Technol.* **24**, 1118–1126 (2008).
35. Natio, M., Otsu, Y., Kamegawa, R., Hayashi, K., Uchida, S., Kim, H. J., Miyata, K. Tunable non-enzymatic degradability of N-substituted polyaspartamide main chain by amine protonation and alkyl spacer length in side chains for enhanced messenger RNA transfection efficiency. *Sci. Technol. Adv. Mater.* **20** 105–115 (2019).

36. Thi, T. T. H., Suys, E. J. A., Lee, J. S., Nguyen, D. H., Park, K. D., Truong, N. P. Lipid-based nanoparticles in the clinic and clinical trials: from cancer nanomedicine to COVID-19 vaccines. *Vaccines* **9** 359 (2021).
37. Swingle, K. L., Hamilton, A. G., Mitchell, M. J. Lipid nanoparticle-mediated delivery of mRNA therapeutics and vaccines. *Trends Mol. Med.* **27** 616–617 (2021).
38. Patel, S., Kim, J., Herrera, M., Mukherjee, A., Kabanov, A. V., Sahay, G. Brief update on endocytosis of nanomedicines. *Adv. Drug Deliv. Rev.* **144**, 90–111 (2019).

Chapter 2

Polyaspartamide derivatives with varying hydrophobicity for antisense oligonucleotide delivery

2.1. Chapter introduction

Cationic amphiphilic polyaspartamide derivatives (PAsp(DET/R)s) tailored with diethylenetriamine (DET) and hydrophobic (R) moieties in the side chains were recently developed for efficient messenger RNA (mRNA) delivery (**Fig. 1-8**) [1]. As aforementioned in **Chapter 1**, the DET moiety achieves efficient endosomal escape due to its special protonation behavior at acidic pH in the endosome. Various R moieties were examined in order to optimize the polyplex stability for enhanced mRNA delivery efficiency by adjusting the hydrophobicity, which was quantified by an octanol–water (at pH 7.3) distribution coefficient, $\log D_{7.3}$. As a result, the mRNA transfection efficiency was associated with the $\log D_{7.3}$ value of the PAsp(DET/R)s [1]. The threshold in $\log D_{7.3}$ value of the PAsp(DET/R)s was determined as approximately -2.4 for efficient mRNA delivery. PAsp(DET/R)s with higher $\log D_{7.3}$ values than -2.4 exhibited efficient mRNA transfection, 1,000 times higher than those with a hydrophobicity below the threshold. Among a series of PAsp(DET/R)s, the cyclohexylamine (CHE) moiety-installed polyaspartamide derivative (PAsp(DET/CHE)) exhibited the highest mRNA transfection efficiency in the cultured cells, and achieved efficient mRNA delivery in the brain *via* intracerebroventricular (ICV) and intrathecal administration [1].

In **Chapter 2**, the applicability of PAsp(DET/R) carriers for the delivery of different types of nucleic acid drugs, *i.e.*, chemically modified antisense oligonucleotides (ASOs), is investigated. Specifically, as ASO has a different structure and length than mRNA, the possibility of forming an ASO-loaded polyplex and the effect of PAsp(DET/R)s on the ASO transfection efficiency has not yet been determined. Therefore, this chapter focusses on the formation of polyplexes encapsulating ASO molecules, and associating the PAsp(DET/R) $\log D_{7.3}$ value with the ASO transfection efficiency in the cultured cells. Furthermore, PAsp(DET/R)s were also

examined for *in vivo* ASO delivery *via* various local administrations, *i.e.*, ICV and intratracheal (IT) injection to the brain and lungs, respectively.

2.2. Materials and methods

2.2.1. Materials

A series of PAsp(DET/R)s with the degree of polymerization (DP) of 21 was helpfully provided by Dr. Hyun Jin Kim (Inha University) (**Fig. 1-8a**). In brief, poly(β -benzyl-L-aspartate) (PBLA), as a parent polymer, was prepared by ring-opening polymerization of *N*-carboxy anhydride of β -benzyl-L-aspartate (BLA-NCA) with the initiation of *n*-butylamine [1,4,5]. Then, PAsp(DET/R)s were synthesized by the aminolysis reaction of PBLA with the mixture of DET and amines having hydrophobic moieties [1,4,5]. GL3 luciferase-targeted ASO (GL3-ASO) and metastasis-associated lung adenocarcinoma transcript 1 (Malat1) lncRNA targeted ASO (Malat1-ASO) were synthesized by Gene Design, Inc. (Osaka, Japan). All ASOs were synthesized with phosphorothioate backbone chemistry. The sequences of ASOs are summarized in **Table 2-1**. Fluorescently labeled ASOs were prepared by the conjugation of Alexa Fluor 647 dye to the 3'-end of the ASO. HEPES buffer (1 M, pH 7.3) was purchased from Amresco, Inc. (Solon, OH, USA). Ultrapure agarose was purchased from Thermo Fisher Scientific (Waltham, MA, USA). Human cervical cancer cells expressing GL3 luciferase (HeLa-Luc) were purchased from PerkinElmer Inc. (Waltham, MA, USA). Human pancreatic and mouse breast cancer cells both expressing GL3 luciferase (Panc1-Luc and 4T1-Luc) were purchased from the American Type Culture Collection (Manassas, VA, USA). Fetal bovine serum (FBS) was purchased from Biosera (Nuaille, France). Dulbecco's modified Eagle's medium (DMEM), Roswell Park Memorial Institute Medium (RPMI-1640), Dulbecco's phosphate-buffered saline (D-PBS(-)), and Dextran sulfate sodium (~500,000 Da, DSS) were purchased from FUJIFILM Wako Pure Chemical Industries, Ltd. (Osaka, Japan). DMEM with 10% FBS was utilized as a culture medium for HeLa- and Panc1-Luc cells. RPMI with 10% FBS was utilized as a culture medium for 4T1-Luc cells. Trypsin-ethylenediaminetetraacetic acid (trypsin-EDTA) was purchased from Sigma-

Aldrich Co. (St. Louis, MO, USA). Passive Lysis 5× Buffer was purchased from Promega (Madison, WI, USA) and diluted to 1× (passive lysis buffer) for use in the experiment. All primers for a qRT-PCR assay were purchased from Hokkaido System Science Co., Ltd. (Hokkaido, Japan). RNeasy Mini Kit was purchased from Qiagen (Hilden, Germany). KOD SYBR qPCR Mix (with ROX) was purchased from Toyobo (Osaka, Japan). BALB/c white mice (6–8-week-old females) were purchased from Charles River Laboratories Japan, Inc. (Yokoyama, Japan). All animal experiments were performed according to the Guidelines for the Care and Use of Laboratory Animals at The University of Tokyo.

Table 2-1. The sequence of GL3- and Malat1-ASO.

ASO	Sequence*
GL3-ASO [6]	5'-TCGAagtactcagcgtaaGTT-3'
Malat1-ASO [7]	5'-GGGtcagctgccaatgcTAG-3'

*Uppercase and lowercase letters represent locked nucleic acid (LNA) (C denotes LNA methylcytosine) and DNA, respectively.

2.2.2. Formation and characterization of antisense oligonucleotide (ASO)-loaded polyplexes

PAsp(DET/R) solutions (in 10 mM HEPES buffer, pH 7.3) were gently mixed with GL3-ASO solutions (50 μM in 10 mM HEPES buffer, pH 7.3) to prepare polyplex samples (final ASO concentration: 10 μM) at various molar ratios of amines in the DET unit to phosphorothioates in ASO (N/P ratio). To confirm the association of ASO with PAsp(DET/R)s, an agarose gel electrophoresis assay was performed. Various 10 μL polyplex samples (10 μM ASO in 10 mM HEPES buffer, pH 7.3) were prepared at N/P ratios of 0, 1, 2, 3, 4, and 5. Glycerol (15 vol.%, 5 μL) was added to the mixed solutions. Then, 10 μL of the mixtures were electrophoresed on an agarose gel (2 wt.% of agarose gel, 1 × TAE buffer, 135 V, 10 min). After

the electrophoresis, ASO molecules on the gel were stained with SYBR[®] Green II for 30 min and visualized using a GelDoc Go Imaging System (Bio-Rad, Hercules, CA). The hydrodynamic diameter (cumulant size) and polydispersity index (PDI) of the polyplexes were determined by dynamic light scattering using a Zetasizer (Malvern Instruments, Worcestershire, UK) equipped with a He–Ne Laser ($\lambda = 633$ nm) at a detection angle of 173° . The cumulant size and PDI were obtained by analysis of the decay rate in the photon correlation function using the method of cumulants. The ζ -potential of the polyplexes was calculated by the electrophoretic mobility measured in a Zetasizer using the Smoluchowski equation. The cumulant size, PDI, and ζ -potential of polyplexes were measured at 25°C .

2.2.3. Evaluation of ASO transfection efficiency in cultured luciferase-expressing cells

HeLa-Luc and Panc1-Luc cells (5.0×10^3 cells/well in $100\ \mu\text{L}$ medium) were seeded into a 96-well plate and incubated for 24 h. Polyplex samples ($5\ \mu\text{M}$ ASO, N/P = 5) prepared from GL3-ASO and naked GL3-ASO were added to each well ($500\ \text{nM}$ ASO), after changing to a fresh medium. Naked scrambled-ASO and polyplex samples encapsulating scrambled-ASO, as the control, were also added in the same manner. After incubation for 24 h, the medium was removed and a passive lysis buffer ($50\ \mu\text{L}$) was added to each well. The photoluminescence intensity of cell lysates was measured with a luminescence microplate reader (Mithras LB 940, Berthold Technologies, Bad Wildbad, Germany) by using a Luciferase Assay System (Promega). The luminescence intensity obtained from the each well was normalized by that obtained from non-treated controls.

2.2.4. Cell viability

HeLa-Luc cells (5.0×10^3 cells/well in 100 μ L medium) were seeded into a 96-well plate and incubated for 24 h. Polyplex samples (5 μ M ASO, N/P = 5) were prepared from GL3-ASO. The samples were then added to each well (500 nM ASO), after having changed to a fresh medium. After incubation for 24 h, 10 μ L of Cell Counting Kit-8 (CCK-8, Dojindo, Kumamoto, Japan) solution was added to each well. After an additional 2 h incubation, the absorbance of each well was measured at 450 nm by using a microplate reader (Spark 20M, Tecan Group Ltd., Männedorf, Switzerland). Cell viability was calculated as a percentage value relative to the absorbance level of non-treated wells (normalized to 100 %).

2.2.5. Evaluation of cellular uptake efficiency

HeLa-Luc cells (1.0×10^5 cells/well in 1 mL medium) were seeded into a 96-well plate and incubated for 24 h. Polyplex samples (5 μ M ASO, N/P = 5) prepared from Alexa647 labeled scrambled-ASO (Alexa647-ASO) and naked Alexa647-ASO were added to each well (500 nM ASO/well) and incubated for 4 h. The cells were washed by PBS twice, followed by trypsin-EDTA treatment. The cells were then suspended in PBS and measured using flow cytometry (BD LSR II, BD Biosciences, San Jose, CA, USA), equipped with FACSDiva software (BD Biosciences).

2.2.6. Polyplex stability against the polyion exchange reaction

Polyplex samples (10 μ M ASO, N/P = 5) encapsulating Alexa647-ASO were prepared, after which 5 μ L of the polyplex solutions were mixed with 5 μ L of the DDS solutions (in 10 mM HEPES buffer, pH 7.3) corresponding to a molar ratio of 6 relative to the sulfates in the dextran unit to the phosphorothioates in ASO (S/P ratio = 6), and then the mixed solutions were incubated

at 37 °C for 1 h. Subsequently, 5 µL of a 15 vol.% glycerol solution was added to the DSS-treated sample solutions, after which 10 µL of the mixtures were electrophoresed on an agarose gel (2 wt.% of agarose gel, 1 × TAE buffer, 135 V, 10 min). After electrophoresis, the Alexa647-ASO was visualized using a GelDoc Go Imaging System (Bio-Rad, Hercules, CA).

2.2.7. *In vitro* gene silencing efficiency of PAsp(DET/R)s by using Malat1-ASO.

4T1-Luc cells (5.0×10^4 cells/well in 1 mL medium) were seeded into a 12-well plate and incubated for 24 h. Polyplex samples (N/P = 5) containing Malat1-ASO were prepared at ASO concentrations of 20, 40, and 100 nM. After 2 days, the cells were washed by PBS and then lysed in RLT buffer with a small amount of β-mercaptoethanol. RNAs were extracted from the cell lysates by using the RNeasy Mini Kit, and then 500 ng of RNAs was reverse transcribed to synthesize a complementary DNA (cDNA). The prepared cDNA (equivalent to 50 ng of RNA), the forward and reverse primers, and KOD SYBR qPCR Mix (with ROX) were mixed. The qRT-PCR of the mixed solutions was performed by using an ABI 7500 Fast Real-time PCR System (Applied Biosystems, Foster City, CA, USA), according to the manufacturer's protocol. The quantification of Malat1 lncRNA in the samples was calculated by using GAPDH mRNA as an endogenous housekeeping gene. The primer sequences for Malat1 and GAPDH are summarized in **Table 2-2**.

Table 2-2. The primer sequences for Malat1 and GAPDH

Primer	Sequence
Malat1 forward primer	5'-GAGCTCGCCAGGTTTACAGT-3'
Malat1 reverse primer	5'-AACTACCAGCAATTCCGCCA-3'
GAPDH forward primer	5'-TGTGTCCGTCGTGGATCTGA-3'
GAPDH reverse primer	5'-TTGCTGTTGAAGTCGCAGGAG-3'

2.2.8. Animal experiments

PAsp(DET/CHE) was further investigated with respect to *in vivo* gene silencing efficiency by delivering Malat1-ASO *via* ICV and IT administration to the brain and lungs, respectively. For ASO delivery to the brain, a polyplex sample (N/P = 5, 10 μ L, ASO 1 μ g in 10 mM HEPES, pH 7.3) formed by PAsp(DET/CHE) was prepared, and then injected into the 3rd ventricle in the brain of the BALB/c white mouse. After 2 days, the brain tissue parts with a width of 2 mm around the injection site were excised. For ASO delivery to the lungs, a polyplex sample (N/P = 5, 50 μ L, ASO 5 μ M in 10 mM HEPES, pH 7.3) formed by PAsp(DET/CHE) was intratracheally injected into the BALB/c white mouse by using a micro-sprayer aerosolizer (KN-34700-1; Natsume Seisakusho Co., Ltd., Tokyo, Japan). After 2 days, the lung tissue parts were excised. PBS and naked Malat1-ASO were also intracerebroventricularly and intratracheally injected as the controls. Each tissue was washed by PBS, and immersed in 1 mL of RNAlater RNA Stabilization Reagent (Qiagen) overnight. Total RNAs were extracted using an RNeasy Mini kit, and then 1 μ g of RNAs was reverse transcribed to synthesize a complementary DNA (cDNA). The prepared cDNA (equivalent to 50 ng of RNA), the forward and reverse primers and FastStart Universal SYBR Green Master (ROX) were mixed. Then qRT-PCR was performed by using an ABI 7500 Fast Real-time PCR System (Applied Biosystems, Foster City, CA, USA), according to the manufacturer's protocol. The quantification of Malat1 lncRNA was calculated in the manner mentioned in **Chapter 2.2.7**.

2.3. Results and Discussion

2.3.1. Formation and characterization of antisense oligonucleotide (ASO)-loaded polyplexes

Polyplex samples were prepared by the mixing of PAsp(DET/R) solutions with GL3-ASO solutions in a 10 mM HEPES buffer (pH 7.3) at N/P ratios of 0, 1, 2, 3, 4, and 5. For simplification, the polyplex samples are denoted R_N -polyplexes, where R and N indicate hydrophobic moiety and its introduction number in the side chains of PAsp(DET/R), respectively. In the case of PAsp(DET), the polyplex is termed a DET-polyplex. The ASO capsulation into the polyplex was determined by agarose gel electrophoresis (**Fig. 2-1**). Whereas free ASO bands were observed at N/P ratios of 0 and 1 in all electrophoresed gels, free ASO bands disappeared at $N/P \geq 2$. This indicates that all ASO molecules were associated with PAsp(DET/R)s at $N/P \geq 2$. This result is convincing due to the formation of charge neutrality between PAsp(DET/R)s and ASO at the N/P ratio of 2, considering that the protonation of DET moieties is 50 % [5,8]. Next, the characteristics, *i.e.*, D_H , PDI, ζ -potential, of polyplex samples prepared at an N/P ratio of 5 were measured with a Zetasizer (**Table. 2-3**). Regardless of varying $\log D_{7.3}$ values, all polyplexes exhibited similar values of D_H around 150 nm, and a ζ -potential around 30 mV, with a relatively narrow PDI lower than 0.2. Ultimately, the results demonstrated that ASO-loaded polyplexes were successfully formed by the mixing of PAsp(DET/R)s with GL3-ASO molecules in an aqueous buffer.

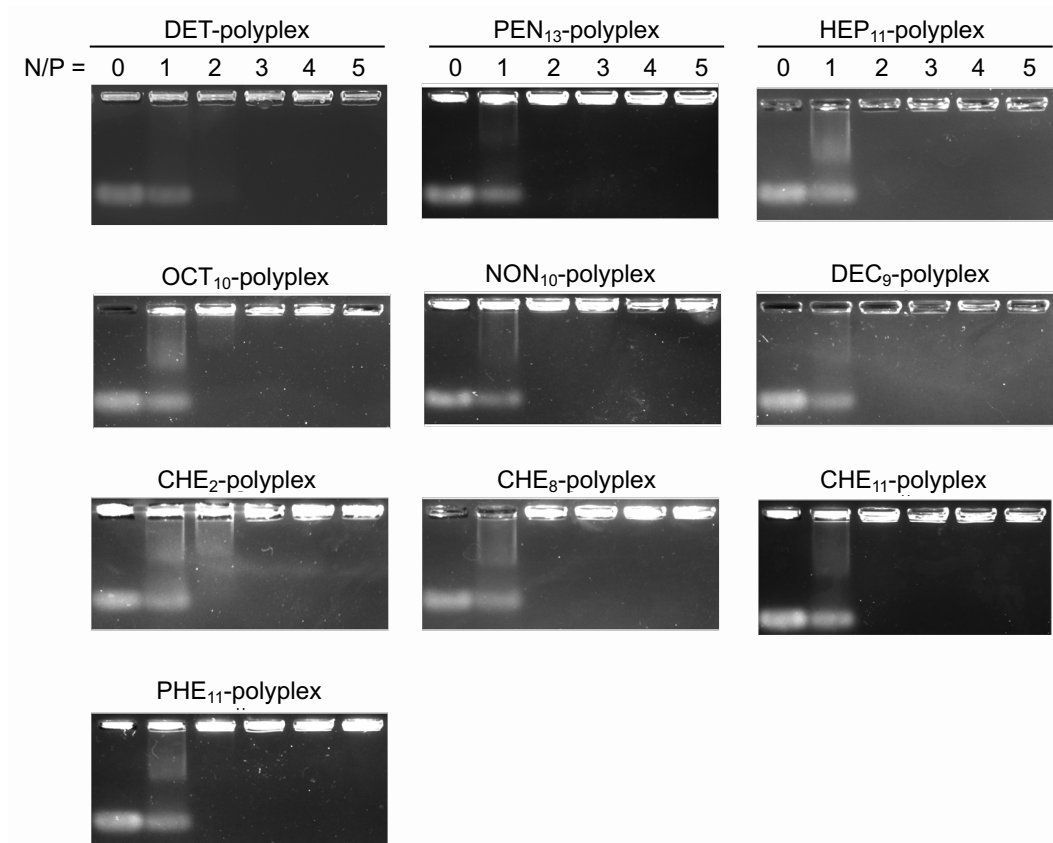


Fig. 2-1. Agarose gel electrophoresis of polyplexes prepared by mixing of PAsp(DET/R)s and GL3-ASO at various N/P ratios. The ASO on the gel was stained with SYBR[®] Green II for 30 min.

Table 2-3. Compositions and $\log D_{7.3}$ values of PAsp(DET/R)s, and characteristics of polyplexes at N/P = 5 (mean \pm SD, $n = 3$).

R moiety	Introduction number of R moiety	Log $D_{7.3}$ of the polymer	Characteristics of polyplexes (N/P = 5)		
			D_H (nm)	PDI	ζ -potential (mV)
DET	—	—	143 \pm 7	0.10 \pm 0.01	27.2 \pm 0.6
PEN	13	-2.45 \pm 0.03	150 \pm 5	0.13 \pm 0.01	43.3 \pm 3.0
HEP	11	-2.15 \pm 0.02	149 \pm 1	0.11 \pm 0.01	20.7 \pm 6.3
OCT	10	-2.06 \pm 0.05	155 \pm 5	0.14 \pm 0.01	40.0 \pm 1.7
NON	10	-1.92 \pm 0.02	151 \pm 4	0.13 \pm 0.02	33.5 \pm 1.7
DEC	9	-2.09 \pm 0.02	154 \pm 6	0.15 \pm 0.00	32.2 \pm 0.7
CHE	2	-2.59 \pm 0.03	153 \pm 5	0.16 \pm 0.00	27.4 \pm 4.1
	8	-2.45 \pm 0.08	153 \pm 5	0.15 \pm 0.01	41.9 \pm 1.1
	11	-2.31 \pm 0.04	158 \pm 10	0.15 \pm 0.03	38.4 \pm 7.1
PHE	11	-2.45 \pm 0.01	154 \pm 3	0.15 \pm 0.02	39.5 \pm 2.8

^a Values were determined as a relative molar ratio to BLA unit in PBLA.

^b Values were determined from ¹H-NMR spectra.

^c Values are expressed as mean \pm SD ($n = 3$).

2.3.2. ASO transfection efficiency in cultured tumor cells

The ASO transfection efficiencies of the polyplexes were evaluated by using a luciferase assay. The polyplex samples containing GL3-ASO were transfected into the cultured HeLa-Luc and Panc1-Luc cells, and the luminescence intensities of the cell lysates were measured with a luminescence plate reader after a 24-hour incubation. The ASO transfection efficiency was determined by the decrease in luminescence intensity. The transfection efficiencies of scrambled-ASO-loaded polyplexes, as negative controls, were also measured (**Fig. 2-2a, b**). The luminescence intensity profiles obtained from HeLa-Luc and Panc1-Luc cells were fairly similar. The polyplex samples containing scrambled-ASO exhibited similar intensities to non-treated controls, which indicates that PAsp(DET/R)s have no effect on the inhibition of gene expression. On the other hand, in the case of GL3-ASO transfection, naked ASO and PAsp(DET) showed no

luminescence reduction. This result indicates that hydrophobic R moieties are essential for efficient ASO transfection. However, polyplexes displayed different luminescence intensities according to the R moieties. In a comparison among the polyplexes formed by polyaspartamide derivatives with linear alkyl chains as the R moieties, HEP₁₁-, OCT₁₀-, NON₁₀-, and DEC₉-polyplexes showed noticeably lower luminescence intensities than PEN₁₃-polyplexes. This indicates that the alkyl side chains, as the R moieties, with more than 7 carbons are preferred for the effective ASO transfection into cultured cancer cells. On the other hand, in the case of R moieties with a ring structure, CHE₁₁-polyplex showed lower luminescence intensity than PHE₁₁-polyplex, despite having the same eight carbons in the R moieties. The introduction rate of the CHE moieties also affected the luminescence intensities. Whereas the CHE₁₁-polyplex displayed lower luminescence intensities, polyplexes formed by PAsp(DET/CHE) with relatively lower introduction rates of the CHE moieties, *i.e.*, CHE₂- and CHE₈-polyplexes, exhibited higher luminescence intensities, comparable to those of the non-treated controls. The chemical structure and introduction rates of the R moiety affect the ASO delivery efficiency. Among all the R_N-polyplexes, the NON₁₀- and CHE₁₁-polyplexes showed the lowest luminescence intensities in both cells. Additionally, the cytotoxicity of the polyplexes is considered to be negligible, due to the maintained luminescence intensities after scrambled-ASO-loaded polyplex treatment. Indeed, the result of the CCK-8 assay indicated that all polyplex samples showed negligible impact on cell viability (**Fig. 2-3**).

To provide an overall interpretation, the effect of the hydrophobicity of the PAsp(DET/R)s on ASO transfection efficiency was investigated. The ratio of luminescence intensities obtained from the cells transfected with GL3-ASO and scrambled-ASO (GL3/scramble) were plotted against $\log D_{7.3}$ of the PAsp(DET/R)s (**Fig. 2-4**). A threshold for efficient ASO transfection was noticeably observed for $\log D_{7.3}$ values around -2.4 .

PAsp(DET/R)s with higher $\log D_{7.3}$ values than -2.4 exhibited appreciably reduced luminescence intensities. On the other hand, PAsp(DET/R)s with lower $\log D_{7.3}$ values than -2.4 showed almost no decrease in luminescence intensities. This indicates that polyaspartamide derivatives with hydrophobicity above a certain level ($\log D_{7.3}$ of -2.4) enables the effective ASO delivery into the cultured cells. Interestingly, the threshold value of $\log D_{7.3}$ for efficient ASO transfection is closely similar to that for efficient mRNA transfection [1].

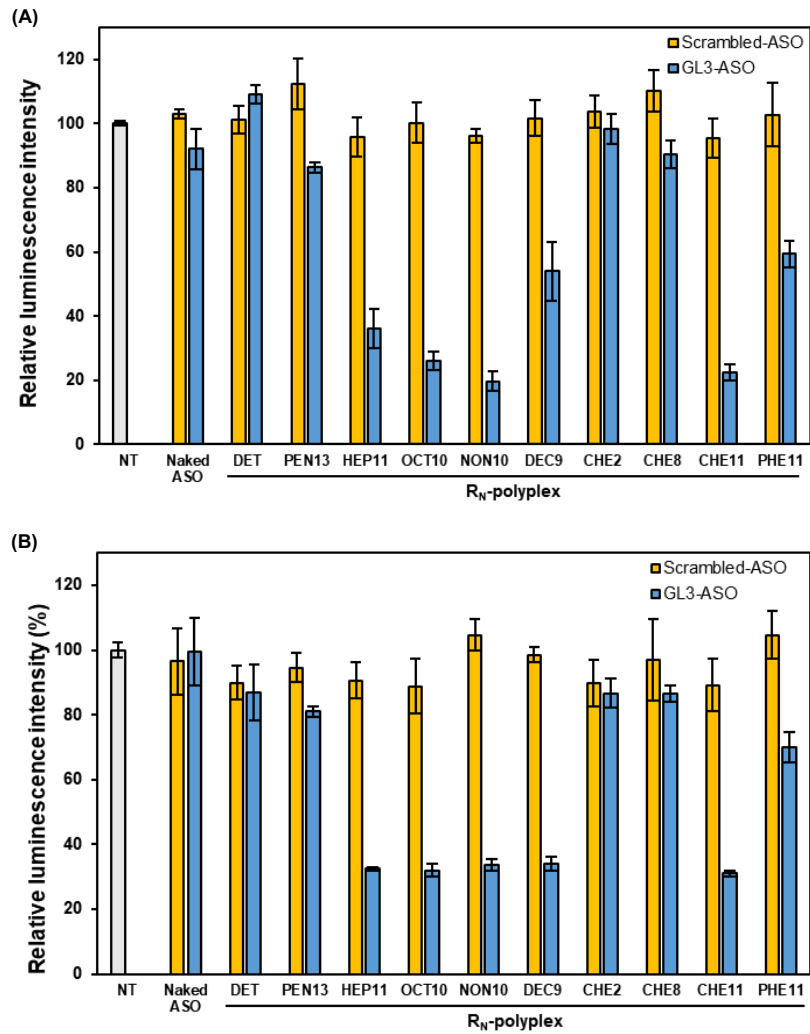


Fig. 2-2. Luminescence intensities of luciferase-expressing cancer cells, HeLa-Luc (A) and Panc1-Luc (B) cells, transfected with scrambled- and GL3-ASO (500 nM) for 24 h. The luminescence intensities were normalized to that obtained from non-treated (NT) cells. (mean \pm SD, $n = 4$)

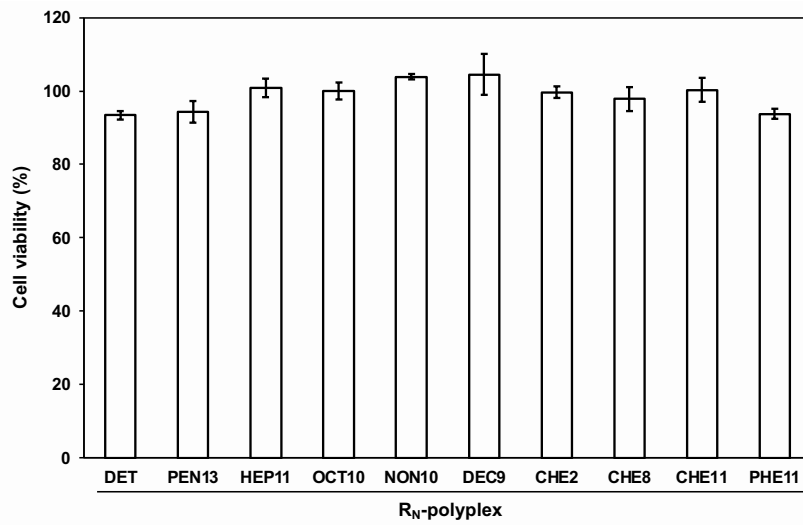


Fig. 2-3. Cell viability of HeLa-Luc cells transfected with polyplexes containing GL3-ASO for 24 h. (mean \pm SD, $n = 4$)

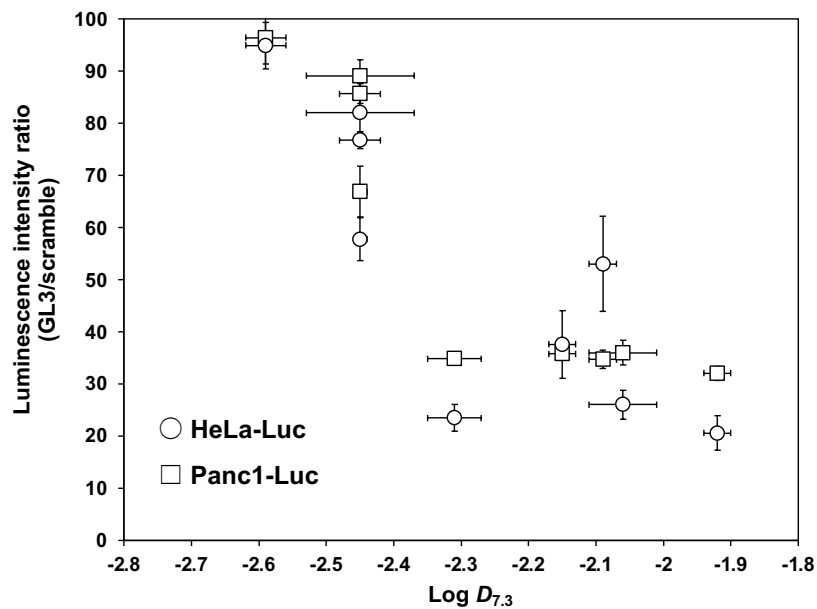


Fig. 2-4. Luminescence intensity ratio vs. the log $D_{7.3}$ value of the PAsp(DET/R)s. The luminescence intensity ratio was calculated from luminescence intensities obtained from GL3-ASO-treated cells by dividing by those from scrambled-ASO-treated cells.

2.3.3. Cellular uptake and polyplex stability

In order to further understand the mechanism underlying the varying ASO transfection efficiency of PAsp(DET/R)s, the cellular uptake efficiency was evaluated by using Alexa647-ASO. Naked Alexa647-ASO and polyplex samples containing Alexa647-ASO were transfected into HeLa-Luc cells, and then incubated for 4 h. The cellular uptake efficiency was measured using the fluorescence intensity derived from Alexa-647 in the cells by flow cytometric analysis (**Fig. 2-5**). In the linear alkyl group as the R moiety of PAsp(DET/R)s, polyplexes having more than five carbons in the alkyl chain, *i.e.*, HEP₁₁-, OCT₁₀-, NON₁₀-, and DEC₉-polyplexes, showed higher mean fluorescence intensities obtained from Alexa647-ASO than those having no or shorter alkyl chains, *i.e.*, the DET-, PEN₁₃-polyplexes. In another group possessing ring structures, the mean fluorescence intensity from CHE₁₁-polyplexes was higher than that from the PHE₁₁-polyplex. In addition, CHE₁₁-polyplexes exhibited a higher mean fluorescence intensity than those with lower introduction rates of CHE moieties, CHE₂- and CHE₈-polyplexes. The obtained profile of cellular uptake is consistent with that of the ASO transfection efficiency, suggesting that the efficient ASO delivery was attributed to the higher cellular uptake of polyplexes encapsulating ASO. Considering the consistency of the two profiles, the cellular uptake efficiency was plotted relative to the $\log D_{7.3}$ value of PAsp(DET/R)s (**Fig. 2-6**). In the correlation, a $\log D_{7.3}$ threshold for efficient cellular uptake was observed at -2.4 . The polyplexes with larger $\log D_{7.3}$ values than -2.4 showed higher cellular uptake efficiencies. This value of the $\log D_{7.3}$ threshold for higher cellular uptake is the same as that for efficient ASO transfection efficiency.

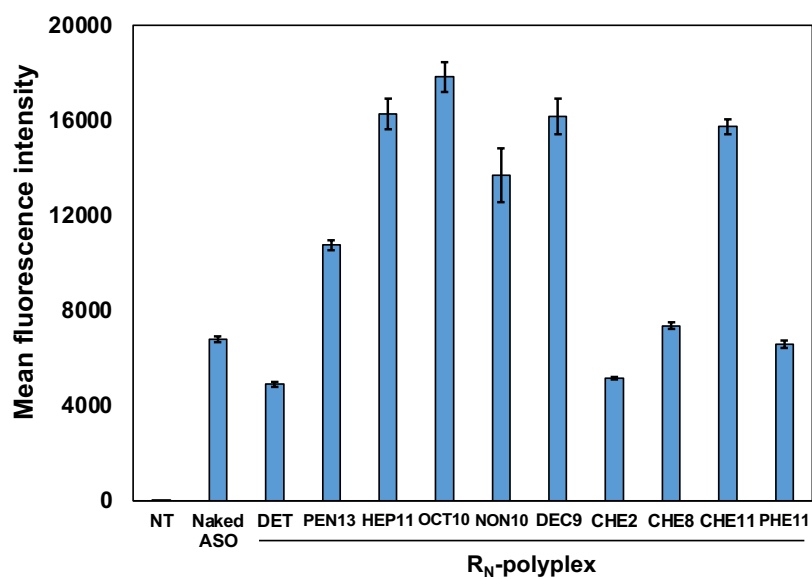


Fig. 2-5. Cellular uptake efficiencies of polyplexes containing Alexa647-ASO in cultured HeLa-Luc cells after incubation for 4 h. (mean \pm SD, $n = 3$)

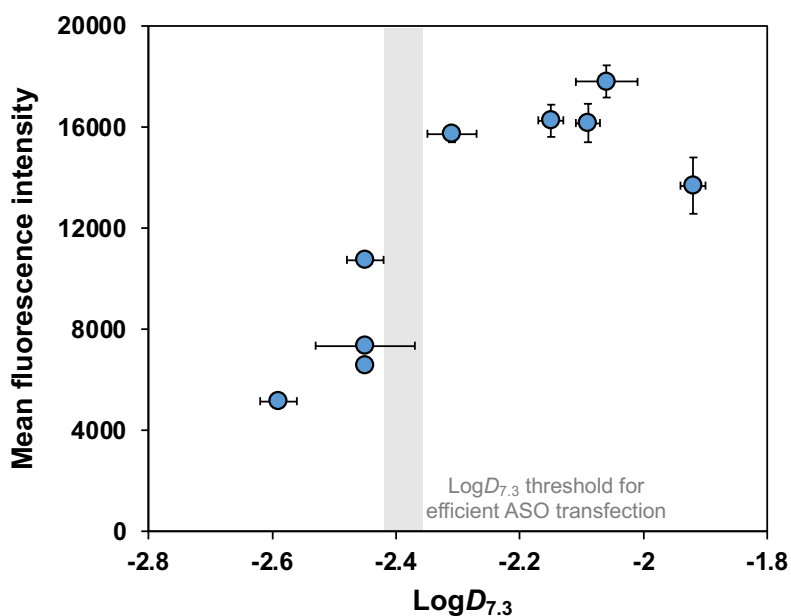


Fig. 2-6. Correlation between cellular uptake efficiency of polyplexes and the $\log D_{7.3}$ value of the PAsp(DET/R)s.

Considering the polyplex with lower hydrophobicity showed limited cellular uptake efficiencies, these might possess lower stability in the cell culture medium. Therefore, the stability of polyplexes was evaluated against the polyion exchange reaction. The polyion exchange reaction is one of the main reasons that polyplexes formed with nucleic acid are dissociated in the extracellular milieu [9,10]. Various anionic molecules including glycosaminoglycans can destabilize a polyplex *via* the polyion exchange reaction. In this experiment, polyionic dextran sulfates were added into the Alexa-ASO-loaded polyplex solution (S/P = 6) at 37 °C for 1 h, followed by agarose gel electrophoresis to measure the amount of dissociated ASO (or polyplex stability) (**Fig. 2-7**). Although released ASO bands from all samples were clearly observed, the fluorescence intensities from the ASO bands were different. DET-, CHE₂-, and CHE₈-polyplexes showed strong fluorescence intensities of released ASO bands. In contrast, OCT₁₀-, NON₁₀-, DEC₉-, and CHE₁₁-polyplexes displayed lower fluorescence intensities and PEN₁₃-, HEP₁₁-, and PHE₁₁-polyplexes exhibited intermediate free-ASO-band intensities. In the correlation between the amount of released ASO (or polyplex stability) and the hydrophobicity of PAsp(DET/R)s, R_N-polyplexes with $\log D_{7.3} > -2.4$ showed higher polyplex stability (**Fig. 2-8**). These results indicate that the higher hydrophobicity of PAsp(DET/R)s induced effective polyplex stability, leading to higher cellular uptake and ASO transfection.

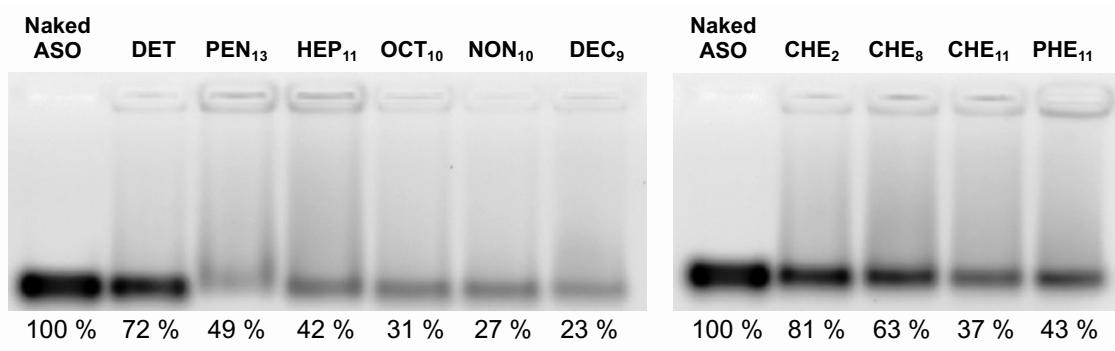


Fig. 2-7. Agarose gel electrophoresis of polyplexes containing Alexa647-ASO. The values under the gels indicate the fluorescence intensity from the released ASO of each polyplex, normalized by that of naked ASO.

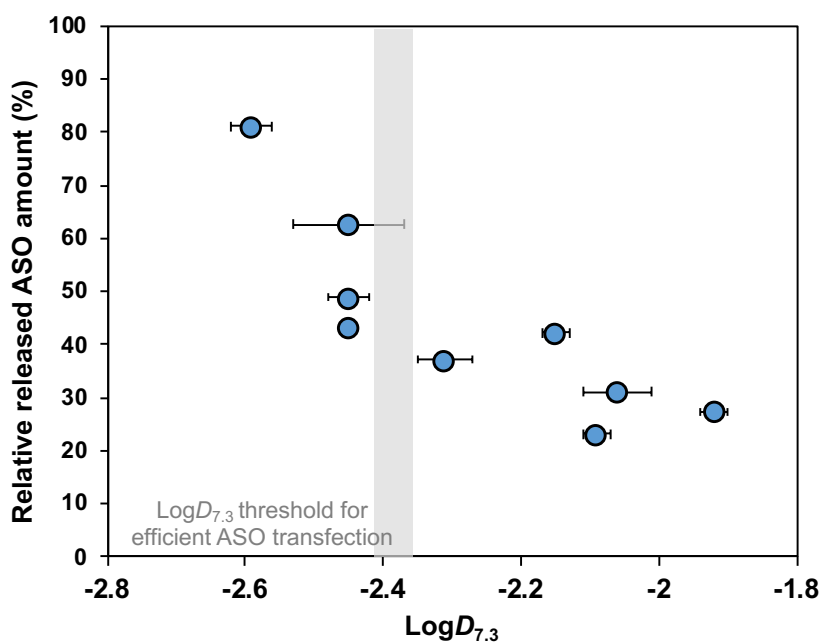


Fig. 2-8. Correlation between relative amount of released ASO from the polyplex after the polyion exchange reaction and the $\log D_{7.3}$ value of the PAsp(DET/R)s.

2.3.4. *In vitro* gene silencing efficiency of polyplexes by using Malat1-ASO

Before *in vivo* studies, *in vitro* gene silencing efficiency was examined by using Malat1-ASO. Among the R_N-polyplexes, PEN₁₃-, NON₁₀-, and CHE₁₁-polyplexes were selected to compare the gene silencing efficiencies, as they showed varying transfection efficiencies in the prior experiment using GL3-ASO. Naked Malat1-ASO and polyplexes encapsulating Malat1-ASO were transfected in 4T1-Luc cells at various ASO concentrations, *i.e.*, 20, 40, 100 nM. *In vitro* gene silencing efficiencies were measured two days after transfection by using the qRT-PCR assay (**Fig. 2-9**). As a result, significantly lower Malat1 lncRNA was observed in the cultured cells treated with polyplexes compared to the non-treated control. Although the NON₁₀-polyplex (transfection ASO concentration: 40 nM) showed slightly higher Malat1 lncRNA than the other samples, there was no significant difference. In addition, NON₁₀-polyplex at a lower ASO concentration (20 nM) lowered the amount of Malat1 lncRNA. According to these results, all R_N-polyplexes containing Malat1-ASO exhibited efficient gene silencing in cultured cells. However, naked Malat1-ASO also displayed a higher gene silencing efficiency, comparable to the R_N-polyplexes. To further investigate the comparison of gene silencing efficiency using Malat1-ASO between polyplexes and naked ASO, gene silencing evaluation at lower concentrations is required.

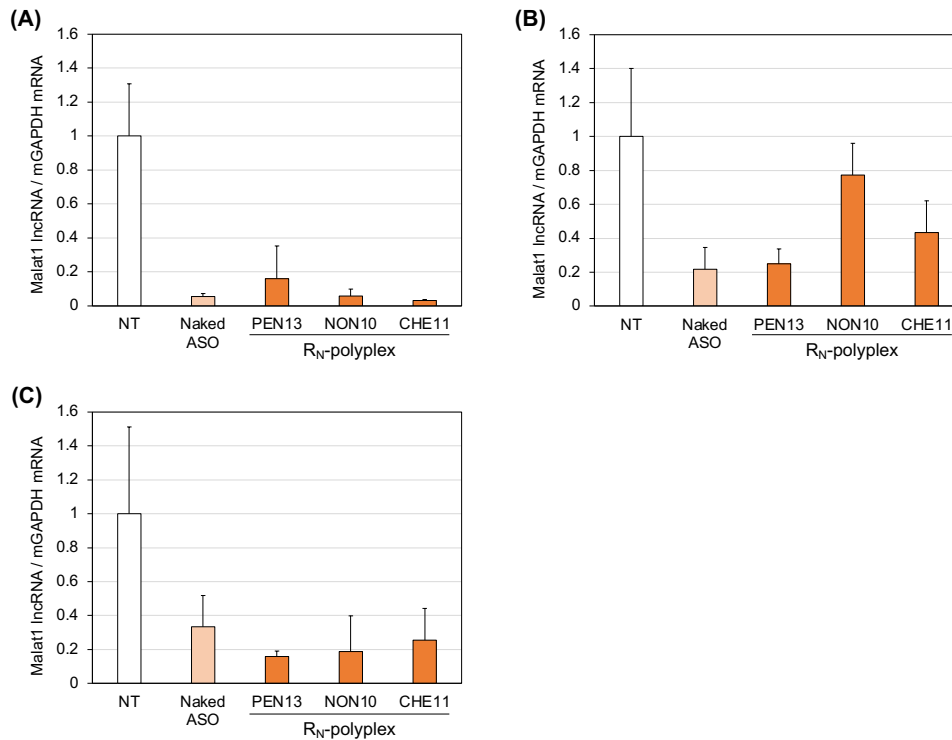


Fig. 2-9. Malat1 lncRNA levels in cultured 4T1-Luc cells treated with Malat1-ASO at various concentrations of 100 nM (A), 40 nM (B), and 20 nM (C) for 2 days. The RNA levels were determined by qRT-PCR. (mean \pm SD, $n = 3$)

2.3.5. *In vivo* gene silencing efficiency of Malat1-ASO-loaded polyplex

In vivo gene silencing efficiencies were evaluated two days after local administration, *i.e.*, ICV and IT administration, of naked Malat1-ASO or Malat1-ASO-loaded CHE₁₁-polyplex, exhibiting higher transfection efficiencies in the previous experiments (**Fig. 2-10**). The CHE₁₁-polyplex showed considerable gene silencing efficiency in each brain and lung tissue after two types of local administration. However, naked ASO also exhibited a transfection efficiency comparable to the polyplex. Similar results were observed from a previous *in vitro* gene silencing assay in that ASO itself possessed efficient gene silencing. To further investigate the comparison

between Malat1-ASO and naked ASO with respect to *in vivo* gene silencing efficiency in the brain, additional gene silencing evaluation at lower ASO concentrations is required.

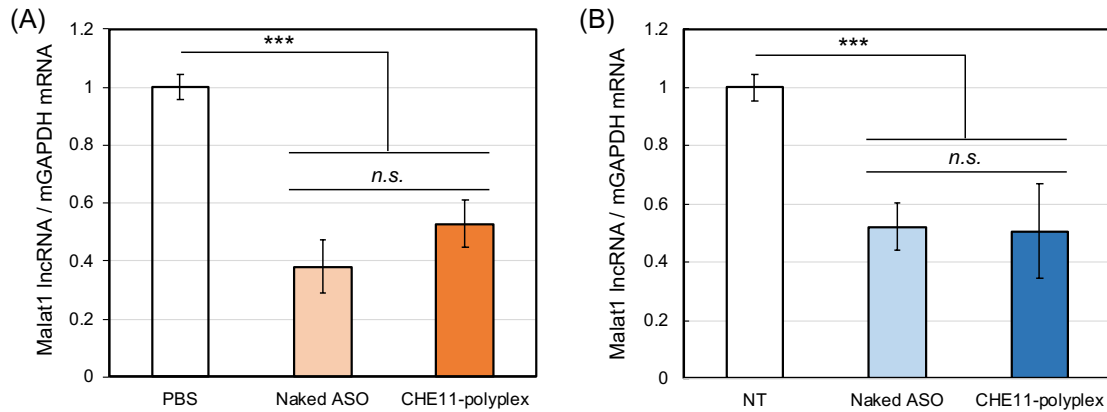


Fig. 2-10. Malat1 lncRNA levels in the brain (A) and lungs (B) 2 days after ICV and IT administration, respectively. Naked Malat1-ASO and Malat1-ASO-loaded CHE₁₁-polyplex were injected (ICV: 10 μ L, ASO 1 μ g/mouse, IT: 50 μ L, ASO 5 μ M). The RNA levels were determined by qRT-PCR. (mean \pm SD, ICV: $n = 3$, IT: $n = 4$)

2.4. Conclusion

In this chapter, the ASO delivery efficiencies of the PAsp(DET/R) library were evaluated and the impact of R moieties on the ASO transfection efficiency was revealed. Regardless of the R moieties, all R_N-polyplexes exhibited an equivalent hydrodynamic diameter (~150 nm) and positive ζ -potential (~30 mV) with relatively narrow PDI. *In vitro* mRNA delivery efficiencies substantially varied according to the R moiety. In the correlation analysis between mRNA transfection efficiency and the hydrophobicity, *i.e.*, the $\log D_{7.3}$ value of PAsp(DET/R)s, a threshold for efficient mRNA delivery was clearly observed. The R_N-polyplexes with $\log D_{7.3}$ values higher than -2.4 elicited higher *in vitro* transfection efficiencies than the counterparts with lower $\log D_{7.3}$ values than -2.4. This was likely due to enhanced cellular uptake of ASO-loaded polyplex induced by higher polyplex stability against competition with polyanions. The present study demonstrates the potential of fine-tuning R moieties in PAsp(DET/R) for the optimal design of ASO-loaded polyplexes toward therapeutic ASO delivery.

Reference

1. Kim, H. J., Ogura, S., Otabe, T., Kamegawa, R., Sato, M., Kataoka, K., Miyata, K. Fine-tuning of hydrophobicity in amphiphilic polyaspartamide derivatives for rapid and transient expression of messenger RNA directed toward genome engineering in brain. *ACS Cent. Sci.* **5**, 1866–1875 (2019).
2. Crooke, S. T., Baker, B. F., Crooke, R. M., Liang, X. H. Antisense technology: an overview and prospectus. *Nat. Rev. Drug Discov.* **20**, 427–453 (2021).
3. Wan, W. B., Seth, P. P., The medicinal chemistry of therapeutic oligonucleotides. *J. Med. Chem.* **59**, 9645–9667 (2016).
4. Uchida, H., Itaka, K., Nomoto, T., Ishii, T., Suma, T., Ikegami, M., Miyata, K., Oba, M., Nishiyama, N., Kataoka, K. Modulated protonation of side chain aminoethylene repeats in N-substituted polyaspartamides promotes mRNA transfection. *J. Am. Chem. Soc.* **135**, 12396–12405 (2014).
5. Miyata, K., Oba, M., Nakanishi, M., Fukushima, S., Yamasaki, Y., Koyama, H., Nishiyama, N., Kataoka, K. Polyplexes from poly(aspartamide) bearing 1,2-diaminoethene side chains induce pH-selective, endosomal membrane destabilization with amplified transfection and negligible cytotoxicity. *J. Am. Chem. Soc.* **130**, 16287–16294 (2008).
6. Pühr, M., Hofer, J., Neuwirt, H., Eder, I. E., Kern, J., Schäfer, G., Geley, S., Heidegger, I., Klocker, H., Culig, Z. PIAS1 is a crucial factor for prostate cancer cell survival and a valid target in docetaxel resistant cells. *Oncotarget* **5**, 12043–12056 (2014).
7. Min, H. S., Kim, H. J., Naito, M., Ogura, S., Toh, K., Hayashi, K., Kim, B. S., Fukushima, S., Anraku, Y., Miyata, K., Kataoka, K. Systemic brain delivery of antisense oligonucleotides across the blood–brain barrier with a glucose-coated polymeric nanocarrier. *Angew. Chem. Int. Ed.* **59**, 8173–8180 (2020).
8. Miyata, K., Nishiyama, N., Kataoka, K. Rational design of smart supramolecular assemblies for gene delivery: chemical challenges in the creation of artificial viruses. *Chem. Soc. Rev.* **41**, 2562–2574 (2012)
9. Burke, R. S., Pun, S. H. Extracellular barriers to in vivo PEI and PEGylated PEI polyplex-mediated gene delivery to the liver. *Bioconjugate Chem.* **19**, 693–704 (2008).
10. Zuckerman, J. E., Choi, C. H. J., Han, H., Davis, M. E. Polycation-siRNA nanoparticles can disassemble at the kidney glomerular basement membrane. *PNAS.* **109**, 3137–3142 (2012).

11. Choi, H. S., Ashitate, Y., Lee, J. H., Kim, S. H., Matsui, A., Insin, N., Bawendi, M. G., Semmler-Behnke, M., Frangioni, J. V., Tsuda, A. Rapid translocation of nanoparticles from the lung airspaces to the body. *Nat. Biotechnol.* **28**, 1300–1303 (2010).
12. Kim, B. S., Osawa, S., Naito, M., Ogura, S., Kamegawa, R., Ishida, H., Kim, H. J., Uchida, S., Miyata, K. A 50-nm-sized micellar assembly of thermoresponsive polymer-antisense oligonucleotide conjugates for enhanced gene knockdown in lung cancer by intratracheal administration. *Adv. Therap.* **3**, 1900123 (2020).

Chapter 3

Molecular design of polyaspartamide derivatives for efficient messenger RNA delivery

3.1. Chapter introduction

As aforementioned, a series of polyaspartamide derivatives (PAsp(DET/R)s) tailored with diethylenetriamine (DET) and various hydrophobic R moieties in the chains showed varying mRNA delivery efficiencies, depending on the hydrophobicity (R moiety) [1]. These derivatives with a $\log D_{7.4}$ value higher than -2.4 exhibited more efficient mRNA transfection efficiency in cultured tumor cells than the counterparts with a $\log D_{7.4}$ value lower than -2.4 .

In **Chapter 3**, the PAsp(DET/R) design is expanded by highlighting the R moiety in the side chains of PAsp(DET/R)s for efficient and systemic mRNA transfection, with an initial focus on the chemical structure of the R moiety. In a previous study, PAsp(DET/CHE) accomplished the highest mRNA transfection efficiency among PAsp(DET/R)s in cultured tumor cells, and its mRNA transfection efficiency level was around 100,000 times higher than that of PAsp(DET) with no hydrophobic moiety [1]. In addition, it was reported that cycloalkyl groups showed higher affinity to the cell membrane than alkyl and phenyl groups, presumably due to having a relatively larger hydrophobic area [2,3]. Based on the chemical structure of PAsp(DET/CHE), various alicyclic moieties with slightly different structures from the CHE moiety were introduced to the side chains of the PAsp(DET/R)s (**Fig. 3-1**). Specifically, two alicyclic moiety groups were selected as the new R moieties of the PAsp(DET/R)s. One group, the cyclohexyl series, has the cyclohexyl moieties with varying alkyl spacers, while the other group, the ethylene series, has various ring structures with ethylene spacers. Secondly, the main chain of PAsp(DET/R)s was designed to have a short degree of polymerization (DP) of around 20 for the minimization of toxicity derived from the cationic components for application to *in vivo* mRNA delivery to be covered in **Chapter 4** [4]. Lastly, the introduction rate of the R moieties is investigated and the mRNA transfection efficiencies of PAsp(DET/CHE)s with different introduction rates of CHE moieties are compared (**Fig. 3-2**). PAsp(DET/CHE) with a 57% introduction rate of CHE moieties

showed higher mRNA expression than the previously synthesized PAsp(DET/CHE) having a 40% introduction rate of CHE moieties [1]. Therefore, PAsp(DET/R)s with alicycle moieties were synthesized to have around a 57% introduction rate of R moieties in the side chains.

In this study, the aim is to synthesize a new PAsp(DET/R) library for improved and systemic mRNA delivery and investigate the effect of R moieties (or hydrophobicity) on mRNA transfection efficiency in cultured cells. To this end, the characteristics of polyplexes formed by new synthesized PAsp(DET/R)s and mRNA transfection efficiency profiles were evaluated. Then, the mechanism of how the R moieties affect the mRNA delivery steps was studied, *i.e.*, cellular uptake, polyplex stability, and endosomal escape in cultured cells.

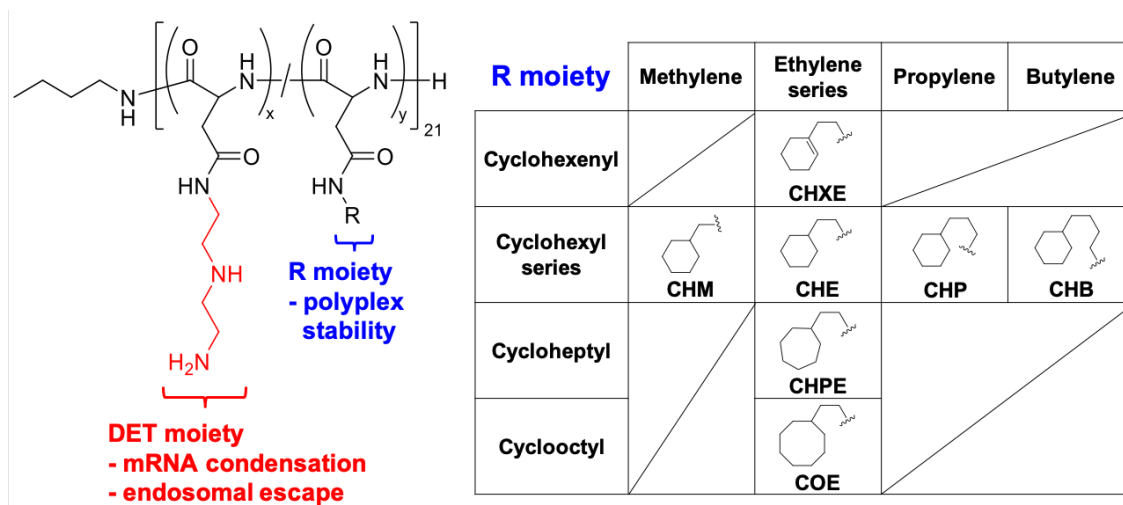


Figure 3-1. Design of a series of PAsp(DET/R)s with alicyclic moieties in the side chains.

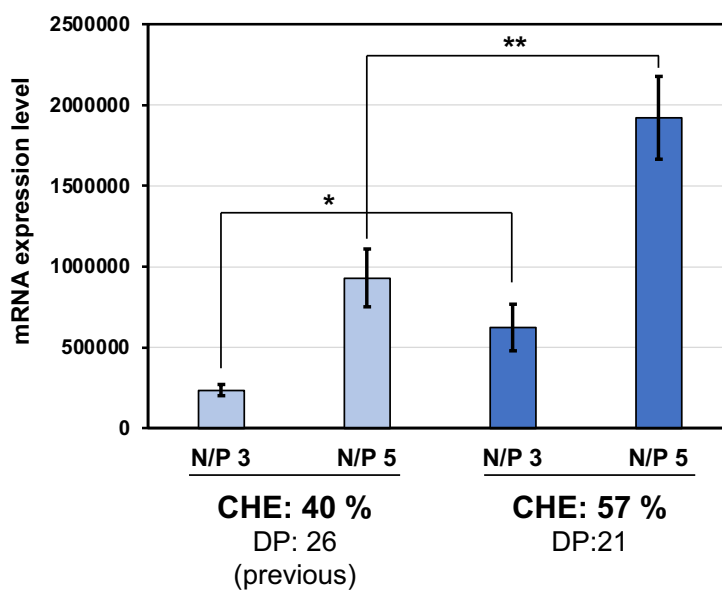


Figure 3-2. mRNA transfection efficiencies of PAsp(DET/CHE)s with different introduction rates of CHE moieties (40 and 57%). Results are expressed as mean \pm SD ($n = 4$). Statistical significance: * $p < 0.05$, ** $p < 0.1$.

3.2. Materials and methods

3.2.1. Materials

β -Benzyl-L-aspartate *N*-carboxy-anhydride (BLA-NCA) was purchased from Chuo Kaseihin Co., Inc. (Tokyo, Japan). Diethylenetriamine (DET), *n*-butylamine, dichloromethane (DCM), *N,N*-dimethylformamide (DMF), *N*-methyl-2-pyrrolidone (NMP), methanol (MeOH), hydrochloric acid (HCl), Dulbecco's phosphate-buffered saline (D-PBS(-)), and Dulbecco's modified Eagle's medium (DMEM) were purchased from FUJIFILM Wako Pure Chemical Industries, Ltd. (Osaka, Japan). DET, *n*-butylamine, DCM, DMF, and NMP were distilled before use. The companies from which the alicyclic amines were purchased are summarized in **Table 3-1**. Diethyl ether was obtained from Showa-Ether Co. (Tokyo, Japan). 1-Octanol and trypsin-ethylenediaminetetraacetic acid (trypsin-EDTA) were purchased from Sigma-Aldrich Co. (St. Louis, MO, USA). Alexa Fluor 647 NHS ester, ultrapure agarose, and Lipofectamine MessengerMAX (LipoM) were purchased from Thermo Fisher Scientific (Waltham, MA, USA). *N,N*-Diisopropylethylamine (DIPEA) was purchased from Tokyo Chemical Industry Co., Ltd. (Tokyo, Japan). HEPES buffer (1 M, pH 7.3) was purchased from Amresco (Solon, OH, USA). Novex Tris-borate-EDTA (TBE) gel (4–20%) was purchased from Invitrogen (Carlsbad, CA, USA). Fetal bovine serum (FBS) was purchased from Biosera (Nuaille, France). Human lung carcinoma (A549) cells were purchased from the American Type Culture Collection (Manassas, VA, USA). Gaussia and firefly luciferase 2-coded (GLuc and Luc2) mRNAs were prepared as previously reported [1,5]. In brief, luciferase-coded plasmid DNAs (pDNAs) were linearized and purified to construct pDNA templates, followed by *in vitro* transcription of the pDNA templates to prepare GLuc- or Luc2-mRNA. Plasmid DNA, luciferase-expressing and poly A/T (120 base pairs) sequences tandemly inserted into pSP73, were kindly provided from Dr. Satoshi Uchida (Kyoto Prefectural University of Medicine). Fluorescently labeled mRNA was prepared by

conjugation of Cy5 dyes to mRNA by using a Label IT Cy5 labeling kit (Mirus Bio Corporation, Madison, WI, USA).

Table 3-1. List of companies manufacturing alicyclic amines utilized in **Chapter 3**.

Alicyclic amine	Reagent company
Cyclohexanemethylamine	Sigma-Aldrich Co. (St. Louis, MO, USA)
2-Cyclohexyl-ethylamine	Tokyo Chemical Industry Co., Ltd. (Tokyo, Japan)
3-Cyclohexyl-propylamine	Enamine Ltd. (Monmouth Junction, NJ, USA)
4-Cyclohexyl-butylamine	J&W PharmLab, LLC (Levittown, PA, USA)
2-(1-Cyclohexenyl)ethylamine	Sigma-Aldrich Co. (St. Louis, MO, USA)
2-Cycloheptyl-ethylamine	ChemBridge Corporation (San Diego, CA, USA)
2-Cyclooctyl-ethylamine	Fluorochem Ltd. (Glossop, UK)

3.2.2. Synthesis of polyaspartamide derivatives tailored with diethylenetriamine and alicyclic moieties (PAsp(DET/R)s)

The PAsp(DET/R)s were synthesized by the aminolysis of PBLA with DET and various alicyclic amines, according to a previous report [1,5,6]. The PAsp(DET/R) synthetic scheme is shown in **Figure 3-3**. First, PBLA was prepared by ring-opening polymerization of BLA-NCA using *n*-butylamine as an initiator. BLA-NCA (500 mg, 2.02 mmol) was dissolved in a mixture of DCM and DMF (9:1 v/v, 5 mL), and *n*-butylamine (8.66 μ L, 0.0876 mmol) was diluted in DCM (870 μ L). The BLA-NCA solution and the *n*-butylamine solution were mixed and reacted under an Ar atmosphere at 35 °C for 72 h. After the reaction, the PBLA solution was purified by precipitation into diethyl ether. The polymer powder was then obtained by vacuum drying overnight. The obtained PBLA was analyzed by gel permeation chromatography (GPC) and ¹H-NMR to calculate the molecular weight distribution (M_w/M_n) and degree of polymerization (DP), respectively. The GPC system (HLC-8220), which was equipped with two TSK gel columns

(TSK-gel Super AW4000 and Super AW3000, TOSOH CORPORATION, Tokyo, Japan), was eluted with lithium chloride (10 mM) dissolved DMF at 0.8 mL/min.

Next, a series of PAsp(DET/R)s were prepared by an aminolysis reaction of the obtained PBLA with the mixed solution of DET and alicyclic amines [1]. PBLA and the mixed amine solution were individually dissolved in NMR (2 mL). Then, after the solutions were cooled to 5 °C, the PBLA solution was added dropwise into the amine solution. The mixture was stirred overnight under an Ar atmosphere at 5 °C. The resulting solution was precipitated in diethyl ether and filtered to remove the unreacted amines. The filtered product was dissolved in cooled 0.01 M HCl at 5 °C. The polymer solution was subsequently purified by sequential dialysis against 0.01 M HCl and distilled water at 4 °C. The polymer powder was obtained by lyophilization of the dialyzed solution. The conversion of benzyl ester moieties to DET/alicyclic moieties and the quantitative amount of DET/alicyclic moieties were confirmed in the ¹H-NMR spectra of the obtained PAsp(DET/R)s.

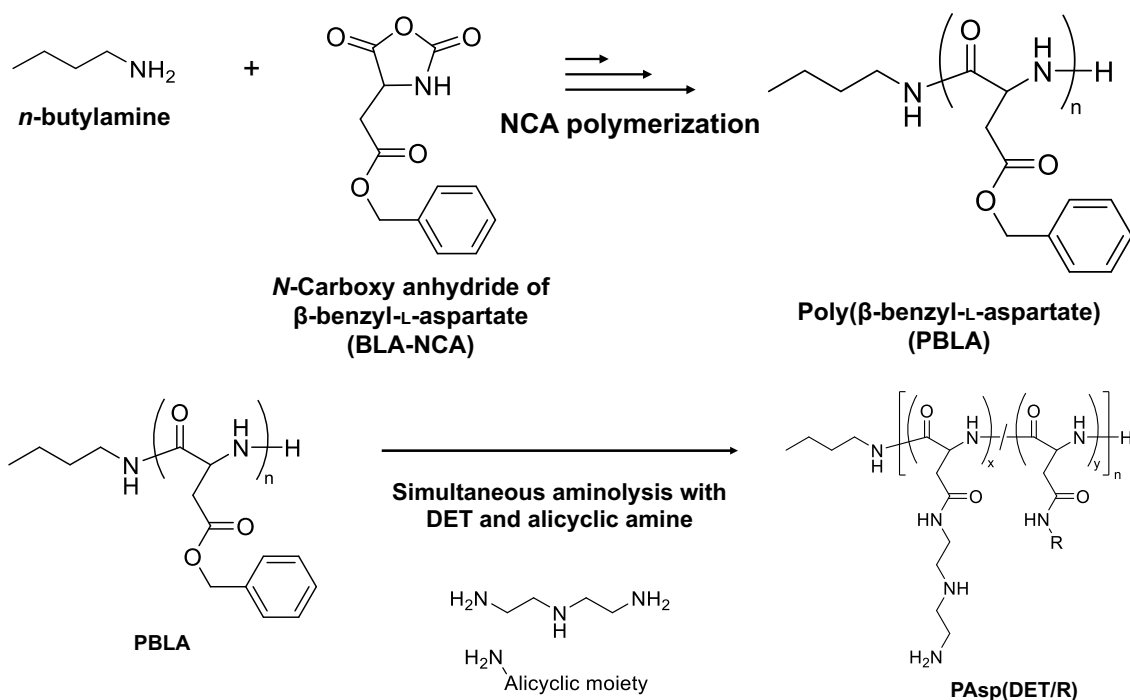


Figure 3-3. Synthetic routes of PAsp(DET/R)s.

3.2.3. Measurement of the hydrophobicity of the PAsp(DET/R)s

The hydrophobicity of PAsp(DET/R)s was quantified by an octanol–water (or buffer at pH 7.3) distribution coefficient ($\log D_{7.3}$), as detailed in a previous study [1]. $\log D_{7.3}$ values of PAsp(DET/R)s were determined from the fluorescence intensity ratio of the 1-octanol layer to the HEPES buffer layer obtained from the mixture of 1-octanol and 10 mM HEPES buffer (1:1 v/v) at pH 7.3 dissolved with fluorescently labeled PAsp(DET/R)s. The labeled PAsp(DET/R)s were prepared by a conjugation reaction with the Alexa Fluor 647 NHS ester (Alexa647) in MeOH with a small amount of DIPEA. After solvent exchange to 0.01 M HCl, the reactants were purified using a PD-10 column and sequentially dialyzed against 0.01 M HCl and distilled water at 4 °C. The final product was obtained by lyophilization. The 10 mM HEPES buffer (pH 7.3) with dissolved Alexa647-labeled PAsp(DET/R)s (100 μ M, 50 μ L) was mixed with 1-octanol (50 μ L), followed by vortexing at 2,500 rpm for 30 min using a MixMate (Eppendorf, Hamburg, Germany).

After a short centrifugation, the mixture was incubated at 4 °C for 1 h to separate into 1-octanol and HEPES buffer layers. The fluorescence intensities of separately obtained 1-octanol and HEPES buffer layers were measured using a spectrofluorometer (FP-8300, Jasco, Tokyo, Japan).

3.2.4. Formation and characterization of *in vitro* messenger RNA (IVT mRNA)-loaded polyplexes

The polyplexes (20 ng/μL mRNA) were prepared by gentle mixing of the PAsp(DET/R) solution with an IVT mRNA solution (100 ng/μL mRNA) at various molar ratios of the amino group in PAsp(DET/R) to the phosphate group in IVT mRNA (N/P ratio). A gel electrophoresis assay was performed to confirm the polyplex formation. The polyplex solutions at N/P ratios of 0, 1, 2, 3, 4, and 5 were prepared *via* the method mentioned in **Chapter 2**. The polyplex solutions (100 ng mRNA) were mixed with glycerol (final glycerol concentration: 8 vol.%), followed by loading into 1 wt.% agarose gel with a small amount of ethidium bromide. The loaded samples were electrophoresed in a 1 × TBE buffer at 135 V for 10–15 min. The mRNA stained with ethidium bromide on the gel was visualized using a Pharos FX Molecular Imager (Bio-Rad, Hercules, CA, USA). The hydrodynamic diameter (cumulant size) and polydispersity index (PDI) of the polyplexes were determined by dynamic light scattering using a Zetasizer (Malvern Instruments, Worcestershire, UK) equipped with a He–Ne Laser ($\lambda = 633$ nm) at a detection angle of 173°. The cumulant size and PDI was obtained by analysis of the decay rate in the photon correlation function using the method of cumulants. The ζ -potential of polyplexes was calculated by the electrophoretic mobility measured in a Zetasizer using the Smoluchowski equation. The cumulant size, PDI, and ζ -potential of the polyplexes were measured at 25 °C.

3.2.5. Evaluation of mRNA transfection efficiency in cultured cells

Human lung carcinoma (A549) cells were used for this experiment. DMEM with 10 % FBS was utilized as a cell culture medium. The cells (5.0×10^3 cells/well in 100 μ L medium) were seeded into 96-well plates and incubated for 24 h. Following exchange with a fresh medium, polyplex samples (N/P = 5) containing GLuc- and Luc2-mRNA were added to each well (50 ng mRNA/well) and then incubated for either 4 h or 24 h. The expression efficiencies of GLuc- and Luc2-mRNA were determined from the luminescence intensities of the cell supernatants diluted 40 times and cell lysates, respectively, by using the luciferase assay (GLuc: Renilla Luciferase Assay System (Promega, Madison, WI, USA); Luc2: Luciferase Assay System (Promega)). The luminescence intensities of diluted supernatants and lysates transferred to the plate (10 μ L/well) were measured with a luminescence microplate reader.

3.2.6. Cell viability

A549 cells (5.0×10^3 cells/well in 100 μ L medium) were seeded into 96-well plates and incubated for 24 h. After exchange with a fresh medium (DMEM with 10% FBS), polyplex samples (N/P = 5) containing GLuc-mRNA were added to each well (50 ng mRNA/well) and then incubated for 24 h. The medium was then exchanged and 10 μ L of Cell Counting Kit-8 (CCK-8, Dojindo, Kumamoto, Japan) solution was added to each well. After an additional 2 h incubation, the absorbance of each well was measured at 450 nm by using a microplate reader (Spark 20M, Tecan Group Ltd., Männedorf, Switzerland). Cell viability was calculated as a percentage value relative to the absorbance level of the non-treated wells (normalized to 100 %).

3.2.7. Evaluation of cellular uptake efficiency

The cellular uptake efficiencies of the polyplexes were determined by fluorescence intensities derived from Cy5-labeled GLuc-mRNA (Cy5-mRNA) in the cells measured with flow cytometry and confocal laser scanning microscopy (CLSM). For the flow cytometry measurement, A549 cells (1.0×10^5 cells/well in 1 mL medium) were seeded into 12-well plates and incubated for 24 h. After a medium (DMEM with 10% FBS) exchange, polyplex samples (N/P = 5) containing Cy5-mRNA were added to each well (1 μ g mRNA/well) and then incubated for 4 h. The cells were washed with PBS twice, followed by trypsin-EDTA treatment. Then, the cells were suspended in PBS and measured using flow cytometry (BD LSR II, BD Biosciences, San Jose, CA, USA), equipped with FACSDiva software (BD Biosciences). For CLSM measurement, A549 cells (5.0×10^3 cells/well in 300 μ L medium) were seeded into an 8-well Lab-Tek chamber (Nalge Nunc International, Rochester, NY, USA) and incubated for 24 h. After exchanging the medium, polyplex samples (N/P = 5) containing Cy5-mRNA were added to each well (50 ng mRNA/well) and incubated for 4 h, after which Hoechst 33258 (5 μ g/mL, 1 μ L, Dojindo, Kumamoto, Japan) was added to stain the nuclei of the cells for 5 min. After being rinsed by PBS, the cells were fixed with 4% paraformaldehyde for 30 min. The cells were then observed using a CLSM (ZEISS LSM 880, Carl Zeiss, Oberkochen, Germany) equipped with a C-Apochromat 40 \times objective (Carl Zeiss) with the excitation wavelength set to 633 nm (He-Ne laser). In addition, the mechanism of cellular uptake was examined by CLSM observation under different temperatures (4 $^{\circ}$ C and 37 $^{\circ}$ C).

3.2.8. Protein absorption in 10% FBS-containing PBS

The protein absorption (or size change) was evaluated by the change of diffusion time after incubation in 10% FBS-containing PBS (10% FBS). Polyplex samples (cyclohexyl series)

with Cy5-mRNA were incubated in 10% FBS at 37 °C for 10 min. Incubated and unincubated polyplex samples were transferred to the well plate. The diffusion times of polyplex samples were then measured by fluorescence correlation spectroscopy (FCS, MF20, Olympus Corporation, Tokyo, Japan).

3.2.9. Effect of protein absorption on mRNA transfection efficiency

The mRNA transfection experiment was performed using a slightly modified protocol from the method mentioned in **Chapter 3.2.5**. The difference being that DMEM with 10% FBS and DMEM without FBS were used as cell culture media before polyplex transfection. A549 cells (5.0×10^3 cells/well in 100 μ L medium) were seeded into 96-well plates and incubated for 24 h. After exchanging cell culture media to DMEM with 10% FBS or DMEM without FBS, the polyplex samples (N/P = 5, cyclohexyl series) containing GLuc-mRNA were added to each well (50 ng mRNA/well) and then incubated for 24 h. The expression efficiencies of GLuc-mRNA were determined from the luminescence intensities of the cell supernatants diluted 40 times using the luciferase assay.

3.2.10. Polyplex stability in FBS-containing medium

Polyplex stability was evaluated by acrylamide gel electrophoresis in PBS containing 10% FBS (10% FBS). Polyplex samples (N/P = 5) encapsulating GLuc-mRNA (50 ng mRNA, 2.5 μ L) were incubated with 10% FBS at 37 °C for 1 h, followed by the purification of mRNA in the solutions using an RNeasy Mini Kit (Qiagen, Hilden, Germany). The purified mRNA solutions were mixed with NuPAGE LDS sample buffer (4 \times , Thermo Fisher Scientific) and distilled water, up to 10 μ L. The mixtures were then electrophoresed in Novex TBE gel (1 \times TBE buffer, 200 V, 50 min). The electrophoresed gel was immersed in SYBR Green II solution (Lonza, Basel,

Switzerland) for 15 min to stain the mRNA molecules on the gel, followed by observation of stained mRNA molecules using the GelDoc Go Imaging System (Bio-Rad).

3.2.11. Evaluation of endosomal escape efficiency

The endosomal escape efficiencies of the polyplexes were determined by the fluorescence signal derived from Cy5-mRNA in the cells measured with CLSM. A549 cells (5.0×10^3 cells/well in 300 μ L medium) were seeded into an 8-well Lab-Tek chamber (Nalge Nunc International). After 8 h, the cell culture media was exchanged to a media containing CellLight™ Lysosomes-GFP (Thermo Fisher Scientific, 10 μ L in 200 μ L medium) and incubated for 24 h. After rinsing with PBS and changing to a fresh medium, polyplex samples (N/P = 5) containing Cy5-mRNA were added to each well (50 ng mRNA/well) and incubated for 5 h. After rinsing with PBS, Hoechst 33258 (5 μ g/mL, 1 μ L, Dojindo) was added to stain the nuclei of the cells for 5 min. After being rinsed with PBS, the cells were fixed with 4% paraformaldehyde for 30 min. The cells were then observed using a CLSM (ZEISS LSM 880).

3.3. Results and discussion

3.3.1. Synthesis of the polyaspartamide derivatives library bearing alicyclic moieties

First, PBLA, the parent polymer, was synthesized by the ring-opening polymerization of BLA-NCA initiated by *n*-butylamine. The M_w/M_n and the DP of PBLA were determined to be 1.10 and 21 from the GPC chart (Fig. 3-4a) and $^1\text{H-NMR}$ spectrum (Fig. 3-4b), respectively. Then, a series of PAsp(DET/R)s were synthesized by the simultaneous aminolysis reactions of PBLA with DET and various alicyclic amines. As a negative control, PAsp(DET) was also synthesized. It was confirmed that all PAsp(DET/R)s had comparable introduction rates of hydrophobic moieties to the side chains (~55%, Table 3-2) from the $^1\text{H-NMR}$ spectra (Fig. 3-5). The $\log D_{7.3}$ values of PAsp(DET/R)s ranged from -2.68 to -1.17 (Table 3-2). The tendency of hydrophobicity of PAsp(DET/R)s did not perfectly match that of the alicyclic moiety, because of the different introduction rates of alicyclic moieties. Meanwhile, The $\log D_{7.3}$ value ($\log D_{7.3} = -1.36$) of PAsp(DET/CHE) synthesized in this experiment was higher than that ($\log D_{7.3} = -2.31$) in the previous study, due to the higher introduction rate of the CHE moiety.

Table 3-2. Compositions and $\log D_{7.3}$ of PAsp(DET/R)s

Polymer	R moiety	Feed ratio ^a		Introduction number ^b		Introduction rate of R moiety (%)	Log $D_{7.3}$ ^c
		DET	Alicyclic amine	DET moiety	R moiety		
PAsp(DET)	—	50	—	21	—	0	—
PAsp(DET/CHM)	cyclohexylmethyl	20	80	11	10	48	-2.68 ± 0.05
PAsp(DET/CHE)	2-cyclohexylethyl	25	80	9	12	57	-1.36 ± 0.04
PAsp(DET/CHP)	3-cyclohexylpropyl	20	80	10	11	52	-1.64 ± 0.10
PAsp(DET/CHB)	4-cyclohexylbutyl	20	80	10	11	52	-1.17 ± 0.07
PAsp(DET/CHXE)	2-(1-cyclohexenyl)ethyl	20	80	9	12	57	-1.74 ± 0.10
PAsp(DET/CHPE)	2-cycloheptylethyl	20	80	8	13	62	-1.46 ± 0.09
PAsp(DET/COE)	2-cyclooctylethyl	20	80	9	12	57	-1.32 ± 0.09

^a Values were determined as a relative molar ratio to BLA unit in PBLA.

^b Values were determined from $^1\text{H-NMR}$ spectra.

^c Values are expressed as mean \pm SD ($n = 3$).

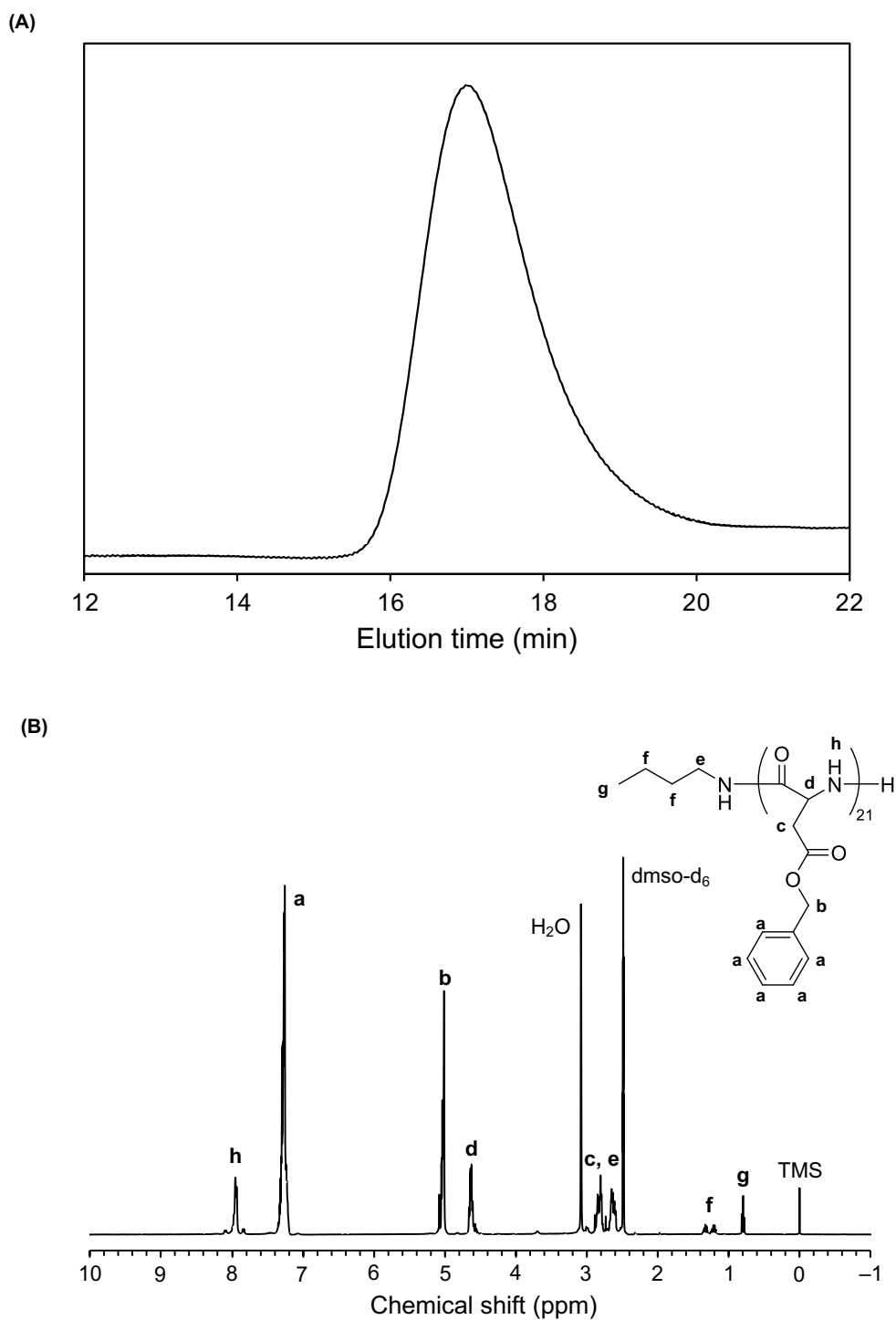


Figure 3-4. (A) GPC chart of PBLA (10 mM lithium chloride in DMF, 0.8 mL/min). (B) ^1H -NMR spectrum of PBLA (400 MHz, 10 mg/mL, DMSO-d_6 , 25 $^\circ\text{C}$).

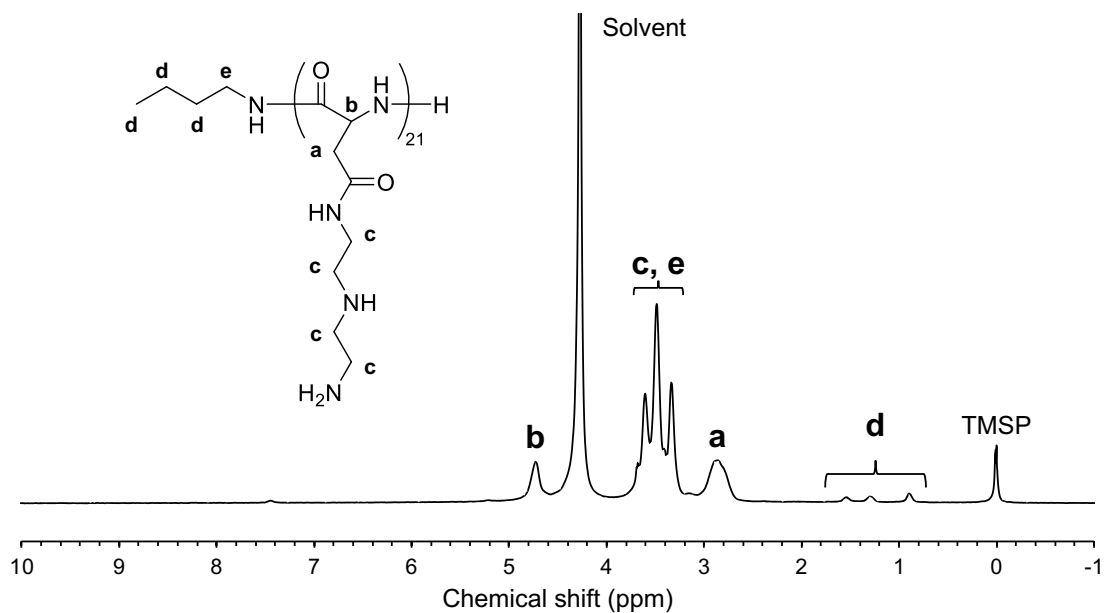


Figure 3-5. (A) ^1H -NMR spectra of a series of PAsp(DET) with DP = 21 (400 MHz, 10 mg/mL, DMSO- d_6 , 25 $^\circ\text{C}$).

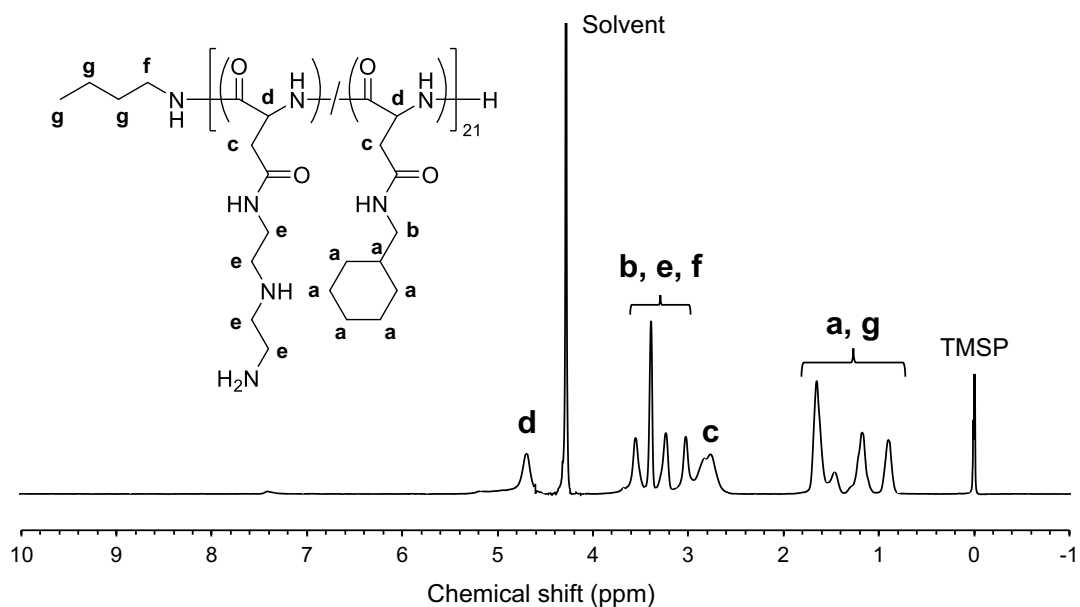


Figure 3-5. (B) ^1H -NMR spectra of a series of PAsp(DET/CHM) with DP = 21 (400 MHz, 10 mg/mL, DMSO- d_6 , 25 $^\circ\text{C}$).

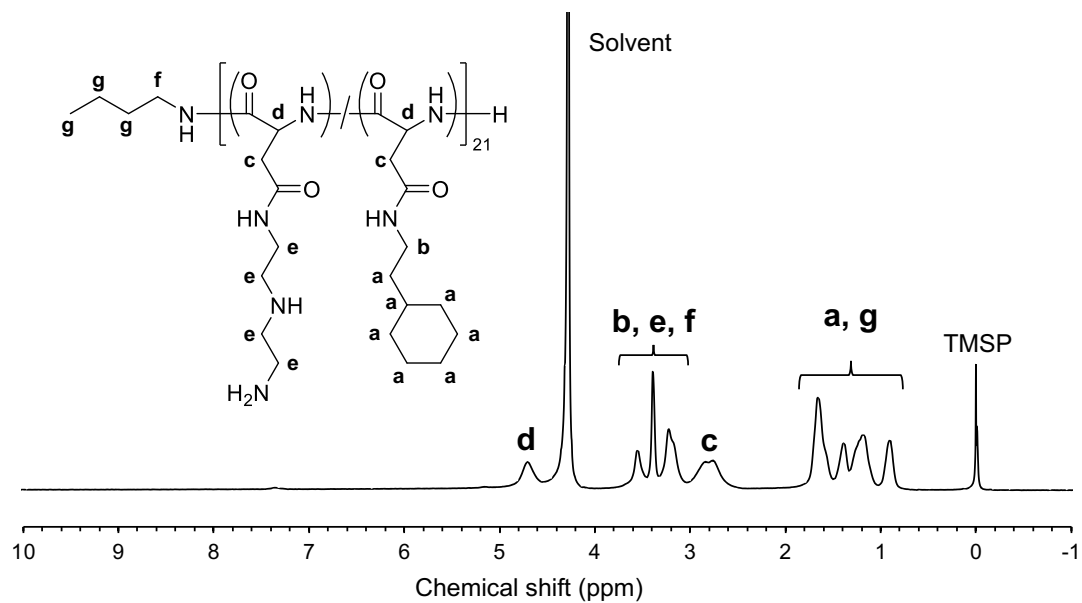


Figure 3-5. (C) $^1\text{H-NMR}$ spectra of a series of PAsp(DET/CHE) with DP = 21 (400 MHz, 10 mg/mL, DMSO- d_6 , 25 °C).

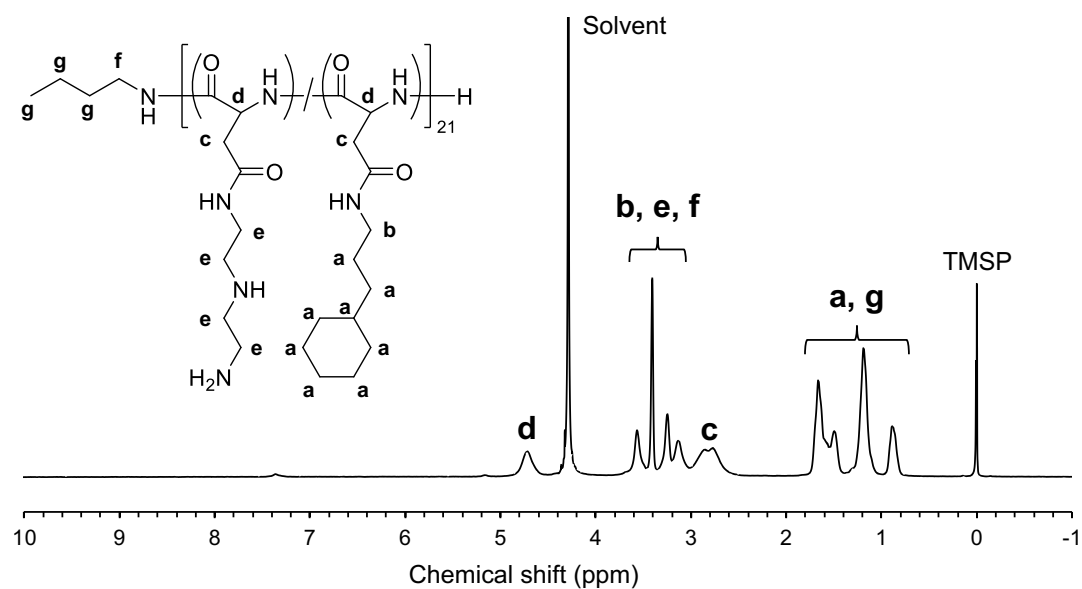


Figure 3-5. (D) $^1\text{H-NMR}$ spectra of a series of PAsp(DET/CHP) with DP = 21 (400 MHz, 10 mg/mL, DMSO- d_6 , 25 °C).

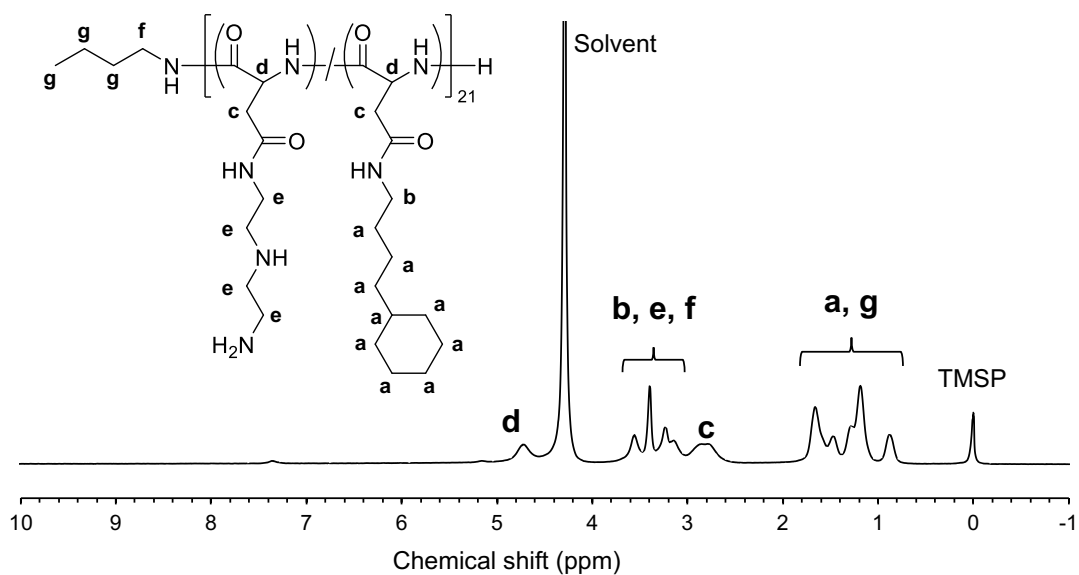


Figure 3-5. (E) $^1\text{H-NMR}$ spectra of a series of PAsp(DET/CHB) with DP = 21 (400 MHz, 10 mg/mL, DMSO- d_6 , 25 $^\circ\text{C}$).

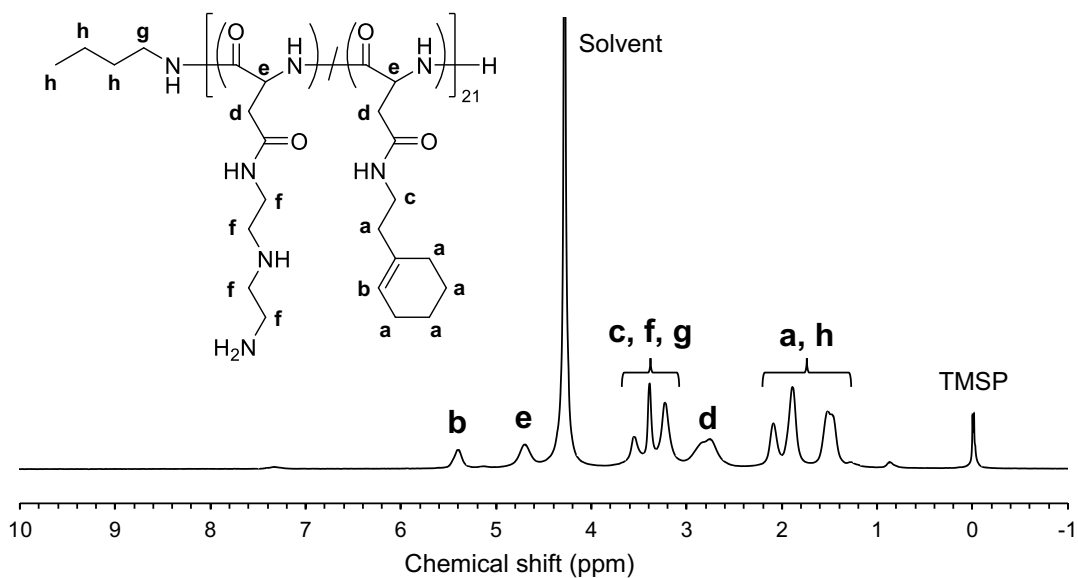


Figure 3-5. (F) $^1\text{H-NMR}$ spectra of a series of PAsp(DET/CHM) with DP = 21 (400 MHz, 10 mg/mL, DMSO- d_6 , 25 $^\circ\text{C}$).

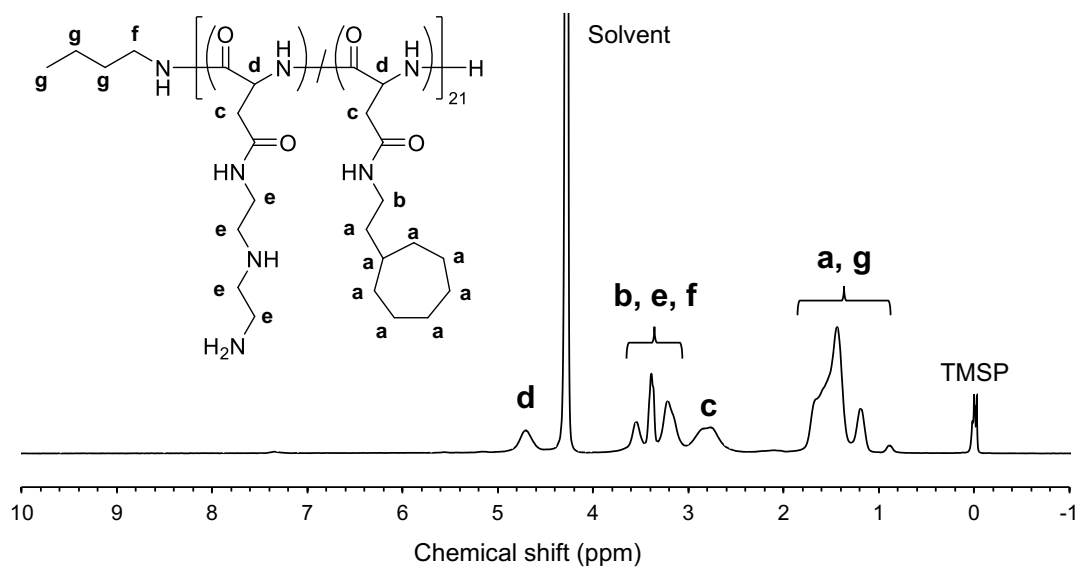


Figure 3-5. (G) $^1\text{H-NMR}$ spectra of a series of PAsp(DET/CHXE) with DP = 21 (400 MHz, 10 mg/mL, DMSO- d_6 , 25 °C).

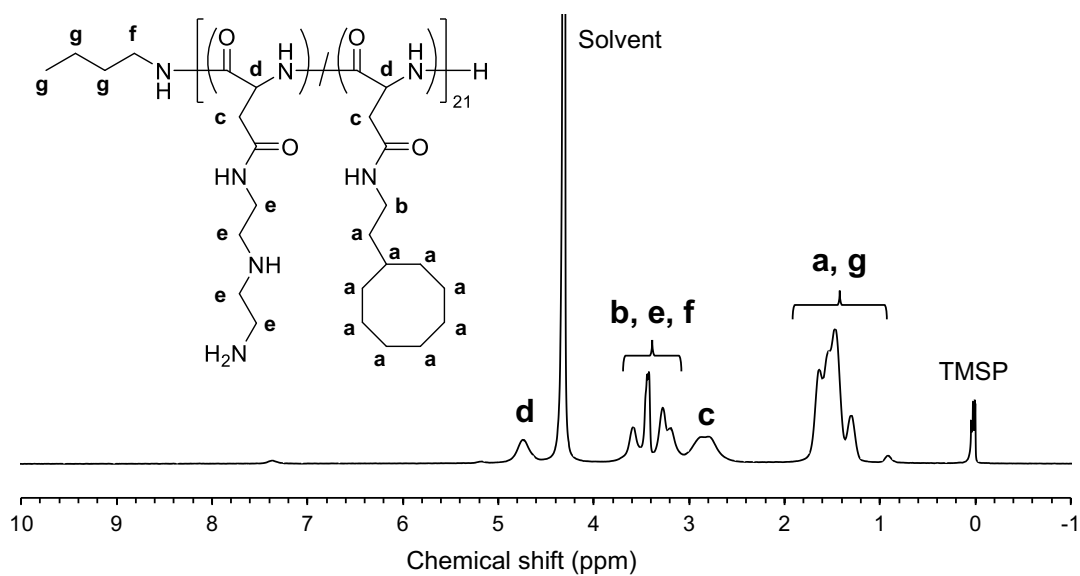


Figure 3-5. (H) $^1\text{H-NMR}$ spectra of a series of PAsp(DET/COE) with DP = 21 (400 MHz, 10 mg/mL, DMSO- d_6 , 25 °C).

3.3.2. Preparation and characterization of mRNA-loaded polyplexes

A series of PAsp(DET/R)s were mixed with GLuc-mRNA in a 10 mM HEPES buffer (pH 7.3) at various N/P ratios. The polyplex samples are expressed as DET- or R-polyplexes, where R indicates the alicyclic unit, for simplicity. The encapsulation of GLuc-mRNA in the polyplexes was determined with a gel electrophoresis assay (**Fig. 3-6**). In the electrophoresed agarose gels, there were no free mRNA bands at $N/P \geq 2$, indicating all mRNAs were encapsulated in the polyplexes at $N/P \geq 2$. This result is reasonable due to stoichiometric charge neutralization between mRNA and the derivatives at $N/P = 2$, given that the protonation degree of DET moieties is approximately 50% at pH 7.3 [6,7]. The characteristics, *i.e.*, hydrodynamic diameter (D_H), PDI, and ζ -potential, of the polyplex samples ($N/P = 5$) were measured with the Zetasizer (**Table 3-3**). The polyplexes exhibited D_H values of approximately 150 nm with a relatively narrow PDI below 0.2. The ζ -potentials of the polyplexes were determined to be ~ 30 mV. The polyplex samples exhibited similar values of D_H and ζ -potential regardless of introduced hydrophobic moieties in PAsp(DET/R). From these data, all polyplex samples were successfully formed by the mixing of PAsp(DET/R)s with IVT mRNA in 10 mM HEPES buffer (pH 7.3) at $N/P = 5$, and a series of polyplexes prepared at an N/P ratio of 5 were utilized in the following experiments.

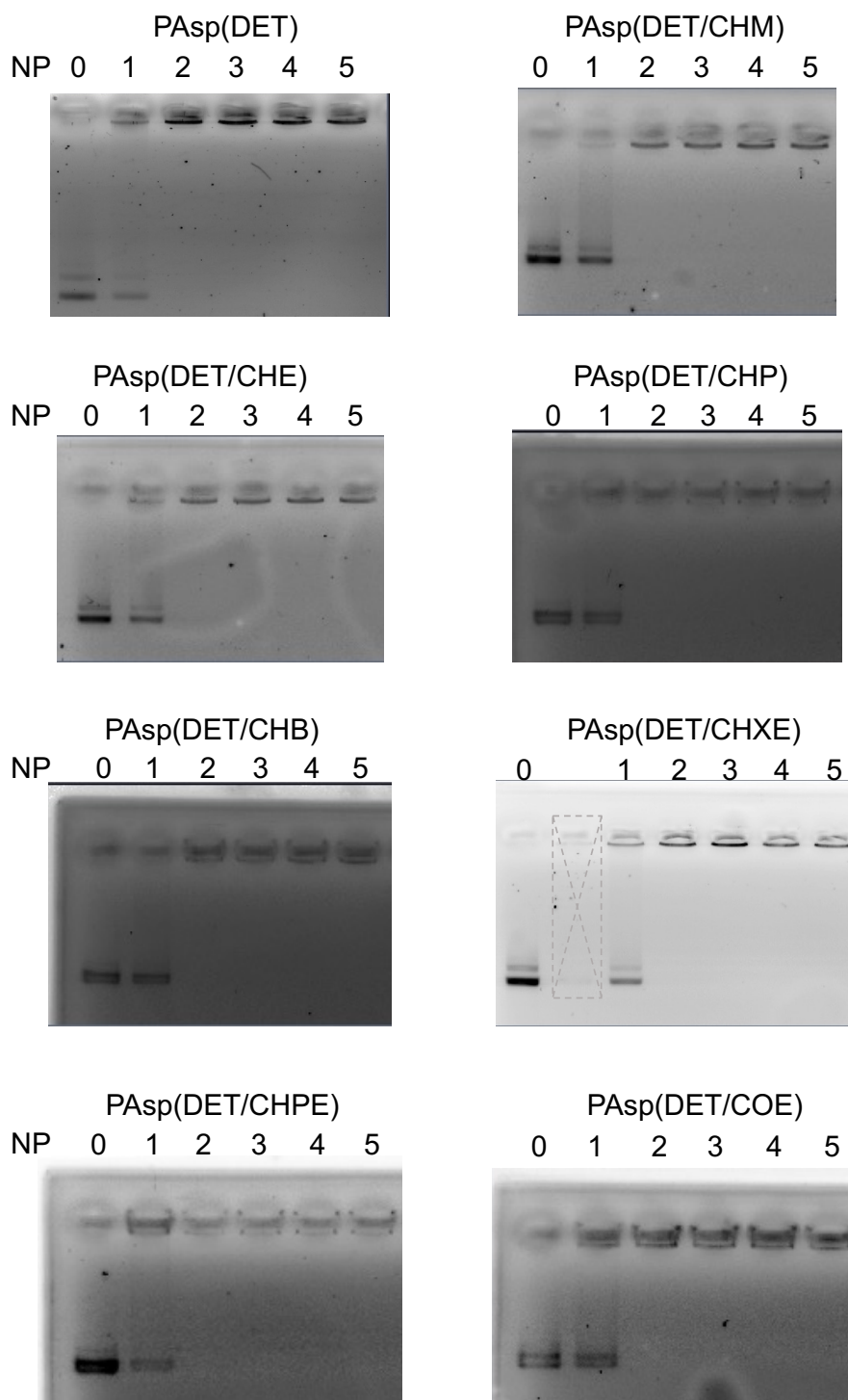


Figure 3-6. Agarose gel electrophoresis of GLuc-mRNA-loaded polyplexes at various N/P ratios. The mRNA molecules were stained with ethidium bromide. Note: The lane marked with dotted lines on PAsp(DET/CHXE) gel is irrelevant.

Table 3-3. D_H , PDI, and ζ -potential of polyplexes containing GLuc-mRNA at N/P = 5 (mean \pm SD, $n = 3$).

Polyplex	D_H (nm)	PDI	ζ-potential (mV)
DET-polyplex	104 \pm 9	0.19 \pm 0.03	24.8 \pm 11.6
CHM-polyplex	120 \pm 9	0.12 \pm 0.02	14.9 \pm 8.9
CHE-polyplex	117 \pm 5	0.18 \pm 0.02	25.1 \pm 8.3
CHP-polyplex	123 \pm 7	0.17 \pm 0.01	25.0 \pm 6.9
CHB-polyplex	116 \pm 7	0.18 \pm 0.00	24.7 \pm 7.1
CHXE-polyplex	106 \pm 10	0.17 \pm 0.01	16.3 \pm 5.3
CHPE-polyplex	107 \pm 5	0.14 \pm 0.02	25.2 \pm 9.5
COE-polyplex	106 \pm 7	0.16 \pm 0.02	24.1 \pm 7.5

3.3.3. *In vitro* transfection assay of the polyplexes in cultured cells

The mRNA delivery efficiencies of polyplexes were determined in cultured A549 cells. PAsp(DET/R)s were mixed with GLuc-mRNA to prepare the polyplex samples (N/P = 5). The polyplex samples were transfected into the cells at 50 ng mRNA/well. Commercially available Lipofectamine MessengerMAX (LipoM) was also transfected as a positive control. The cells were incubated for 4 and 24 h, and GLuc expression levels were measured with a luminescence plate reader (**Fig. 3-7**). Among the cyclohexyl series, the CHE- and CHP-polyplexes showed higher luminescence intensities than the CHM- and CHB-polyplexes. In the ethylene series, the luminescence intensities of the CHE- and CHPE-polyplexes were higher than those of the other polyplexes. Interestingly, the PAsp(DET/R)s with high mRNA expression efficiencies (R = CHE, CHP, CHPE) commonly have 7 or 8 carbons in the hydrophobic moiety. Nevertheless, all PAsp(DET/R)s, except for PAsp(DET/CHM), showed comparable luminescence intensities to LipoM. Note that the luminescence intensity profile obtained from A549 cells transfected with Luc2-mRNA-loaded polyplexes was similar to that transfected with GLuc-mRNA-loaded polyplexes (**Fig. 3-8**).

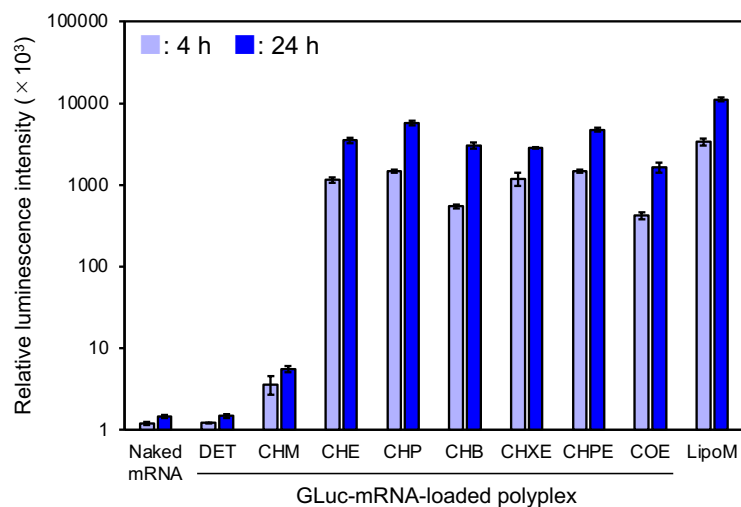


Figure 3-7. Relative luminescence intensities of A549 cells transfected with GLuc-mRNA (50 ng) *via* polyplexes or LipoM-based delivery. Results are expressed as mean \pm SD ($n = 4$).

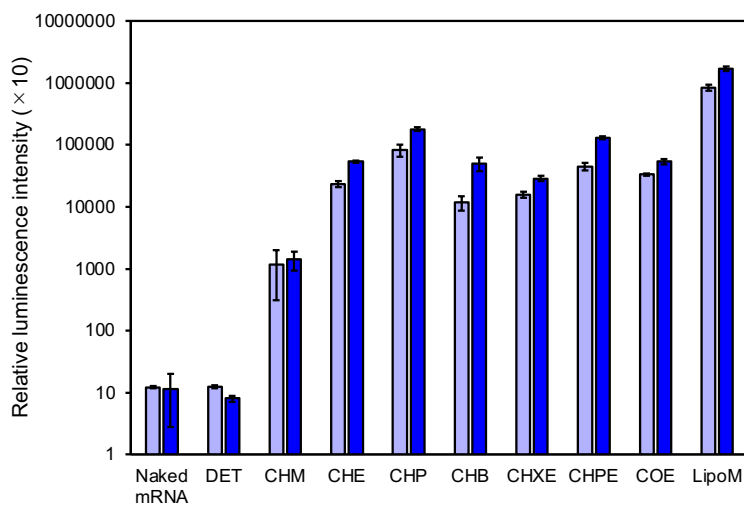


Figure 3-8. Relative luminescence intensities of A549 cells transfected with GLuc-mRNA (50 ng) *via* polyplexes or LipoM-based delivery. Results are expressed as mean \pm SD ($n = 4$).

In the correlation between luminescence intensity and $\log D_{7.3}$, the trend of the correlation was consistent with the previous findings (**Fig. 3-9**). PAsp(DET/R)s with $\log D_{7.3}$ values higher than -2.4 , which is the threshold for higher mRNA expression revealed from the previous study, showed higher mRNA expression efficiencies [1]. Only PAsp(DET/CHM) having a lower $\log D_{7.3}$ value exhibited a negligible mRNA expression level.

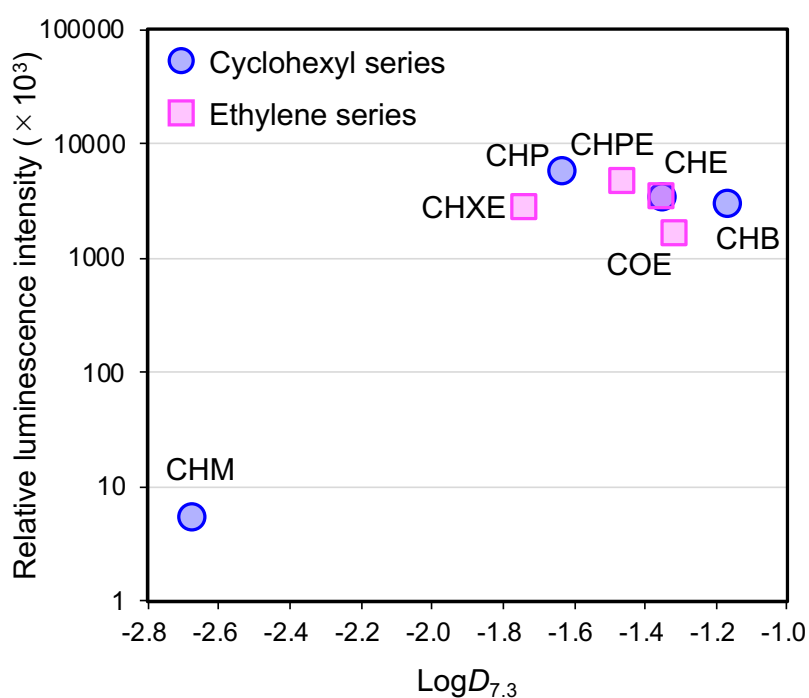


Figure 3-9. Correlation between relative luminescence intensities of A549 cells treated with GLuc-mRNA-loaded polyplexes and the $\log D_{7.3}$ value of PAsp(DET/R)s

Furthermore, the cytotoxicity of polyplexes was determined by the viability of A549 cells treated with polyplexes (50 ng mRNA/well). After incubating for 24 h, the viability was measured using the Cell Counting Kit-8 assay (**Fig. 3-10**). It was found that all polyplexes exhibited no severe cytotoxicity at the transfection condition.

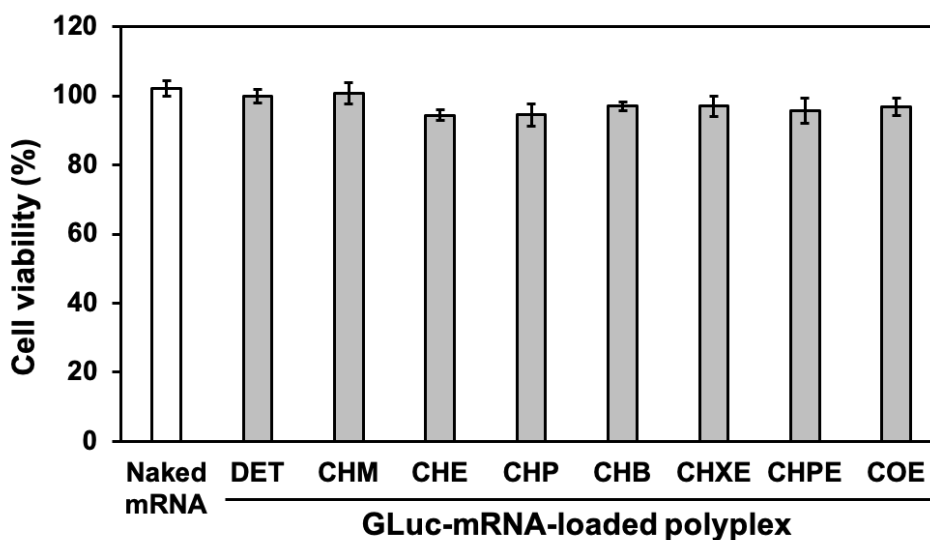


Figure 3-10. Cell viability of A549 cells treated with GLuc-mRNA-loaded polyplex for 24 h. Results are expressed as mean \pm SD ($n = 4$).

3.3.4. Cellular uptake efficiency and polyplex stability

To further investigate why PAsp(DET/CHM) showed a lower mRNA delivery efficiency, cellular uptake analysis was conducted by using Cy5-mRNA. Naked Cy5-mRNA and Cy5-mRNA-loaded polyplex samples were transfected into A549 cells. After incubating for 4 h, the mean fluorescence intensities derived from Cy5 in mRNA were measured using flow cytometry (Fig. 3-11). The profile of the mean fluorescence intensities correlated strongly with that of the transfection efficiencies in cultured cells. All PAsp(DET/R)s, except for PAsp(DET/CHM), exhibited higher mean fluorescence intensities, indicating efficient cellular uptake. On the other hand, PAsp(DET/CHM) exhibited a lower mean fluorescence intensity, comparable to naked mRNA and PAsp(DET), *i.e.*, limited cellular uptake. From the perspective of hydrophobicity ($\log D_{7.3}$), the polyplexes with $\log D_{7.3}$ value higher than -2.4 showed appreciably efficient cellular uptake compared to the CHM polyplexes ($\log D_{7.3} < -2.4$). Thus, the

efficient mRNA expression obtained from polyplexes with higher hydrophobicity ($\log D_{7.3} < -2.4$) was attributed to their increased cellular uptake.

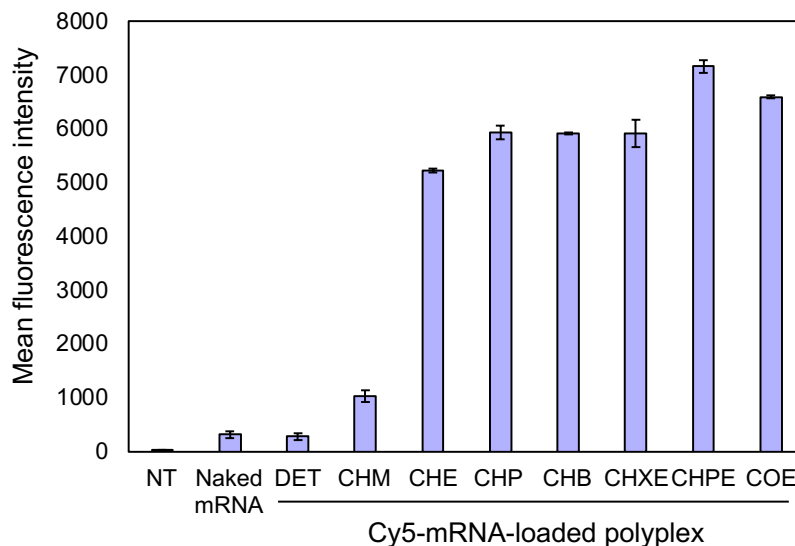


Figure 3-11. Mean fluorescence intensity (cellular uptake efficiency) of labeled mRNA, measured with flow cytometry, at 4 h after polyplex treatment. Results are expressed as mean \pm SD ($n = 3$).

In addition, the cellular uptake of labeled mRNA was checked by CLSM observation (**Fig. 3-12**). The CHE-, CHP-, and CHPE-polyplexes exhibited a larger number of fluorescent spots derived from labeled mRNA than the DET- and CHM-polyplexes and naked mRNA. This indicates the polyplexes with a higher $\log D_{7.3}$ value than -2.4 exhibited efficient cellular uptake of mRNA, which is consistent with the result obtained from the flow cytometry assay. In addition, to investigate whether the polyplex is taken into the cells *via* energy-dependent endocytosis, the cellular uptake of CHE-polyplex was examined by CLSM observation under different temperature conditions, 4 °C and 37 °C (**Fig. 3-13**). Whereas a larger number of red fluorescent mRNA spots were observed in the cells incubated at 37 °C, there were almost no mRNA spots in

the cell incubated at 4 °C. This indicates that polyplexes were internalized into the cell *via* energy-dependent endocytosis.

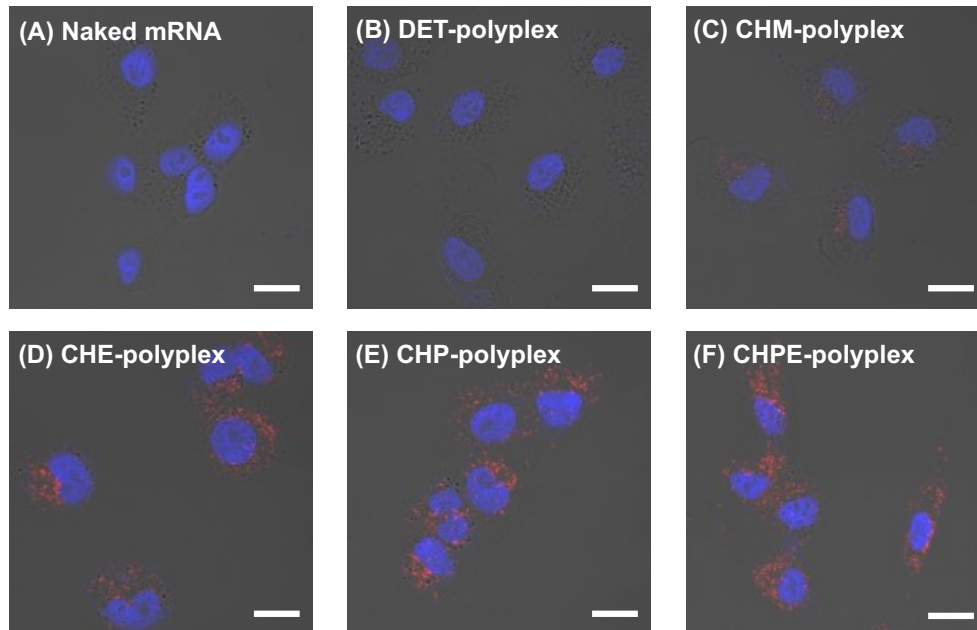


Figure 3-12. CLSM images of A549 cells treated with the naked Cy5-mRNA and Cy5-mRNA-loaded polyplexes for 4 h. ((A) naked Cy5-mRNA, (B) DET-polyplex, (C) CHM-polyplex, (D) CHE-polyplex, (E) CHP-polyplex, (F) CHPE-polyplex). Red and blue dots indicate Cy5 and nuclei (stained with Hoechst 33528), respectively. The scale bar represents 20 μm .

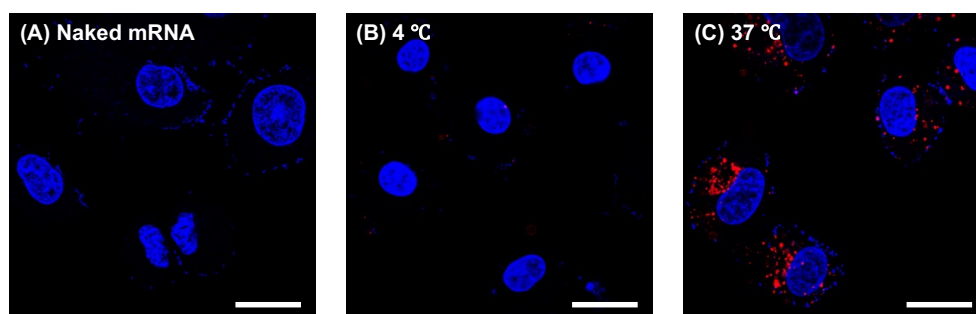


Figure 3-13. CLSM images of A549 cells treated with the naked Cy5-mRNA and Cy5-mRNA-loaded CHE-polyplexes for 4 h. ((A) naked Cy5-mRNA, 37 °C, (B) CHE-polyplex, 4 °C, (C) CHE-polyplex, 37 °C). Red and blue dots indicate Cy5 and nuclei (stained with Hoechst 33528), respectively. The scale bar represents 20 μm .

To investigate the mechanism underlying the varying cellular uptake efficiencies of the polyplexes, the conformation of the polyplex in 10% FBS (mimicking the extracellular milieu) was investigated. First, to check the protein absorption on the surface of the polyplex, the size change of the polyplexes (cyclohexyl series) was investigated by measuring the diffusion time with FCS after incubation in 10% FBS (**Fig. 3-14**). Whereas the diffusion time of polyplexes in HEPES was around 7000 μs , the diffusion time increased by a factor of approximately 3.5 after FBS treatment. This indicates that proteins in the FBS adsorbed to the polyplex and formed a protein corona. Furthermore, to investigate the effect of the protein corona on *in vitro* mRNA delivery, *in vitro* mRNA expression efficiency was evaluated depending on the presence or absence of FBS (**Fig. 3-15**). Although mRNA expression levels decreased in the presence of FBS, the magnitude of the decrease differed depending on the $\log D_{7.3}$ value. The mRNA expression levels of the polyplex with higher $\log D_{7.3}$ value were slightly decreased in the presence of FBS. Only the CHM-polyplex with a lower $\log D_{7.3}$ value exhibited a significantly decreased mRNA expression level in 10% FBS.

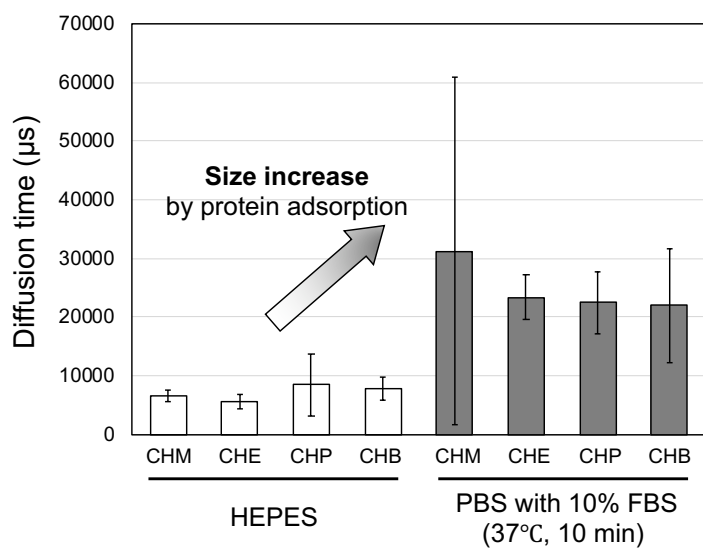


Figure 3-14. Diffusion time of the polyplexes (cyclohexyl series) in HEPES or 10% FBS measured by FCS.

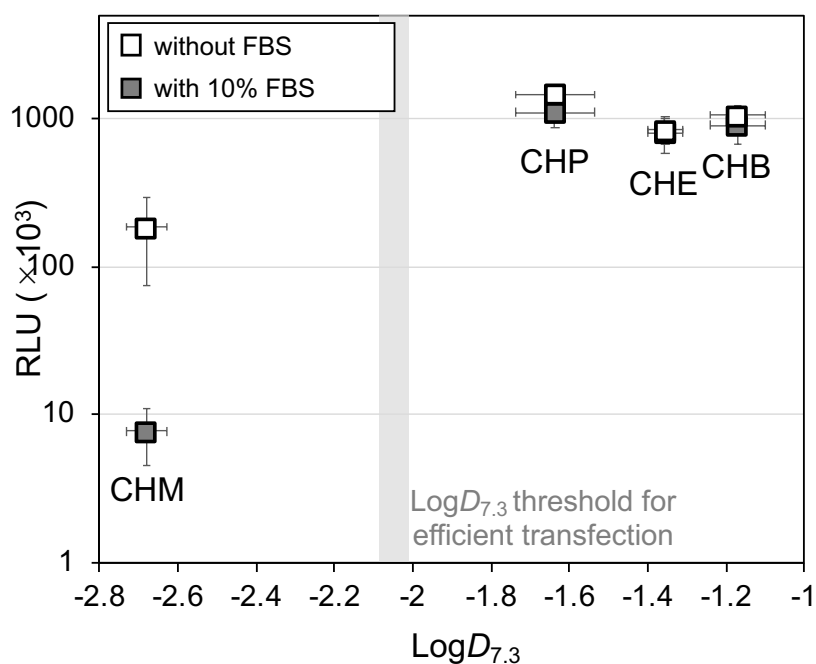


Figure 3-15. Relative luminescence intensities of A549 cells transfected with GLuc-mRNA (50 ng) *via* polyplex (cyclohexyl series)-based delivery in the presence or absence of FBS. Results are expressed as mean \pm SD ($n = 4$).

According to the appreciably lower $\log D_{7.3}$ value of PAsp(DET/CHM) compared to the other PAsp(DET/R)s, the decreased mRNA transfection of PAsp(DET/CHM) in the presence of FBS might be attributable to insufficient polyplex stability derived from low hydrophobicity. Therefore, the polyplex stability was examined by acrylamide gel electrophoresis of GLuc-mRNA, which was extracted from polyplexes after 1 h incubation in 10% FBS at 37 °C. The intact mRNA band was obviously detected from all polyplex lanes on the gel, except for the DET- and CHM-polyplexes, and the intensities of the intact mRNA band were comparable to that of the non-treated mRNA band. On the contrary, the DET- and CHM-polyplexes exhibited significantly lower intensities of the intact mRNA band. This result strongly supports the assumption that insufficient DET- and CHM-polyplex stability derived from lower hydrophobicity limited the cellular uptake efficiency. Therefore, the polyplexes with $\log D_{7.3}$ values higher than -2.4 exhibited enhanced stability in the cell medium, resulting in increased cellular uptake and mRNA delivery efficiency.

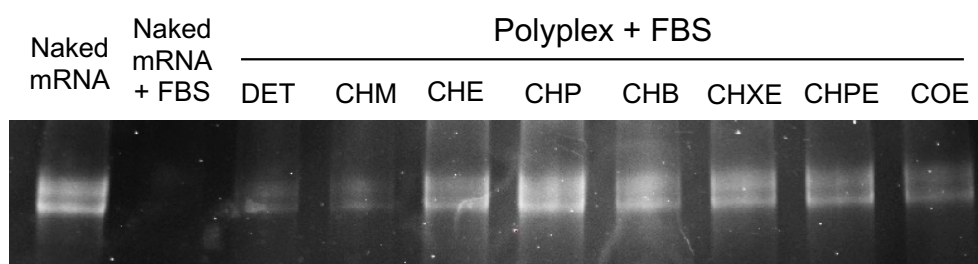


Figure 3-16. Acrylamide gel electrophoresis of GLuc-mRNA. The mRNA was extracted from polyplex samples after 1 h incubation in 10% FBS at 37 °C by using an RNeasy Mini Kit.

Additionally, the endosomal escape efficiency of the polyplexes with efficient cellular uptake, *i.e.*, the CHE-, CHP-, and CHB-polyplexes, was evaluated by CLSM observation after a 5-hour incubation. From the CLSM images, the endosomal escape ratio of R-polyplexes was

calculated and compared. It was found that the polyplexes displayed a only negligible difference in endosomal escape ratio, which led to similar mRNA expression efficiencies.

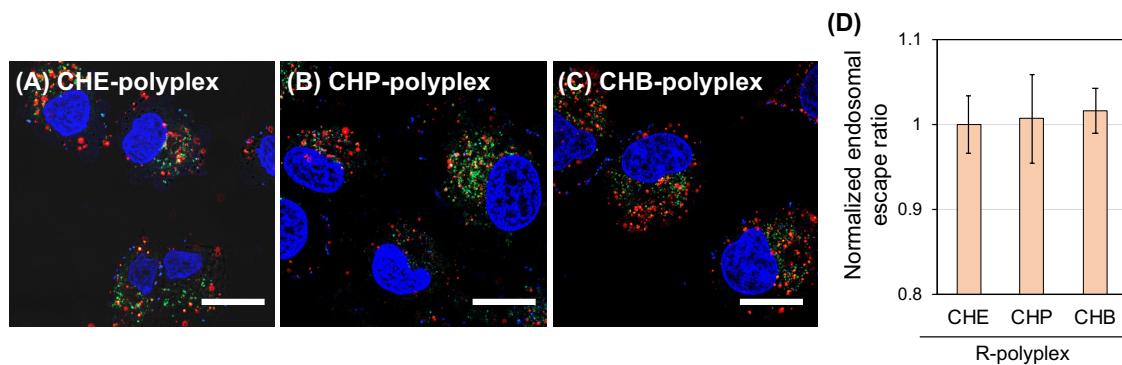


Figure 3-17. CLSM images of A549 cells treated with the Cy5-mRNA-loaded polyplexes for 5 h. ((A) CHE-, (B) CHP-, and (C) CHB-polyplex). Red, Green, and blue dots indicate Cy5, endosome, and nuclei, respectively. The scale bar represents 20 μ m. (D) Normalized endosomal escape ratio calculated from CLSM images.

3.4. Conclusions

In this chapter, a series of PAsp(DET/R)s bearing various alicyclic moieties were synthesized and a comparison of the effect of the R moieties on the enhancement of the mRNA delivery efficiency in cultured cells was presented. All PAsp(DET/R)s were synthesized with about a 55% introduction rate of R moieties, and polyplexes were prepared to have a similar hydrophobic diameter (~110 nm) and positive ζ -potential (~20 mV) with narrow size distribution, regardless of R moieties. However, the mRNA delivery efficiency depends on the R moiety. In the correlation of hydrophobicity ($\log D_{7.3}$) to mRNA delivery efficiency in cultured cells, an optimal $\log D_{7.3}$ range exhibiting efficient transfection was observed, which is consistent with the previously determined range ($\log D_{7.3} > -2.4$). The polyplexes achieved significantly improved *in vitro* mRNA delivery, comparable to a commercially available transfection agent (Lipofectamine MessengerMAX), other than CHM-polyplex ($\log D_{7.3} = -2.7$). This might be attributable to an enhanced cellular uptake of payload (mRNA) derived from increased polyplex stability against the adsorption of the anionic proteins. Among the PAsp(DET/R) library, the CHE, CHP, and CHPE units correspond to the optimized R moieties for *in vitro* mRNA delivery.

Reference

1. Kim, H. J., Ogura, S., Otabe, T., Kamegawa, R., Sato, M., Kataoka, K., Miyata, K. Fine-tuning of hydrophobicity in amphiphilic polyaspartamide derivatives for rapid and transient expression of messenger RNA directed toward genome engineering in brain. *ACS Cent. Sci.* **5**, 1866–1875 (2019).
2. Barnoud, J., Rossi, G., Marrink, S. J., Monticelli, L. Hydrophobic compounds reshape membrane domains. *PLoS Comput. Biol.* **10**, e1003873 (2014).
3. Mineo, H., Ogita, A., Kanayama, N., Kawagishi, M., Sato, E., Yamamoto, N., Arai, K., Izawa, M. A. Effects of the chemical specificity of benzoic acid and its analogs on osmotic fragility in erythrocytes of Sprague-Dawley rats in vitro. *Eur. J. Pharmacol.* **702**, 142–148 (2013).
4. Fischer, D., Bieber, T., Li, Y. X., Elsässer, H. P., Kissel T. A novel non-viral vector for DNA delivery based on low molecular weight, branched polyethylenimine: effect of molecular weight on transfection efficiency and cytotoxicity. *Pharm. Res.* **16**, 1273—1279 (1999).
5. Uchida, H., Itaka, K., Nomoto, T., Ishii, T., Suma, T., Ikegami, M., Miyata, K., Oba, M., Nishiyama, N., Kataoka, K. Modulated protonation of side chain aminoethylene repeats in N-substituted polyaspartamides promotes mRNA transfection. *J. Am. Chem. Soc.* **135**, 12396–12405 (2014).
6. Miyata, K., Oba, M., Nakanishi, M., Fukushima, S., Yamasaki, Y., Koyama, H., Nishiyama, N., Kataoka, K. Polyplexes from poly(aspartamide) bearing 1,2-diaminoethene side chains induce pH-selective, endosomal membrane destabilization with amplified transfection and negligible cytotoxicity. *J. Am. Chem. Soc.* **130**, 16287–16294 (2008).
7. Miyata, K., Nishiyama, N., Kataoka, K. Rational design of smart supramolecular assemblies for gene delivery: chemical challenges in the creation of artificial viruses. *Chem. Soc. Rev.* **41**, 2562–2574 (2012).

Chapter 4

Systemic messenger RNA delivery by using polyaspartamide derivatives

4.1. Chapter introduction

In previous research, polyaspartamide derivatives (PAsp(DET/R)) tailored with diethylenetriamine (DET) and hydrophobic (R) moieties in the chains were synthesized. Among them, the derivative (PAsp(DET/CHE)) bearing a cyclohexylethyl (CHE) moiety achieved efficient mRNA delivery in the brain *via* intracerebroventricular/intrathecal administration [1]. However, the *in vivo* mRNA delivery efficiency of PAsp(DET/R)s was not evaluated in systemic delivery. Systemic mRNA delivery is attractive for direct access to circulatory organs and can be utilized for protein replacement therapies and cancer immunotherapies [2,3]. Despite the potential of systemic delivery, mRNA is rapidly degraded in the extracellular milieu and cleared by the kidney due to its small size [4,5]. The presence and design of mRNA carriers are important to protect mRNA payloads and efficiently deliver them into the cell cytoplasm.

In **Chapter 4**, the PAsp(DET/R)s synthesized in **Chapter 3** were utilized for systemic mRNA delivery and the impact of R moieties on *in vivo* mRNA activities was studied after intravenous administration of mRNA-loaded polyplexes. A new PAsp(DET/R) library was synthesized to possess a short degree of polymerization (DP) of approximately 20 to decrease *in vivo* toxicity [6,21], and the derivatives with higher hydrophobicity were confirmed to exhibit efficient mRNA expression in cultured tumor cells in **Chapter 3**. The *in vivo* mRNA transfection efficiency and biodistribution of these PAsp(DET/R)s was evaluated *via* intravenous administration of polyplexes into the tail vein of mice (**Fig. 4-1**), and the optimized R moieties for *in vivo* mRNA delivery were investigated. Moreover, *in vivo* safety profiles of PAsp(DET/R)s were also examined.

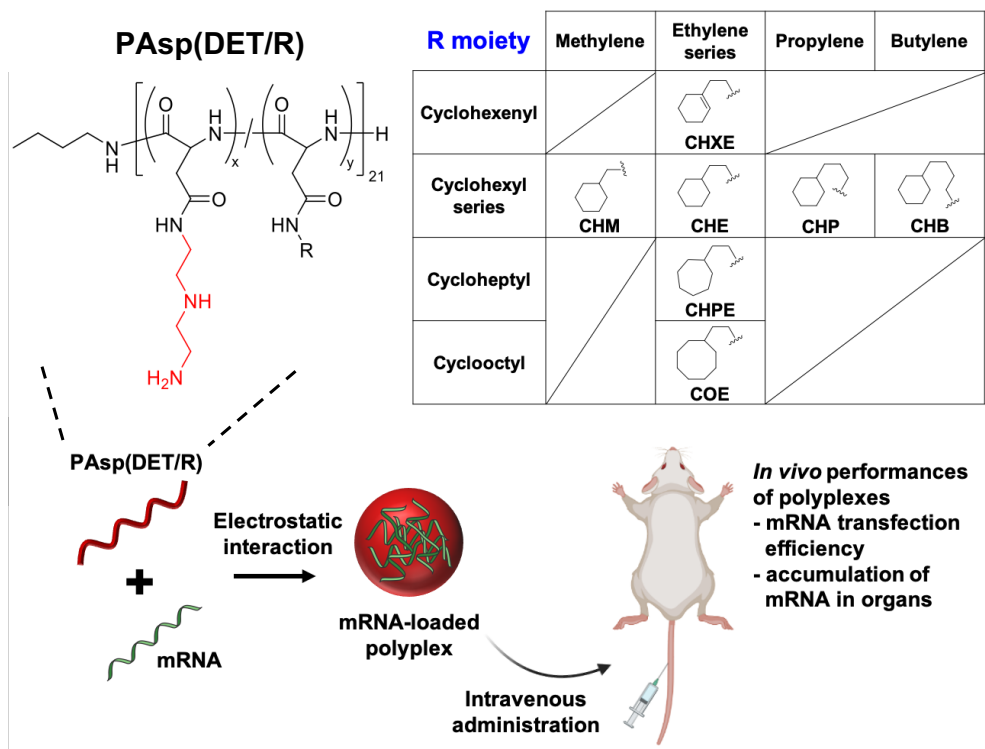


Figure 4-1. Schematic illustration of the study in **Chapter 4**. A series of PAsp(DET/R)s were utilized for systemic mRNA delivery.

4.2. Materials and methods

4.2.1. Materials

A series of PAsp(DET/R)s, luciferase-coded mRNAs (including Cy5-labeled GLuc-mRNA (Cy5-mRNA)), Lipofectamine MessengerMAX (LipoM), and HEPES buffer were purchased as abovementioned in **Chapter 3**. The polyplexes (R-polyplexes) were prepared by the association of PAsp(DET/R) and mRNA, according to the procedure detailed in **Chapter 3**. BALB/c white mice (6–8-week-old females) were purchased from Charles River Laboratories Japan, Inc. (Yokoyama, Japan). VivoGlo™ Luciferin (*in vivo* grade luciferin) and Renilla Luciferase Assay Lysis Buffer (lysis buffer) were purchased from Promega (Madison, WI, USA). All primers for a qRT-PCR assay were purchased from Hokkaido System Science Co., Ltd. (Hokkaido, Japan). RNeasy Mini Kit was purchased from Qiagen (Hilden, Germany). FastStart Universal SYBR Green Master (ROX) was purchased from Roche Diagnostics (Mannheim, Germany).

4.2.2. *In vivo* transfection efficiency via systemic messenger RNA (mRNA) delivery

A polyplex solution (N/P = 5) loading 3.0 µg Luc2-mRNA (150 µL, 10 mM HEPES) was mixed with a 20% glucose solution (50 µL, distilled water) for equivalent osmotic pressure in body fluids [7]. The mixed samples were intravenously injected into the tail of a BALB/c white mouse. Each organ/tissue was excised and homogenized with a lysis buffer. Luc2 expression levels were determined as relative luminescence unit (RLU) values of tissue lysates by a luminescence microplate reader (Mithras LB 940, Berthold Technologies, Bad Wildbad, Germany) with Luciferase Assay System (Promega, Madison, WI, USA). The obtained RLU values were normalized to the weight of the tissues.

4.2.3. Biodistribution assay derived from fluorescently labeled mRNA

A polyplex solution (N/P = 5) loading 3.0 µg Cy5-mRNA (150 µL, 10 mM HEPES) was mixed with a 20% glucose solution (50 µL, distilled water), and then intravenously injected into the tail of a BALB/c white mouse. After 4 h, each organ was harvested and homogenized in a lysis buffer. Then, the biodistribution of mRNA was determined by the fluorescence intensities of each organ lysate, measured by a microplate reader (Spark 20M, Tecan Group Ltd.).

4.2.4. Quantification of intact mRNA in each organ by qRT-PCR

A polyplex solution (N/P = 5) loading 3.0 µg Luc2-mRNA (150 µL, 10 mM HEPES) was mixed with a 20% glucose solution (50 µL, distilled water), and then intravenously injected into the tail of a BALB/c white mouse. After 4 h, each organ was harvested and lysed in RLT buffer with a small amount of β-mercaptoethanol. In each tissue lysate, RNAs were extracted using the RNeasy Mini Kit, and then 1 µg of RNAs was reverse transcribed to synthesize a complementary DNA (cDNA). The prepared cDNA (equivalent to 50 ng of RNA), the forward and reverse primers, and FastStart Universal SYBR Green Master (ROX) were mixed, and then qRT-PCR was performed using an ABI 7500 Fast Real-time PCR System (Applied Biosystems, Foster City, CA, USA), according to manufacturer's protocol. The quantification of Luc2-mRNA in each tissue sample was calculated by using GAPDH as an endogenous housekeeping gene. The primer sequences for GAPDH and Luc2 are summarized in **Table 4-1**.

Table 4-1. The primer sequences for GAPDH and Luc2

Primer	Sequence
GAPDH forward primer	5'-TGTGTCCGTCGTGGATCTGA-3'
GAPDH reverse primer	5'-TTGCTGTTGAAGTCGCAGGAG-3'
Luc2 forward primer	5'-CATGGATAGCAAGACCGACTAC-3'
Luc2 reverse primer	5'-GATGATCTGGTTGCCGAAGA-3'

4.2.5. Flow cytometric analysis

Flow cytometric analysis was performed to investigate the lung cells following intravenous administration of the polyplex. Specifically, lung tissues were collected at 4 h after intratracheal administration of the Cy5-mRNA-loaded polyplexes. Isolated cell suspensions were prepared by digesting the lung tissues at 37 °C for 1 h using an RPMI-1640 buffer containing 50 U/mL of DNase I (0.125 mg/mL, Sigma) and 300 U/mL and 100 U/mL of collagenase and hyaluronidase (STEMCELL Technologies), respectively. In addition, ACK buffer treatment was performed to lysis red blood cells. To separate immune (CD45 positive) cells from the cell suspension, the cells were modified with CD45 antibody-conjugated magnetic beads by adding 10 µL of CD45 MicroBeads (Miltenyi BioTec), followed by 15 min of incubation at 4 °C. The cells were washed after adding 2 mL of PBS containing 0.5% BSA and 2 mM, which was used as an antibody reaction buffer, and centrifuging for 10 min at 300g and 4 °C, after which they were resuspended in 500 µL of the antibody reaction buffer. The cell suspension was placed in a magnetic holder (EasySep™ Magnet, STEMCELL Technologies) and incubated for 5 min at room temperature. The supernatant was poured out into a different tube to separate the CD45 negative cells. The tube was removed from the magnetic holder, and the CD45 positive cells attached on the bottom of the tube were suspended in 100 µL of the antibody reaction buffer. The antibody staining of CD45 negative cells was performed to distinguish epithelial and endothelial

cells. Before the antibody staining, Fc receptors were blocked to avoid non-specific antibodies by the addition of 0.25 μg (0.5 μL) of TruStain FcXTM PLUS per 1×10^6 cells, which was mixed with the cell suspension followed by 5 min incubation on ice. APC/Cyanine7 anti-mouse CD326 antibody and Alexa Fluor® 488 anti-mouse CD11c antibody were added to the cell suspension and incubated for 15 min at 4 °C. The cell suspensions were washed three times by adding the antibody reaction buffer up to 1.5 mL for centrifugation. The final suspension was obtained with the addition of 500 μL of PBS. Then, dead cells were then stained with 250 μL of PI solution (2 $\mu\text{g}/\text{mL}$) for 20 min at 37 °C in a dark environment. Without washing, the flow cytometric analysis was performed using a flow cytometer, BD AccuriTM C6 Plus.

4.2.6. Evaluation of mRNA transfection efficiency in the cell culture media with various FBS concentrations.

The mRNA transfection experiment was performed using a slightly modified protocol from the method detailed in **Chapter 3.2.5**. The difference being that DMEM with various FBS concentrations (10% FBS, 20% FBS, and 40% FBS) were used as cell culture media. The expression efficiencies of GLuc-mRNA were determined from the luminescence intensities of the cell supernatants diluted 40 times, using a luciferase assay.

4.2.7. *In vivo* safety test

For the evaluation of *in vivo* polyplex safety, the levels of the blood chemistry components, *i.e.*, alanine aminotransferase (ALT), aspartate aminotransferase (AST), creatinine (CRE), and blood urea nitrogen (BUN), were compared in the plasma of polyplex- and non-treated mice. A polyplex solution (N/P = 5) loading 3.0 μg Luc2-mRNA (150 μL , 10 mM HEPES) was mixed with a 20% glucose solution (50 μL , distilled water), and then intravenously injected

into the tail of a BALB/c white mouse. After 24 h, blood was collected and centrifuged at 1,500g for 10 min to obtain the plasma. The levels of blood chemistry components were measured using DRI-CHEM 7000i with each suitable DRI-CHEM slide (Fujifilm, Tokyo, Japan).

4.3. Results and discussion

4.3.1. *In vivo* transfection efficiency of Luc2-mRNA-loaded polyplexes

The *in vivo* mRNA delivery efficiencies of the PAsp(DET/R)s were investigated. Luc2-mRNA-loaded polyplexes (3 μ g mRNA/mouse) were intravenously administered to the mice. LipoM was also injected as a control in the same manner. The luciferase expression efficiency in each organ was quantitatively evaluated by IVIS measurements at 4 h after administration of mRNA-loaded samples (**Fig. 4-2a, b**). The effect of R moieties on mRNA expression efficiencies was slightly different between the *in vitro* and *in vivo* cases. PAsp(DET/CHE), followed by PAsp(DET/CHXE), exhibited the highest *in vivo* mRNA transfection efficiency, but were not the optimal derivatives for *in vitro* mRNA expression. The CHM- and CHB-polyplexes exhibited prominently low *in vivo* transfection efficiency. The tendency of the CHM-polyplex for low transfection efficiency *in vivo* was similar to that *in vitro*, and was probably attributable to the instability of the CHM-polyplex. Meanwhile, the *in vivo* mRNA transfection efficiency of the CHB-polyplex was remarkably different from the *in vitro* transfection efficiency, although the *in vitro* transfection level of the CHB-polyplex was comparable to those of CHE- and CHXE-polyplex. This indicates that excessively higher hydrophobicity ($\log D_{7.3} > -1.2$) might not be suitable for systemic mRNA delivery (**Fig. 4-3**). A previous study found a similar result in which the *in vivo* mRNA expression efficiency drops sharply when the length of the alkyl group (or hydrophobicity) is higher than the optimized length in the side chains of polyester-based polymers [8]. This might be due to the interruption of mRNA release through the formation of aggregates between the polyplexes and blood components [9]. These results indicate that the effective $\log D_{7.3}$ range for systemic mRNA delivery is narrower than that for efficient *in vitro* mRNA transfection (**Fig. 4-3**). In the comparison of the mRNA expression efficiency among the organs, all polyplexes elicited the highest mRNA expression in the lungs, followed by the spleen. Remarkably low

mRNA expression was observed from the other organs, *i.e.*, liver, kidney, heart, and muscle, compared to the lungs and spleen. Notably, in the mice intravenously injected with CHE- and CHXE-polyplexes, approximately 95% of all mRNA expressions were found in the lungs. Similarly, it has been reported that some cationic polymer-carriers exhibit lung-selective mRNA delivery, such as polyesters with amino and alkyl moieties (forming polyplexes) and poly(β -amino ester) terpolymers formulated with a PEG-lipid (forming lipopolyplexes) [10–12]. These mRNA expression profiles of polyplexes were not identical to that of LipoM, which exhibited higher transfection efficiency mainly in the spleen.

From the *in vivo* mRNA expression profile, two questions arise; why does the polyplex mainly deliver mRNA to the lungs, and why does a polyplex with relatively higher hydrophobicity show lower *in vivo* mRNA expression? These questions are further investigated and covered in the following sections.

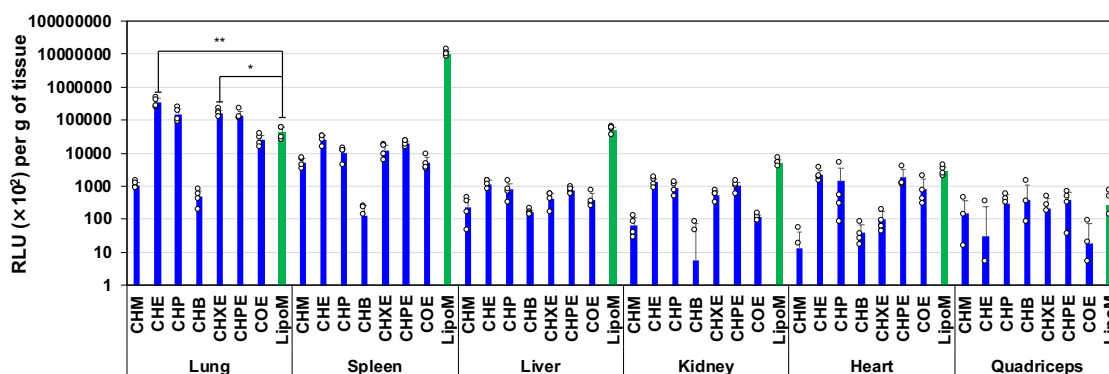


Figure 4-2. (A) mRNA expression levels in various organs/tissues at 4 h after intravenous injection of Luc2-mRNA-loaded polyplexes or LipoM (3 μ g mRNA/mouse). Each organ/tissue was excised and homogenized with a lysis buffer, followed by a luciferase assay of tissue lysates. The obtained RLU values were normalized by the tissue weight. Results are expressed as mean \pm SD ($n = 4$; $*p < 0.05$ and $**p < 0.01$).

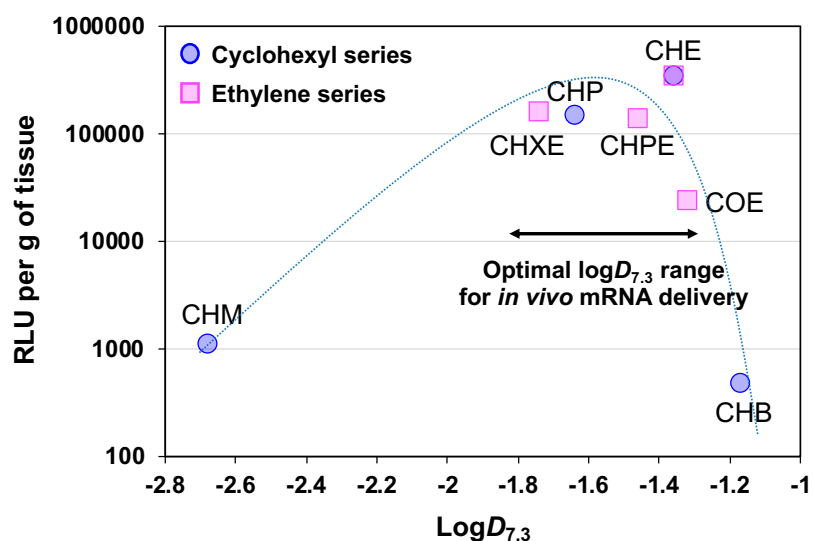


Figure 4-3. Correlation between luminescence intensities in the lung at 4 h after intravenous administration of polyplexes and the $\log D_{7.3}$ value of PAsp(DET/R)s.

4.3.2. Biodistribution assays derived from fluorescently labeled mRNA and intact mRNA

In order to understand the lung-targeting specificity of the polyplexes, the two kinds of biodistribution assays were performed. First, the biodistribution profiles were determined by the Cy5 fluorescence intensities from homogenized organ solutions at 4 h after intravenous injection of Cy5-mRNA-loaded polyplex samples (**Fig. 4-4**). Astonishingly, the mRNA biodistribution profile did not match the *in vivo* expression profile. After intravenous injection, the Cy5-mRNA existed overall in the lungs, the spleen, the liver, and the kidneys, despite the mRNA expression mainly in the lungs. Furthermore, the accumulation levels of Cy5-mRNA in the spleen and the liver were higher than that in the lungs. Several previous studies also reported the inconsistency between the profiles of *in vivo* mRNA expression and biodistribution in the organs after intravenous administration of mRNA-loaded nanoparticles [11,13,14]. This suggests that the Cy5-based biodistribution results might not properly reflect the exact accumulation amount of

bioavailable mRNA, presumably due to the overestimation of Cy5 from inactive (or degraded) mRNA.

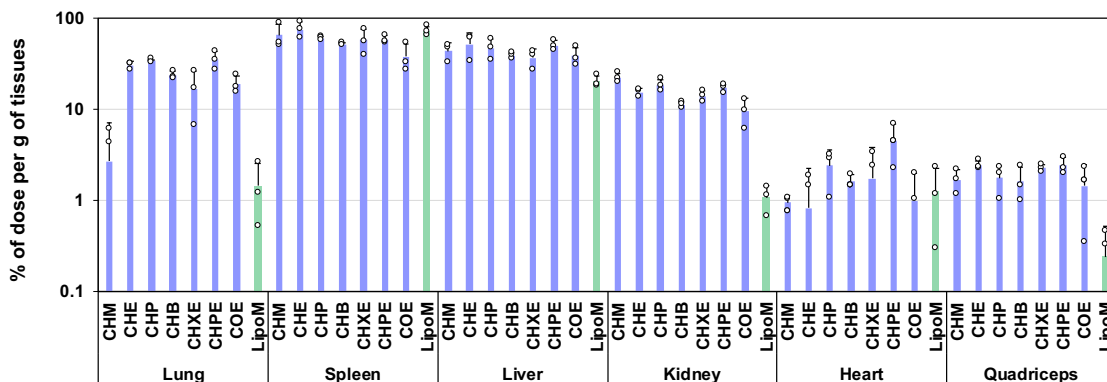


Figure 4-4. Biodistribution of Cy5-mRNA in mice at 4 h after intravenous administration of polyplexes or LipoM. All results are expressed as mean \pm SD ($n = 3$).

Next, the biodistribution of intact mRNA in the organ tissues was measured by using qRT-PCR. The CHE- and CHXE-polyplexes were utilized as the representatives of the R-polyplexes. The accumulation levels of intact mRNA were the highest in the lungs, followed by the spleen and the liver (**Fig. 4-5a, b**). These results matched with the magnitude order of the *in vivo* mRNA delivery efficiency in the organs (**Fig. 4-5d, e**). Meanwhile, in the case of LipoM, the largest amounts of intact mRNA were accumulated in the spleen, followed by the lungs and the liver (**Fig. 4-5c**), which is also consistent with the magnitude order of the *in vivo* transfection efficiency (**Fig. 4-5f**). Thus, the intact mRNA accumulation levels considerably reflected the *in vivo* expression profiles. Although the fundamental mechanisms underlying the lung-specific targeting of the polyplex-based mRNA delivery are not known, there are some possible reasons. First, the lung is the first organ that intravenously injected nanoparticles encounter, except for the heart (**Fig. 4-6a**) [15, 16]. This indicates there is a higher opportunity for delivering large amounts of intact mRNA to the lungs. Indeed, it was confirmed that the highest mRNA amount was

accumulated in the lungs in a short time, 5 min after CHE-polyplex administration (**Fig. 4-6b**). Another possibility is the specific targeting by endogenous proteins. In the bloodstream, hepatocyte targeting proteins, including apolipoprotein E, attached to the surface of the various lipid-based nanoparticles, leading to the delivery of the mRNA payload to the liver [17,18]. The positively charged polyplexes prepared by PAsp(DET/R)s also attach serum proteins in the bloodstream to the surface. Among them, a certain protein might elicit the lung-specific targeting and internalization of the polyplexes into the lungs. Overall, the results indicate that R moieties in PAsp(DET/R)s substantially changed *in vivo* mRNA transfection efficiency after the intravenous administration of polyplexes. The optimized structures, *i.e.*, PAsp(DET/CHE) followed by PAsp(DET/CHXE), achieved effective mRNA delivery to the lungs, and the mRNA transfection efficiency in the lungs was appreciably higher than that of LipoM.

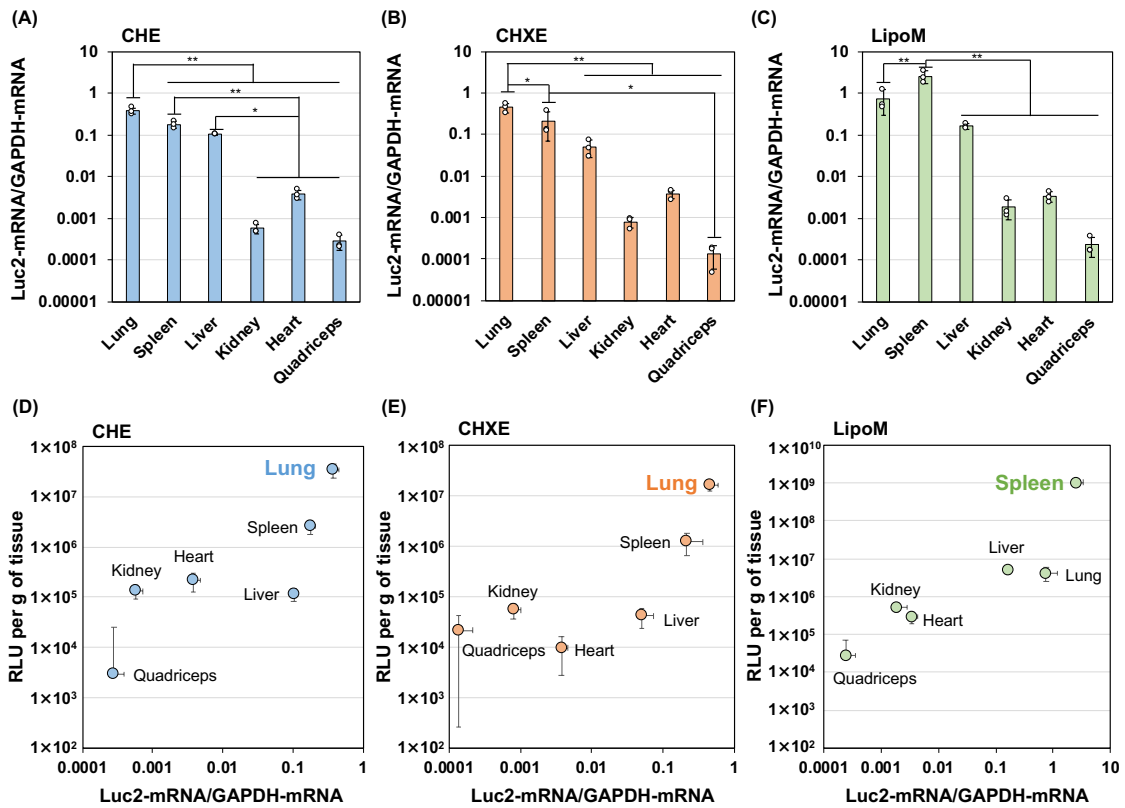


Figure 4-5. Biodistribution of intact mRNA in mice 4 h after intravenous injection of (A) CHE-, (B) CHXE-polyplexes, and (C) LipoM, measured by qRT-PCR. Results are expressed as mean \pm SD ($n = 3$). The *in vivo* Luc2-mRNA expression levels plotted against the distribution of intact mRNA in each organ. (D) CHE-polyplex, (E) CHXE-polyplex, and (F) LipoM.

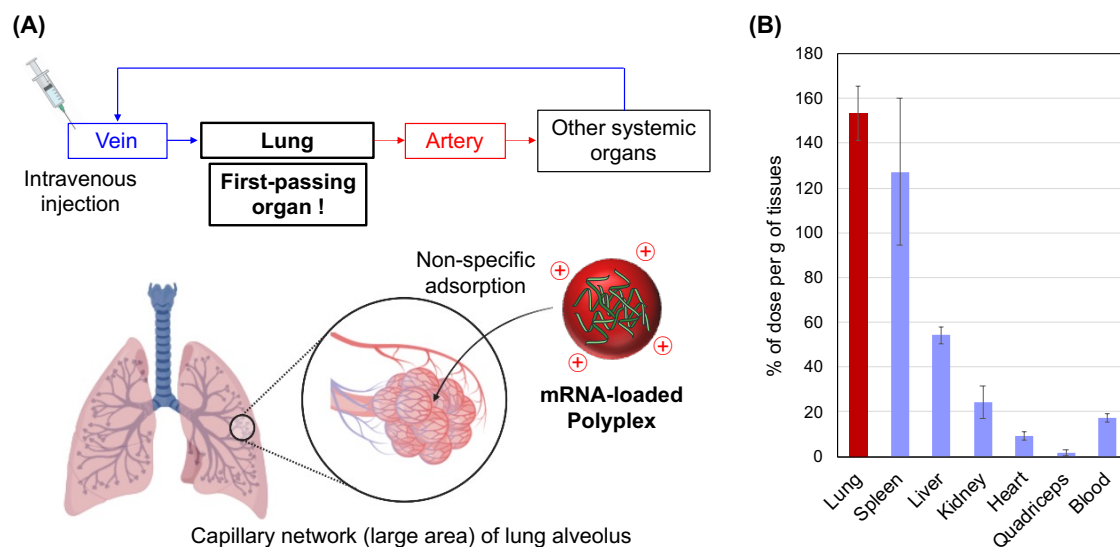


Figure 4-6. (A) Schematic illustrating the lung-preferred delivery of polyplexes after intravenous administration. (B) Biodistribution of Cy5-mRNA in mice at 4 h after intravenous administration of the CHE-polyplex. The results are expressed as mean \pm SD ($n = 3$).

4.3.3. Quantification of intact mRNA in the lung tissues and cellular uptake in the lung cells by flow cytometric analysis

To further investigate why the CHB-polyplex exhibited lower *in vivo* mRNA expression, the amount of intact mRNA in the lung tissues was evaluated by qRT-PCR (**Fig. 4-7**). The CHM-polyplex showed a lower mRNA amount due to its lower stability. However, the CHB-polyplex showed similar intact mRNA accumulation, comparable to the CHE- and CHXE-polyplex, despite its lower *in vivo* mRNA expression. The cellular uptake of the polyplexes in the lung cells was examined by flow cytometric analysis (**Fig. 4-8**), which confirmed that the CHB-polyplex delivered mRNA into the epithelial, endothelial, and immune cells in the lung tissues. Furthermore, this distribution was similar to that of the CHE-polyplex. From the previous two results, the internalization of the CHB-polyplex in the lung cells could be ascertained, indicating that the intracellular activity of the CHB-polyplex was less efficient for mRNA expression.

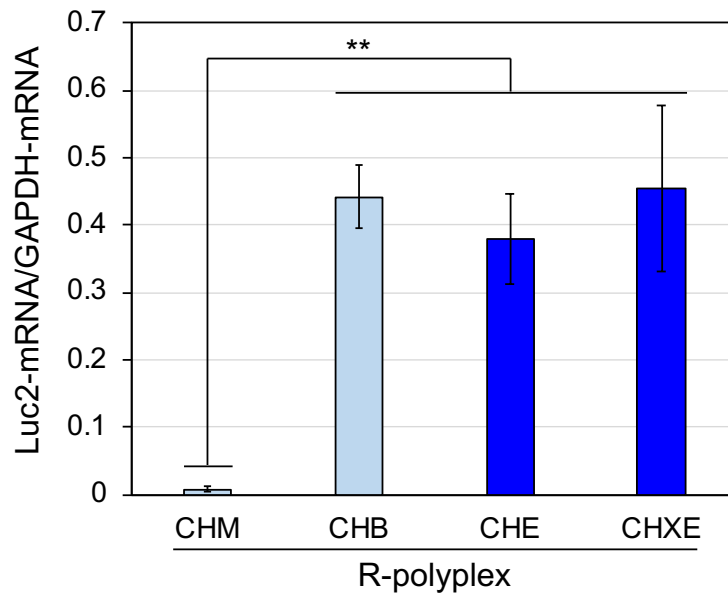


Figure 4-7. The amount of intact mRNA in the lung tissues 4 h after intravenous injection of polyplexes, measured by qRT-PCR. Results are expressed as mean \pm SD ($n = 3$).

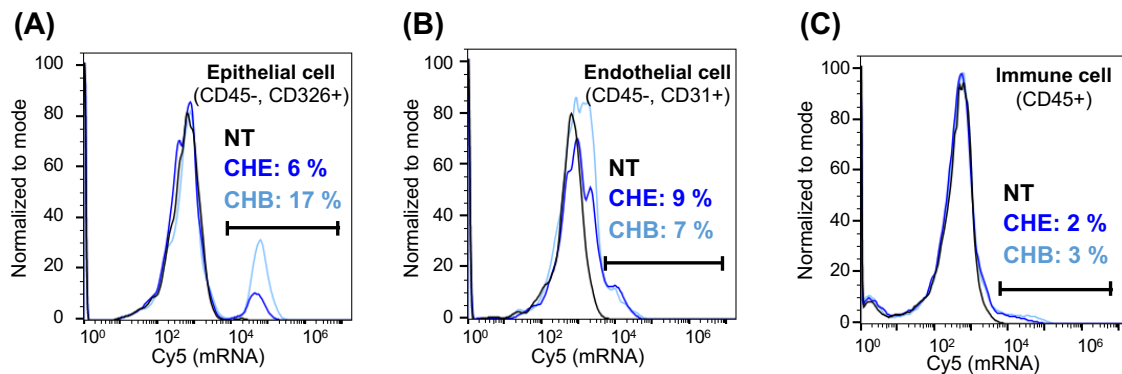


Figure 4-8. Histogram of Cy5 intensities derived from mRNA delivered by CHE- and CHB-polyplex in epithelial (A), endothelial (B), and immune cells (C).

4.3.4. *In vitro* mRNA transfection efficiency in the cell culture media with various FBS concentrations

It is hypothesized that the association of the CHB-polyplex exhibiting higher hydrophobicity with high amounts of proteins in the blood induces the disturbance of mRNA expression. Therefore, mRNA expression was evaluated in the cell culture media with various FBS concentrations (**Fig. 4-9**). Compared to the CHM-, CHE-, and CHP-polyplexes, the CHB-polyplex showed a significant decrease in mRNA expression when the FBS concentration increased from 10% to 40%. Furthermore, the mRNA expression profile in the higher FBS concentration (40 %) was similar to that *in vivo*. This suggests that the interaction between high blood proteins and the CHB-polyplex with the highest hydrophobicity might induce the suppression of mRNA expression. Therefore, it was revealed that the polyplexes with excessive hydrophobicity are less effective in mRNA delivery.

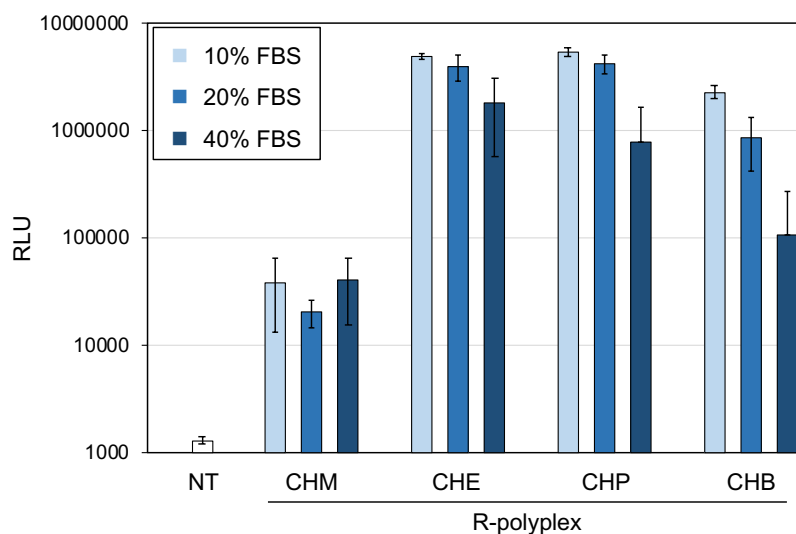


Figure 4-9. Relative luminescence intensities of A549 cells transfected with GLuc-mRNA (50 ng) *via* the polyplex in the cell culture media with various FBS concentrations. Results are expressed as mean \pm SD ($n = 4$).

4.3.4. *In vivo* safety test

To investigate *in vivo* safety of polyplexes, the level of blood chemical parameters, *i.e.*, ALT, AST, CRE, and BUN, were measured in the plasma of mice at 24 h after being treated by the CHE- and CHXE-polyplexes (**Fig. 4-10**). ALT/AST and CRE/BUN are major markers of liver and spleen injury, respectively, because their levels increase after liver and spleen damage [19]. The levels of ALT, AST, and CRE in the plasma of polyplex-treated mice were similar to those of non-treated controls. Although the levels of BUN of polyplex-treated mice was slightly higher than those of the non-treated ones, the levels were within the range of non-treated mice from a previous study conducted using the same protocol and device [20]. These results indicate that CHE- and CHXE-polyplexes have negligible *in vivo* toxicity.

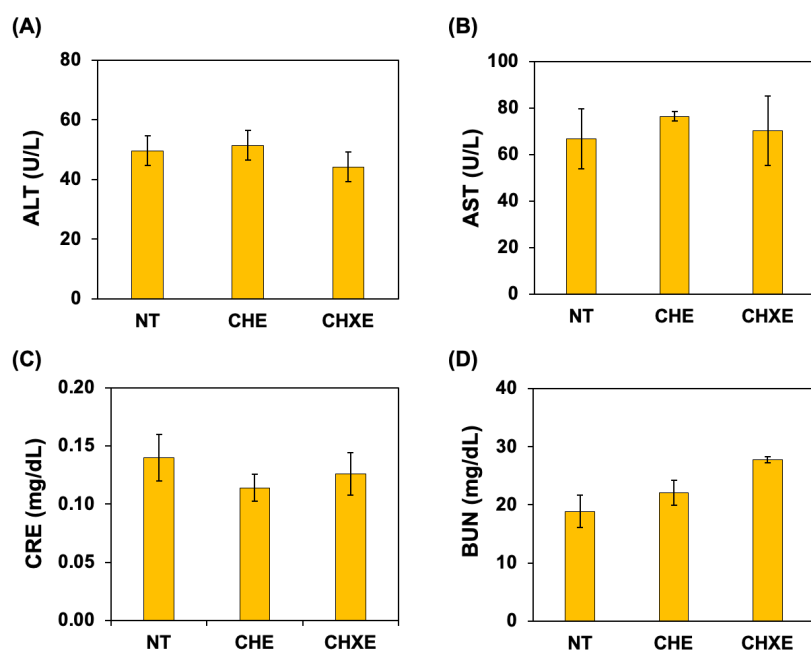


Figure 4-10. The levels of blood chemistry components, (A) ALT, (B) AST, (C) CRE, (D) BUN.

Results are expressed as mean \pm SD ($n = 5$).

4.3. Conclusions

This study aimed at optimizing alicyclic (R) moieties of PAsp(DET/R)s for enhanced systemic mRNA delivery. *In vivo* mRNA delivery efficiency strongly depends on the R moieties of the derivatives. The polyplexes formed by PAsp(DET/R)s having $\log D_{7.3}$ values between -1.8 and -1.3 , elicited efficient systemic mRNA delivery. PAsp(DET/CHM) ($\log D_{7.3} = -2.7$) exhibited extremely limited *in vivo* mRNA delivery efficiency, presumably due to the insufficient polyplex stability caused by low hydrophobicity. In addition, while PAsp(DET/CHB) ($\log D_{7.3} = -1.2$) achieved higher *in vitro* mRNA expression efficiency, it showed remarkably low *in vivo* mRNA expression. This indicates that the optimized $\log D_{7.3}$ range for efficient *in vivo* mRNA delivery was narrower than that for *in vitro* cellular delivery. Interestingly, the polyplex achieved higher *in vivo* transfection efficiencies in the lung, compared to the LipoM, which exhibited mRNA expression mainly in the spleen. The lung-specific targeting by the polyplexes was highly correlated to the accumulation of intact mRNA determined by qRT-PCR, but was inconsistent with the biodistribution of fluorescently labeled mRNA. Overall, this research demonstrates the potential of PAsp(DET/R) with fine-tuned R moieties for effective *in vivo* mRNA delivery, especially to the lungs, indicating that it could be utilized for therapeutic mRNA applications.

References

1. Kim, H. J., Ogura, S., Otabe, T., Kamegawa, R., Sato, M., Kataoka, K., Miyata, K. Fine-tuning of hydrophobicity in amphiphilic polyaspartamide derivatives for rapid and transient expression of messenger RNA directed toward genome engineering in brain. *ACS Cent. Sci.* **5**, 1866–1875 (2019).
2. Karikó, U. K., Türeci, Ö. mRNA-based therapeutics—developing a new class of drugs. *Nat. Rev. Drug Discov.* **13**, 759–780 (2014).
3. Pardi, N., Hogan, M. J., Porter, F. W., Weissman, D. mRNA vaccines – a new era in vaccinology, *Nat. Rev. Drug Discov.* **17**, 261–279 (2018).
4. Seymour, L. W., Duncan, R., Strohalm, J., Kopecek, J. Effect of molecular weight of N-(2-hydroxypropyl) methacrylamide copolymers on body distribution and rate of excretion after subcutaneous, intraperitoneal, and intravenous administration to rats. *J. Biomed. Mater. Res.* **21**, 1341–1358 (1987).
5. Choi, H. S., Liu, W., Misra, P., Tanaka, E., Zimmer, J. P., Ipe, B. I., Bawendi, M. G., Frangioni, J. V. Renal clearance of quantum dots. *Nat. Biotechnol.* **25**, 1165–1170 (2007).
6. Fischer, D., Bieber, T., Li, Y. X., Elsässer, H. P., Kissel T. A novel non-viral vector for DNA delivery based on low molecular weight, branched polyethylenimine: Effect of molecular weight on transfection efficiency and cytotoxicity. *Pharm. Res.* **16**, 1273—1279 (1999).
7. Caon, M. Osmoles, osmolality and osmotic pressure: Clarifying the puzzle of solution concentration. *Contemp. Nurse* **29**, 92–99 (2008).
8. Yu, X., Liu, S., Cheng, Q., Lee, S. M., Wei, T., Zhang, D., Farbiak, L., Johnson, L.T., Wang, X., Siegwart, D. J. Hydrophobic optimization of functional poly(TPAE-co-suberoyl chloride) for extrahepatic mRNA delivery following intravenous administration. *Pharmaceutics* **13**, 1914 (2021).
9. Nomoto, T., Matsumoto, Y., Miyata, K., Oba, M., Fukushima, S., Nishiyama, N., Yamasoba, T., Kataoka, K. In situ quantitative monitoring of polyplexes and polyplex micelles in the blood circulation using intravital real-time confocal laser scanning microscopy. *J. Control. Release* **151**, 104–109 (2011).
10. Yan, Y., Xiong, H., Zhang, X., Cheng, Q., Siegwart, D. J. Systemic mRNA Delivery to the Lungs by Functional Polyester-based Carriers. *Biomacromolecules* **18**, 4307–4315 (2017).
11. Kaczmarek, J. C., Patel, A. K., Kauffman, K. J., Fenton, O. S., Webber, M. J., Heartlein, M.

- W., DeRosa, F., Anderson, D. G. Polymer-lipid nanoparticles for systemic delivery of mRNA to the lungs. *Angew. Chem. Int. Ed.* **55**, 13808–13812 (2016).
12. Kaczmarek, J. C., Patel, A., K., Rhym, L. H., Palmiero, U. C., Bhat, B., Heartlein, M. W., DeRosa, F., Anderson, D. G. Systemic delivery of mRNA and DNA to the lung using polymer-lipid nanoparticles. *Biomaterials* **275**, 120966 (2021).
 13. Verbeke, R., Lentacker, I., Wayteck, L., Breckpot, K., Bockstal, M. V., Descamps, B., Vanhove, C., De Smedt, S. C., Dewitte, H. Co-delivery of nucleoside-modified mRNA and TLR agonists for cancer immunotherapy: Restoring the immunogenicity of immunosilent mRNA. *J. Control. Release* **266**, 287–300 (2017).
 14. Ke, X., Shelton, L., Hu, Y., Zhu, Y., Chow, E., Tang, H., Santos, J. L., Mao, H. Q. Surface-functionalized PEGylated nanoparticles deliver messenger RNA to pulmonary immune cells. *ACS Appl. Mater. Interfaces* **12**, 35835–35844 (2020).
 15. Ruberte, J., Navarro, M., Carretero, A., König, H. E., Circulatory System, in: Ruberte, J., Carretero, A., Navarro, M. (Eds.) Morphological mouse phenotyping: Anatomy, histology and imaging. Elsevier Inc. *Academic Press*. pp. 269–347 (2017).
 16. Blanco, E., Shen, H., Ferrari, M. Principles of nanoparticle design for overcoming biological barriers to drug delivery. *Nat. Biotechnol.* **33**, 941–951 (2015).
 17. Yan, X., Kuipers, F., Havekes, L. M., Havinga, R., Dontje, B., Poelstra, K., Scherphof, G. L., Kamps, J. A. The role of apolipoprotein E in the elimination of liposomes from blood by hepatocytes in the mouse. *Biochem. Biophys. Res. Commun.* **328**, 57–62 (2005).
 18. Akinc, A., Querbes, W., De, S., Qin, J., Frank-Kamenetsky, M., Jayaprakash, K. N., Jayaraman, M., Rajeev, K. G., Cantley, W. L., Dorkin, J. R., Butler, J. S., Qin, L., Racie, T., Sprague, A., Fava, E., Zeigerer, A., Hope, M. J., Zerial, M., Sah, D. W. Y., Fitzgerald, K., Tracy, M. A., Manoharan, M., Kotliansky, V., Fougereolles, A. D., Maier, M. A. Targeted delivery of RNAi therapeutics with endogenous and exogenous ligand-based mechanisms. *Mol. Ther.* **18**, 1357–1364 (2010).
 19. Pratt, D. S., Kaplan, M. M. Evaluation of abnormal liver-enzyme results in asymptomatic patients. *N. Engl. J. Med.* **342**, 1266–1271 (2000).
 20. Lee, J., Kim, D., Son, E., Yoo, S. J., Sa, J. K., Shin, Y. J., Yoon, Y., Nam, D. H. Pharmacokinetics, biodistribution, and toxicity evaluation of anti-SEMA3A (F11) in *in vivo* models. *Anticancer Res.* **38**, 2803–2810 (2018).

21. Moghimi, S. M., Symonds, P., Murray, J. C., Hunter, A. C., Debska, G., Szewczyk, A. A two-stage poly(ethylenimine)- mediated cytotoxicity: Implications for gene transfer/ therapy. *Mol. Ther.* **11**, 990–995 (2005).

Chapter 5
Concluding Remarks

5.1. Concluding Remarks

In this thesis, the author focused on the molecular design of amphiphilic cationic polymers for efficient nucleic acid delivery. **Chapter 1** introduced various kinds of nucleic acids as novel biopharmaceuticals and their reaction mechanisms in the target cells. Next, the author described the delivery strategies of nucleic acids, *i.e.*, chemical modifications and delivery vehicles, to overcome the limitation of naked nucleic acids such as high fragility and inefficient cellular uptake. The strategies elicited enhanced stability and cellular uptake efficiency of nucleic acids. Among the strategies, the author paid specific attention to polymeric nanoparticles (polyplexes), due to the ease of preparation in aqueous buffers and high functionalization by fine-tuning the components of the polymer chemical structure. Then, various polymer designs (functionalization) were described for efficient nucleic acid delivery, in terms of polyplex stability in the extracellular milieu, endosomal escape, and biodegradability. Among the functionalized polymers, amphiphilic polyaspartamide derivatives (PAsp(DET/R)s) with diethylenetriamine (DET) and hydrophobic (R) moieties were discussed as effective mRNA delivery carriers. In PAsp(DET/R)s, the R moieties substantially affect the mRNA transfection efficiencies, and a hydrophobicity ($\log D_{7.4}$) threshold was clearly observed at around -2.4 for efficient *in vitro* mRNA delivery. PAsp(DET/R)s with $\log D_{7.3}$ values larger than -2.4 exhibited appreciably higher mRNA expression efficiencies compared with the counterparts with $\log D_{7.3}$ values lower than -2.4 . Ultimately, a polyaspartamide derivative comprising cyclohexylethyl (CHE) moieties, PAsp(DET/CHE), showed the highest mRNA delivery efficiency in the cultured cells and in the brain *via* local injection. However, the viability of the PAsp(DET/R)s for the delivery of other nucleic acids and systemic mRNA delivery was not determined. In this study, the author focused on the molecular design of polyaspartamide derivatives, by highlighting the R moiety, for efficient

antisense oligonucleotide delivery and systemic mRNA delivery in **Chapter 2**, and **Chapters 3 and 4**, respectively.

In **Chapter 2**, the author studied the impact of R moieties on the *in vitro* ASO transfection efficiency. Before the evaluation of the *in vitro* ASO transfection efficiency, the formation of ASO-loaded polyplexes was confirmed, which exhibited equivalent hydrodynamic size and zeta-potential independent of the various R moieties. It was revealed that the ASO transfection efficiency of PAsp(DET/R)s depends on the R moieties. The presence of a threshold for efficient ASO expression by the polyplexes was observed in the $\log D_{7.4}$ value of PAsp(DET/R)s at approximately -2.4 . The derivatives with a $\log D_{7.4}$ value greater than the threshold exhibited substantially higher ASO delivery, which proved to be due to enhanced cellular uptake of the ASO payloads caused by higher polyplex stability. Consequently, the author determined the optimal R moieties for efficient ASO delivery.

In **Chapters 3 and 4**, the author aimed at improving systemic mRNA delivery *via* polyplex by synthesizing and comparing PAsp(DET/R)s tailored with various alicyclic (R) moieties, which are slightly different from the CHE moiety. The synthetic and *in vitro* transfection results of the new PAsp(DET/R) library were described in **Chapter 3**. While all PAsp(DET/R)s possessed equivalent introduction rates of the alicyclic moieties, they exhibited varying $\log D_{7.3}$ values based on the different R structures. All polyplexes exhibited higher *in vitro* mRNA delivery efficiencies, comparable to the commercially available Lipofectamine MessengerMAX (LipoM) control, except for the polyplex formed by the cyclohexylmethyl (CHM)-installed derivative (PAsp(DET/CHM)). This was attributed to PAsp(DET/CHM) having a lower $\log D_{7.3}$ value, resulting in limited polyplex stability and cellular uptake. The effect of the R moieties in the PAsp(DET/R)s synthesized in **Chapter 3** was investigated with respect to systemic mRNA delivery in **Chapter 4**. The polyplexes with $\log D_{7.3}$ values between -1.8 and -1.3 elicited efficient

systemic mRNA delivery into the lungs, compared to commercially available Lipofectamine MessengerMAX control. Whereas the derivative with a $\log D_{7.3}$ value of -1.3 showed higher *in vitro* mRNA delivery, it exhibited limited *in vivo* expression levels in the organs, indicating the optimized $\log D_{7.3}$ range for systemic mRNA delivery is narrower than that for *in vitro* delivery. Although the reason for the inconsistency between the *in vivo* and *in vitro* expression profiles was not revealed, it is presumed that excessive hydrophobicity interfered with mRNA expression *in vivo*. The lung-preferential mRNA expression by the polyplex was consistent with the amount of intact mRNA measured by qRT-PCR, whereas the biodistribution of fluorescently labeled mRNA was less well matched, probably due to overestimation derived from inactive (degraded) mRNA. This study demonstrates the potential of PAsp(DET/R)s with fine-tuned R moieties for polyplex-based mRNA delivery to the lungs for therapeutic applications.

In this thesis, the author developed PAsp(DET/R)s for efficient nucleic acid delivery by fine-tuning hydrophobic moiety and demonstrated the therapeutic potential of PAsp(DET/R)s for lung-targeted delivery *via* a polyplex. However, the polyplexes in this study have positive zeta-potential, resulting in short blood circulation time, followed by limited nucleic acid delivery. The introduction of biocompatible PEG into the polymer elicits enhanced stability and prolonged circulation time in the bloodstream. However, an excessive amount of PEG components in the polymer might invalidate the lung-selective property. Therefore, it is expected that optimization of the PEG introduction amount will improve the *in vivo* transfection efficiency in the lungs.

Appendix

A. List of publications

1. **J. Yum**, B. S. Kim, M. Naito, H. J. Kim, and K. Miyata, “Efficient antisense oligonucleotides delivery using polyaspartamide derivatives with fine-tuned hydrophobicity to brain via intracerebroventricular administration”, *in preparation*.
2. **J. Yum**, B. S. Kim, S. Ogura, R. Kamegawa, M. Naito, Y. Yamasaki, H. J. Kim, K. Miyata, “Fine-tuning of Polyaspartamide Derivatives with Alicyclic Moieties for Systemic mRNA Delivery”, *Journal of Controlled Release*, *under review*.

B. Other publications

1. B. S. Kim, S. Osawa, **J. Yum**, M. Naito, and K. Miyata, “Installation of thermoswitchable hydrophobic domain into unimer polyion complex for enhanced cellular uptake of siRNA”, *Bioconjugate Chem.* **2020**, 31, 1320–1326.

C. Conferences

1. **J. Yum**, M. Naito, H. J. Kim, K. Miyata, “Size-controlled nano brush polymer carriers to target intractable cancers”, The 15th SNU-UT-TU Workshop, Korea, October 2019.
2. **J. Yum**, M. Naito, and K. Miyata, “Size-controlled polymer brush for intractable cancer targeting”, 2nd G‘L’owing Polymer Symposium in KANTO, Tokyo, Japan, November 2020.
3. **J. Yum**, M. Naito, H. J. Kim, and K. Miyata, “グラフトポリマー型ナノキャリアの設計と固形がんへの集積性に対するサイズ効果の検討”, The 69th SPSJ Annual Meeting, Japan, May 2020.

4. **J. Yum**, M. Naito, H. J. Kim, and K. Miyata, “Design of polyaspartamide derivatives with varying hydrophobic moieties for efficient mRNA delivery to ex vivo T cells”, The 36th Annual Meeting of the Japan Society of Drug Delivery System, Japan, August 2020.
5. **J. Yum**, B. S. Kim, M. Naito, H. J. Kim, and K. Miyata, “Development of amphiphilic polyaspartamide derivatives for systemic messenger RNA delivery to lung”, 2021 CRS Virtual Annual Meeting, Online, July 2021.
6. **J. Yum**, B. S. Kim, M. Naito, H. J. Kim, and K. Miyata, “Development of amphiphilic polyaspartamide derivatives for systemic messenger RNA delivery”, The 6th Annual Meeting of the Nucleic Acids Therapeutics Society of Japan, Online, June 2021.
7. **J. Yum**, B. S. Kim, M. Naito, H. J. Kim, and K. Miyata, “全身投与を介してメッセンジャーRNAを送達するカチオン性/疎水性官能基導入ポリアスパルタミド誘導体の開発”, The 37th Annual Meeting of the Japan Society of Drug Delivery System, Japan, June 2021.
8. **J. Yum**, B. S. Kim, M. Naito, H. J. Kim, and K. Miyata, “Development of amphiphilic polyaspartamide derivatives with alicyclic moieties for systemic messenger RNA delivery to the lungs”, The 16th Annual Meeting of Nano Biomedical Society, Online, November 2021.
9. **J. Yum**, B. S. Kim, M. Naito, H. J. Kim, and K. Miyata, “Development of amphiphilic polyaspartamide derivatives for systemic messenger RNA delivery”, The 43rd Annual Meeting of the Japanese Society for Biomaterials and The 8th Asian Biomaterials Congress, Japan, November 2021.

D. Awards

1. The 48th Annual Meeting of the Controlled Release Society, **Best Poster Award 1st Prize.**
2. The 16th Annual Meeting of Nano Biomedical Society, **奨励賞.**
3. The 43rd Annual Meeting of the Japanese Society for Biomaterials and The 8th Asian Biomaterials Congress, **Excellent Poster Awards ABMC Scession.**

Acknowledgment

The doctoral dissertation is the compilation of the research conducted at Department of Materials Engineering, School of Engineering, The University of Tokyo from 2019 to 2021.

First and foremost, I would like to express my sincere gratitude to my supervisor, Associate Professor Dr. Kanjiro Miyata for invaluable guidance and advice. I have learned various things including an active attitude toward research and knowledge about polymer chemistry and drug delivery systems. It was my honor to conduct the research under his guidance in the doctoral course.

I would like to express my sincere appreciation to Professor Dr. Ryo Yoshida, Associate Professor Dr. Yuichi Yamasaki, Associate Professor Dr. Horacio Cabral, at Department of Materials Engineering, and Professor Dr. Shinsuke Sando, at Department of Chemistry and Biotechnology for their kind suggestions and advice on my doctoral research as referees of the dissertation.

I would like to express my sincere appreciation to Dr. Hyun Jin Kim, an Assistant Professor at Department of Biological Engineering, Inha University, for the guidance with the polymer synthesis and fundamental knowledge about messenger RNA-related studies.

I would like to express my sincere gratitude to Dr. Beob Soo Kim for the experimental suggestions regarding the antisense oligonucleotide delivery studies. In addition, I am thankful for various additional advice beyond the research project.

I would like to express my sincere gratitude to Dr. Mitsuru Naito for the guidance with fundamental experimental skills and kind advice regarding my studies. His support provided a comfortable experimental environment and helped me concentrate on my studies.

I am also greatly appreciated to Ms. Satomi Ogura and Dr. Kaori Taniwaki for their aid and advice regarding animal studies. The experiments were performed efficiently, thanks to them.

I also thank all members of the Miyata Laboratory for their kindness. I was inspired by their active research attitude and was able to have a good time. I was able to live happily in the Miyata Laboratory for three years, thanks to them. I hope you will continue to attain many achievements in the Miyata Laboratory.

Also, I am greatly appreciative of Dr. Ishihara Kazuhiko, the Specially Appointed Professor at the Division of Materials and Manufacturing Science, Osaka University, who was the supervisor of my masters course. I have learned basic knowledge of biomaterials from him, which was very helpful for my research during the doctoral course.

I would like to thank Editage (www.editage.com) for English language editing.

Lastly, I would like to thank my family for their continuous encouragement and help during the doctoral course. Without their help, this study would not have proceeded well.

Jongmin Yum

Department of Materials Engineering,
School of Engineering,
The University of Tokyo
December 2021